Molecular mechanisms of complement activation, regulation and evasion

Jin Wu

邬金

Cover: ‘stereo’ view of the monomeric C3bBb-SCIN model

Molecular mechanisms of complement activation, regulation and evasion

Moleculaire mechanismen van de activatie, regulatie en ontwijking van het complement systeem

(met een samenvatting in het Nederlands)

Proefschrift

ter verkrijging van de graad van doctor aan de Universiteit Utrecht op gezag van de rector magnificus, prof. dr. G.J. van der Zwaan, ingevolge het besluit van het college voor promoties in het openbaar te verdedigen op maandag 30 januari 2012 te 12.45 uur

door

Jin Wu

geboren op 2 januari 1981 te Beijing, China

Promoter: **Prof. dr. P. Gros**

to my dear parents
aan mijn lieve ouders
仅将此论文献给我的父母

Table of Contents

Chapter 1

General Introduction

Complement system-an overview

The complement components were first demonstrated by Jules Bordet in the late of 19th century who found factors in human serum that had bactericidal and bacteriolytic properties. Such phenomena could be destroyed by heating. A few years later, the preliminary concept of "complement system" was introduced by Paul Ehrlich, as a complementary system that has the capacity of killing bacteria in addition to antibodies. Traditionally, complement is recognized as a key component in the innate immune system for its rapid responses against pathogen infections. It leads to the effectors functions such as oponization of the foreigner agents, release of anaphylatoxins and leading to direct bacterial lysis. In the recent decades, the important role of the complement system has been also established with its ability to mediate and activate the adaptive immune system[1-3]. In addition to its ability to eliminate foreign invaders, complement system also participates in removal of cellular debris. Complement deficiencies or decreased levels of complement components can lead to recurrent infections and development of autoimmune diseases[4,5]. Genetic defects on complement regulators may lead to dysfunction of complement activation control, which causes increased susceptibility to certain retinal and renal diseases[6-8]. Therefore, the final outcome of complement largely depends on a delicate balance between complement activation and regulation. Characterization of molecular mechanisms is the central step for understanding complement activation and regulation; it offers opportunities for the design of complement-targeted therapies[9].

The complement cascade

The complement system comprises ~30 plasma and cell surface proteins, which are present in blood as inactive forms. There are three pathways that can be initiated specifically, in the cases of classical and lectin pathways, or spontaneously, in the case of alternative pathway. All three pathways converge at the assembly of C3 convertase complexes. This complex is not only essential for activating the terminal complement pathway, but also critical for the local amplification of the complement responses leading to various effector functions (**Fig. 1**).

Initiation of complement cascade

The classical pathway recognizes pathogens through binding of the C1 complex to antigen-bound antibodies. The C1 complex is a multi-molecular protease composing of a recognition component

C1q and two protease fragments C1r and C1s[10]. C1q is responsible for antigen recognition. Activated C1s enables the protolytic processing of the complement component 4 (C4) into a small fragment C4a and a major product C4b[10]. C4b molecules covalently attach to the cell surface via the nascent thioester, which is highly active to the hydroxyl- or amino-containing substrates present on the cell surface[11,12]. The surface-bound C4b forms complexes with complement component 2 (C2), which then is sequentially processed by the activated protease fragment C1s in the C1 complex. As a result, the pro-peptide C2b is released. The remaining complex C4b2a is the active classical pathway convertase[13].

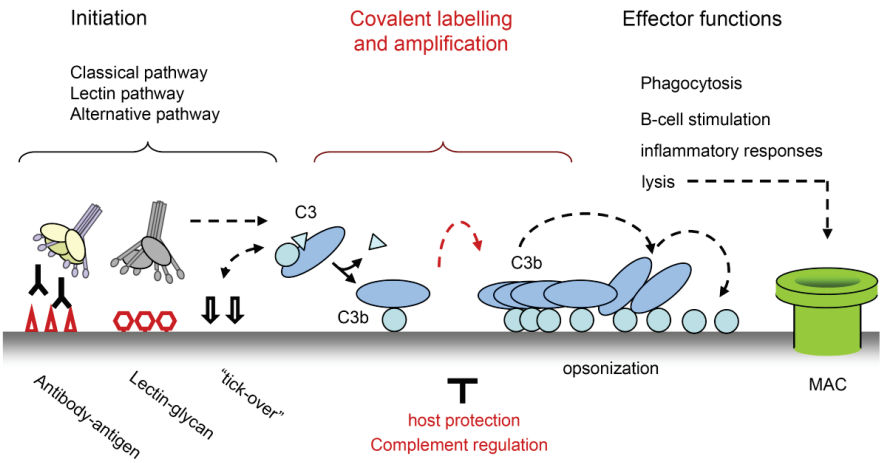

Figure 1 Schematic representation of complement cascade.

The lectin pathway has a similar structure as the classical pathway, but is not initiated by antibodies. This pathway starts when mannose-binding lectin (MBL) and ficolins bind to neutral sugars, such as mannose, glucose and N-acethylglucosamine[14-16]. Similar to the C1 complex, the MBL complex is formed by the recognition molecule MBL and two proteases MBL-associated serine protease-1 (MASP-1) and MASP-2. Activation of this pathway also leads to the proteolytical cleavage of C4 and sequential formation of active C3 convertase C4b2a[16]. In this pathway, protease MASP-2 cleaves C4 releasing C4a and generating C4b[17].

The third pathway is known as the alternative pathway. Differing from the two pathways above, it is activated spontaneously and has a basal level of activation in the body. This pathway is essential for amplification of the complement responses. The internal thioester bond of the C3 molecule is intrinsically instable and spontaneously reacts with water, resulting a hydrolyzed product C3(H_2O).

$C3(H_2O)$ binds to pro-enzyme factor B (FB), forming the complex $C3(H_2O)B$. This complex can be then processed by another protease factor D (FD), which releases the pro-peptide Ba and the remaining complex is the fluid phase C3 convertase[18,19].

Activation and amplification of complement responses

All three pathways converge at the production of the C3 convertases in two forms: C4b2a in the classical and lectin pathways and C3bBb in the alternative pathway. The C3 convertase is critical for complement amplification as these enzyme complexes bind to its substrate C3 and proteolytically process large amount of C3 into C3b. C3b contains a reactive thioester bond that can covalently attach to the cell surface, which brings the complement cascade to the surface[12]. C3b then forms more C3 convertase on the cell surface generating more C3b molecules (**Fig. 2**). This is the so called "tickover loop", which amplifies the complement responses rapidly on the target cell surface. The C3 convertase is labile with a short half-life of ~90s[20,21]. Once the protease fragment Bb dissociates, it cannot rebind to C3b. This short-lived property can be considered as an efficient way of self-regulation that only allows brief and local amplification of complement responses.

Proteolytic activation of C3 to C3b triggers the chemical reaction of the internal thioester and induces massive domain rearrangements with translations up to ~95 Å in distance (**Fig. 2**) [22-25]. As a result of such conformational changes, C3b exposes multiple binding sites for other complement components or pathogen secreted proteins[23,26,27]. The surface-attached C3b is also known as opsonin, which can be recognized by complement receptors on phagocytic cells. Thus, in this way, C3b acts as a labeling molecule on the microbial surface guiding and enhancing phagocytosis and clearance. The proteolytical product of C3b, denoted as iC3b, also acts as an opsonin, which can be recognized by receptors presented on macrophages. iC3b can be further degraded to C3d. Both iC3b and C3d can still attach to pathogen surfaces and interact with complement receptor 2 (CR2). Such interaction stimulates B cells activation, acting as a linkage between the innate and adaptive immune systems.

C3 convertase activity

C3 convertase is crucial for the amplification of complement responses. C3 convertase is known to be assembled through two steps: first assembly of the pro-convertase (C3bB in the alternative

pathway) and then this complex is processed by FD to generate C3bBb as the active enzyme complex[25]. It is known that binding of FB to C3b is via two sites contained in the pro-peptide fragment Ba domain and the von Willebrand factor type A (VWA) domain. The binding of Ba is reversible while binding of VWA domain is Mg^{2+}-dependent[18,21,28]. Binding studies indicate that FB binding upon C3b requires conformational changes, which allows sequential process by FD[29,30]. The proteolytic activity of protease fragment Bb is only present when it is bound in the C3 convertase complex, but not in pro-enzyme FB, pro-convertase C3bB or the isolated protease fragment Bb. C3 convertase shows high specificity towards its substrate C3 and limited activity to the C3 homolog C5[31,32]. Site-directed mutagenesis studies showed the residues near the Mg^{2+} binding sites give significant effects on C3 convertase formation and stability[33]. The type of divalent ion can impact on the stability of C3 convertase. For example, replacement of Mg^{2+} by Ni^{2+} results a more stable C3 convertase[34].

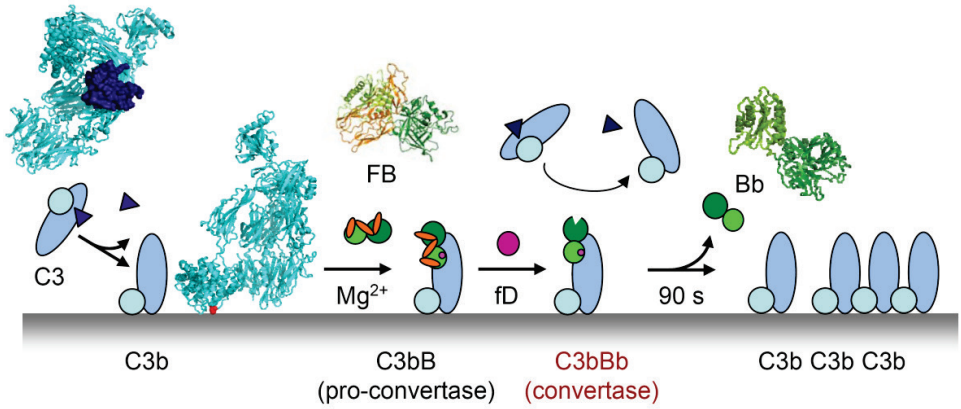

Figure 2 Schematic representation of amplification of complement responses via alternative pathway. The available structures are shown in cartoon representation.

In recent years, structures of complement components have been determined and give insights into molecular mechanisms of complement activation (**Fig. 2**)[22,23,35-37]. Activation from C3 to C3b involves remarkable conformational changes which rearrange domains in C3b that exposes the binding sites for FB as well as for complement regulators. The crystal structure of FB showed a disordered metal ion–dependent adhesion site (MIDAS), suggesting a rearrangement in FB upon C3b binding, resulting in an ordered MIDAS. The domain orientation between VWA domain and serine protease (SP) domain in FB and isolated Bb is dramatically different, which indicates significant changes occurring during convertase assembly[36]. Although the functional importance of C3 convertase has been well established for decades, the structural study on C3 convertase is

considered to be most challenging because of its metastability. It remains unclear how the C3 convertase is assembled, where the substrate C3 binds, what determines the catalytic activity and the irreversible dissociation of protease fragment Bb.

Downstream complement pathway

The amplification of complement responses results in the deposition of high quantities of C3b on target surface and forms more C3 convertase via the "tickover loop". Additional C3b molecules can react with the C3 convertases (C3bBb and C4b2a) forming C3bBbC3b or C4b2aC3b complexes that switch the substrate specificity from C3 to C5, hence they are named the C5 convertases[31,32]. In C5 convertases, the proteolytical subunits are the serine proteases Bb (in C3bBbC3b) and C2a (in C4b2aC3b), as with the C3 convertases. The C5 convertases cleave C5 into C5a and C5b. The small cleavage product C5a is a powerful inflammatory mediator. The major cleavage fragment C5b forms complex with complement component C6, initiating the terminal complement cascade, ultimately resulting in formation of membrane attack complex (MAC) on the target surface. The MAC complex has a ring structure formed by the complex C5b-8 and multiple copies of the C9 molecules[38]. When sufficient amount of pores are formed on pathogen surface, it causes cell lysis and kills Gram-negative bacteria directly.

Regulation of complement pathways

After initiation, complement responses are quickly amplified, generating effector molecules that accumulate on any cell surface without discrimination. Such aggressive effects are potentially dangerous to host cells and may lead to unwanted damage to the host tissues. Therefore, the complement cascade is tightly controlled at multiple levels by various complement regulators[39]. There is a cluster of genes encoding homologous proteins important for controlling the complement activation located on human chromosome lq32 (ref. 40). These are denoted as regulators of complement activation (RCA) and include the soluble regulators (complement factor H, FH and the C4b binding protein, C4bp), the surface-anchored regulator (decay-accelerating factor, DAF) and the membrane-integrated regulators (complement receptor 1, CR1 and the membrane cofactor protein, MCP)[40].

Structure and function of RCA proteins

Members from the RCA family down-regulate the central step of complement amplification by targeting C3b/C4b or C3 convertases (i.e. C3bBb and C4b2a). They can bind to C3b or C4b and have cofactor activity for protease factor I (FI) to degrade C3b/C4b into the inactive form iC3b/iC4b. The second function of those proteins is to dissociate C3 convertases C3bBb or C4b2a, also known as decay-accelerating activity. Most of the regulators have both activities, whereas MCP only has cofactor activity and DAF only has decay accelerating activity (**Fig. 3a** and **3b**).

a

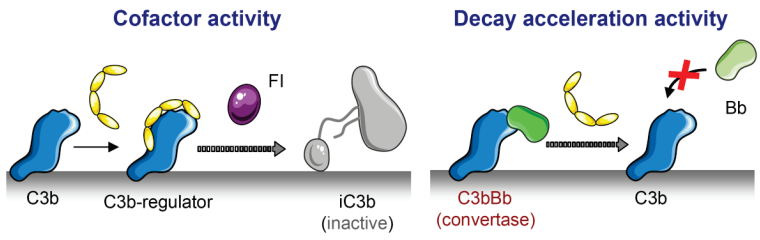

b

Regulator	Form	Cofactor activity	Decay accelerating activity
FH	soluble	✓	✓
CR1	Membrane bound	✓	✓
MCP	Membrane bound	✓	✗
DAF	Membrane bound	✗	✓
C4bp	soluble	✓	✓

c

Figure 3 (**a**) Cartoon representation of two regulatory activities and (**b**) list of regulators of complement activation. (**c**) Structure of a typical CCP domain with conserved residues shown in sticks.

Proteins from RCA family are highly homologous and they are mainly composed of a single module type, denoted as complement control protein modules (CCP domains), also known as short consensus repeats (SCR) domains. Each globular CCP domain contains ~60 residues forming several β-sheets connected by loops. It has a fairly conserved structure stabilized by two invariant disulphide bridges, one tryptophan and several other highly conserved hydrophobic residues (**Fig. 3c**).

Complement factor H (FH)

FH is a single polypeptide chain glycoprotein (~155 kDa) circulating in blood at a concentration approximately 200-500 μg/ml. It was first identified as β1H in 1965 as the fifth component of complement system[41]. FH is the major regulator controlling the alternative pathway that functions both in the fluid phase and on the cell surface. FH is formed by a linear string of 20 copies of CCP domains. The N-terminal four CCP domains (CCP1-4) possess both cofactor and decay accelerating activities[42-44]. In addition, FH suppresses C3 convertase assembly by competing with FB in binding to C3b[45]. The middle fragment of FH (CCP6-8) contains a polyanion binding site that recognizes sialic acid and glycosaminoglycans (GAG) presented on the host cell surface[46,47]. The C-terminus of FH (FH19-20) has a secondary C3b binding site and also binds to the polyanionic carbohydrates, with is important in discriminating self components from non-self[48-51]. It has been shown changing the polyanion concentration induces self-association of FH, possibly through the C-terminal parts of FH, accompanied by increased regulatory activities as well as C3b binding capacity[52].

Table 1 List of determined structures of CCP domains of FH.

	PDB code	Methods	Reference
FH1-2	2RLP	NMR	55
FH2-3	2RLQ	NMR	55
FH1-4	2WII	X-ray	56
FH6-8	2UWN	X-ray	47
FH12-13	2KMS	NMR	57
FH15	1HFI	NMR	58
FH15-16	1HFH	NMR	58
FH19-20	2BZM	NMR	59
	2G7I	X-ray	60

Structural studies of FH have been performed extensively with various methods, including nuclear magnetic resonance (NMR), electron microscopy, small-angle X-ray scattering (SAXS) and X-ray crystallography. The full length protein is highly flexible and extended[53]. A folded-back model of full length FH was proposed based on SAXS data[54]. So far, 13 out of 20 CCP domains of FH were determined by NMR or X-ray crystallography (**Table 1**). Despite of experimentally determined structures of CCP domains, the molecular basis for complement regulatory activities remains poorly understood. This is mainly because the majority of structures were determined as the

isolated single modules which do not give complete information regarding the interaction with the major ligand C3b.

Membrane cofactor protein (MCP)

MCP is a single chain type I transmembrane glycoprotein, also known as CD46. It is composed of four CCP domains at its N-terminus, followed by a serine/threonine-rich (ST) region, a transmembrane domain and a cytoplasmic tail[61]. The CCP domains bind to both C3b and C4b and possess cofactor activity for factor I-mediated cleavage of C3b/C4b in the fluid phase and on the cell surface[62]. Functional studies on MCP using domain-deletion constructs showed that the first CCP domain is not required for C3b binding and cofactor activity[63]. Domains CCP 3 and 4 of MCP contains the major C3b binding, whereas domains 2, 3 and 4 are required for C4b binding[63]. Although CCP2 of MCP only has a minor effect on C3b binding, it is required for the FI-mediated cofactor activity for C3b[63]. In addition to its protective role in controlling complement activation, a number of bacteria and viruses, use MCP (CD46) as a receptor for cell attachment and entry[64-68]. Domains of CCP 1 and 2 have been shown to mediate the binding of adenovirus and measles viruses[69,70]. The interaction between MCP and those viruses are well characterized in recent years by structural studies, giving insights into how pathogens utilize human receptors to enter host cells[71,72].

Decay-accelerating factor (DAF)

DAF is also known as CD55. It has four CCP domains and attaches to the cell membrane via its C-terminal glycosylphosphatidylinositol (GPI) anchor. DAF inhibits all three pathways by its potent capacity to rapidly dissociate C3 convertases C3bBb and C4b2a[73]. The exact mechanism of how DAF affects C3 convertase dissociation is not fully elucidated. Studies showed that DAF interacts with both components of the C3 convertases[30]. DAF binds to C3b with low affinity (~14 μM), whereas it binds to the isolated protease fragment Bb with affinity of ~1-2 μM in the presence of Mg^{2+} (ref. 30). Domains 2 to 4 are critical, whereas CCP 1 is not required for the decay accelerating activity of DAF[74,75]. The crystal structure of full-length DAF (CCP1-4) was determined in 2005, which revealed that four CCP domains form an extended rod-like structure[76].

Complement receptor 1 (CR1)

CR1 is also denoted as CD35, which is a type 1 transmembrane glycoprotein formed by 30 CCP domains at its N-terminus, followed by a transmembrane domain and a cytoplasmic tail. CR1 regulates all complement pathways by acting at levels of C3b/C4b and C3 convertases. It binds to both C3b and C4b and serves as a cofactor for FI-mediated cleavage. CR1 is the only known cofactor that facilitates the process of the third cleavage site in C3b, generating the C3c and C3dg fragments[77]. CR1 also accelerates the dissociation of C3 convertases (C3bBb and C4b2a)[78].

CR1 has the most CCP domains in RCA family. There are three sites that interact with C3b and C4b: CCP1-3, CCP8-10 and CCP15-17 (ref. 79). The first site CCP1-3 has strong decay-accelerating activity and weak cofactor activity[80,81]. The second and third sites are nearly identical with only three amino acid differences (194 amino acids in total). These two sites have potent cofactor activity and little decay-accelerating activity. CCP1-3 binds C3b weakly, whereas CCP8-10 and CCP15-17 binds C3b with relatively high affinity[80,81]. In this sense, CR1 carries one DAF-like site and two MCP-like sites, which makes it a highly efficient complement regulator.

Complement factor I (FI)

FI is a serine protease that has an essential role in complement regulation. It normally circulates in blood as inactive form and only has catalytic activity in the presence of a cofactor protein, such as FH, C4bp, MCP or CR1. FI has high specificity as it only cleaves its natural substrates C3b and C4b under physiological condition. There are three FI cleavage sites in C3b: site 1 (Arg1281-Ser1282), site 2 (Arg1298-Ser1299) and site 3 (Arg932-Glu933). When the first site is cleaved, the product $iC3b_1$ no longer binds to FB so that the complement amplification loop is stopped[82]. In the presence of FH or MCP, FI enables the sequential processing of C3b at the first and second sites generating $iC3b_2$. In the presence of CR1, the third site can be processed, which generates two degraded products C3c and C3dg[77]. FI is able to cleave synthetic substrates but with much lower catalytic activity compared to thrombin[83].

Mature FI has two chains connected by a disulfide bond. The N-terminal non-catalytic heavy chain comprises four domains (FIMAC, SRCR and two LDLr domains) and a serine protease domain forms the C-terminal light chain. The overall arrangement of FI shows two globular parts[53,84]. The crystal structure of full length FI was determined in 2011, which provides new insights into the substrate recognition and formation of the ternary complex FI-C3b-cofactor[85].

Diseases associated with complement regulation

The essential role of complement regulators in host protection is reflected by the strong linkage with several kidney and ocular diseases, such as atypical hemolytic uremic syndrome (aHUS), membranoproliferative glomerulonephritis type II (MPGNII) and age-related macular degeneration (AMD).

Unlike typical HUS caused by *E.coli* infection, aHUS is not triggered by external agents, but in many cases associated with mutations and polymorphisms in the complement alternative pathway genes, including complement regulators (FH, MCP, FI) and complement activators (C3/C3b, FB) (reviewed in 6-8 and 86). Combinations of mutations/polymorphisms in multiple complement regulators/components have been found in aHUS patients. Function characterization of the N-terminal mutations of FH showed significantly reduced regulatory activities[87]. Over 80 FH mutations and polymorphisms have been associated with aHUS. Many of them are clustered at the C-terminus of FH (domains 19 and 20). As the C-terminus of FH has a dual role in host recognition and C3b binding, some of the FH mutants in this region lost the ability to discriminate self from non-self, while others interfere with C3b binding[60,88]. In addition, autoantibodies have been also identified from aHUS patients, which bind to the C-terminal region of FH leading to an impaired C3b-FH interaction[89]. More than 20 MCP mutants have been reported in aHUS patients. Many of MCP mutants are associated with decreased expression levels, while some mutants have normal expression levels but reduced C3b/C4b binding and cofactor activity (reviewed in 90). There are a number of FI mutants that have been identified that give problems either in protein secretion or affect the catalytic activity of FI.

MPGNII is also known as dense deposit disease (DDD), which is characterized by massive deposits of complement components on the basement membrane of kidney glomerli[8,91]. Mutations in FH are linked to this disease, which is linked to FH protein secretion or reduced complement regulatory activities[92,93]. As a consequence, FH is unable to protect the kidney from excess complement activation.

Age-related macular degeneration (AMD) is one of the common causes of blindness in the elderly population. Polymorphisms in the gene encoding FH are linked to an increased risk for developing AMD[94,95]. The polymorphism of Y402H in FH has been extensively studied in order to understand the pathogenetic mechanisms and indicated an alteration in the binding pattern of FH to the

carbohydrates on the host surface.

Complement cascade-immune evasion

To enter and survive within host cells, bacteria and viruses have developed various ways to fight against the sophisticated immune defense system. Complement system is very effective in recognition and removal of invading microbes as well as host cell debris[96]. A large number of complement evading strategies have been described and novel molecules secreted by pathogens are continuously discovered (reviewed in 97-100). The Gram-positive bacteria have thick layer of capsules that protect them from lysis by the membrane attack complex. *Staphylococcus aureus*, secrets diverse proteins that are able to effectively mediate complement responses at many stages[97]. *Neisseria meningitides* produces a surface protein that hijacks the host complement regulator FH, and utilizes it to down-regulate complement responses[101]. Viruses develop strategies to shield themselves from complement recognition and can modulate complement responses in order to increase their chance of survival[96,100]. Certain pox viruses (such as vaccinia virus, smallpox virus) and herpes viruses produce proteins that mimic the host complement regulators[102-105]. Measles and herpes viruses utilize surface-attached complement component such as MCP, DAF for their initial attachment to the host cells and subsequent internalization[68,72,106]. Understanding how pathogens suppress our immune responses is not only important for revealing their role in pathogenesis, but also helps to identify novel pharmaceutical target for drug development.

Staphylococcal complement inhibitors

In the recent years, many staphylococcal inhibitors were identified, which target certain components in the complement cascade. *S. aureus* excretes proteins that help bacteria to evade immune detection and elimination. Staphylococcal complement inhibitor (SCIN) was discovered as an inhibitor that specifically targets the C3 convertases C3bBb and C4b2a[107]. In this way, SCIN can efficiently mediate all three complement pathways by blocking the enzyme activity of C3 convertases. Moreover, SCIN has the unique ability to stabilize C3 convertases on bacteria surface[107]. The active sites of SCIN have been determined by site-direct mutagenesis studies[108]. Without a corresponding atomic structure of the complex, it is unclear where SCIN interacts with the two components C3b and Bb in the C3 convertase, and how SCIN blocks and at same time stabilizes C3 convertase on bacteria suface[107]. Another evasion protein produced by *S. aureus* is Ecb, which blocks the enzyme activity of C3 and C5 convertases[109]. Ecb binds to C3d (TED

domain) region of C3/C3b[110,111]. This contact site overlaps with interaction of CR2 with C3d, so that Ecb also modulates B cell stimulation by inhibiting CR2-C3d interaction[112].

Viral complement inhibitor

Viruses evoke various strategies to fight against immune recognition and eradication. Pox viruses and herpes viruses encode secreted proteins that have potent capacity to down regulate complement activation and they are functionally similar to the host RCA proteins. Vaccinia virus complement control protein (VCP) and its variola homologue, smallpox inhibitor of complement enzymes (SPICE), have four CCP domains each, with only 11 amino acids differences. However, SPICE is ~100 fold more potent than VCP in regulating the alternative pathway[113]. The site-direct mutagenesis data suggests that the four amino acid substitutions in CCP2 domain contribute to the activity difference[114]. It was shown that the electrostatic potential changes in the CCP2 region have great impact on the cofactor activity of viral complement regulators[114,115].

Scope of this thesis

The complement system is an efficient component in the immune system that rapidly responses to pathogen invasion. The importance of complement system is not only to kill bacteria directly, but also to modulate phagocytosis, promote inflammatory responses and stimulate B cell activation. Over-activation of complement can be deleterious as it may cause serious damage to host cells and tissues. The presence of complement regulators on host cell surface are critical for discrimination of self from non-self and prevent unwanted complement attack. Thus, the efficacy of the complement-mediated immune responses relies on a delicate balance between activation and regulation. Bacteria and viruses have evolved strategies to avoid attacks by host immune defense. Many pathogens produce a series of immune evasion proteins in order to increase their survival rate and facilitate infection.

This thesis mainly focuses on the molecular mechanisms of complement activation, regulation and evasion. In **chapter 2** we describe the atomic structure of the alternative pathway C3 convertase C3bBb stabilized by SCIN. These data give unprecedented insights into the assembly, activity and enzyme specificity of the C3 convertase. Moreover, the structure reveals a unique strategy developed by *S. aureus* to freeze C3 convertase in an inactive form to avoid complement attack. In **chapter 3** we describe the structure of the first four N-terminal CCP domains of FH in complex

with the central component C3b. The structure shows in atomic detail how all four CCP domains bind C3b to support decay-accelerating and cofactor activities. This structure, combined with functional data, suggests a general model for complement regulation and offers molecular explanations for mutants associated with diseases induced by disorder of complement regulation. Next, we extended our structural studies to other host complement regulators as well as a viral mimicry protein in **chapter 4**. We try to address questions such as: how is C3b recognized by different regulators; and how do these regulators act as cofactors that are subsequently recognized by the protease factor I? The results provide insights into molecular recognition in the complement network and a comprehensive view of the molecular mechanisms underlying the complement regulatory activities. Finally, results are discussed and summarized in **chapter 5**.

REFERENCES

1. Ricklin, D., Hajishengallis, G., Yang, K. & Lambris, J.D. Complement: a key system for immune surveillance and homeostasis. *Nat Immunol* **11**, 785-797 (2010).
2. Carroll, M.C. The complement system in regulation of adaptive immunity. *Nat Immunol* **5**, 981-986 (2004).
3. Carroll, M.C. The complement system in B cell regulation. *Mol Immunol* **41**, 141-146 (2004).
4. Song, W.C. Complement regulatory proteins and autoimmunity. *Autoimmunity* **39**, 403-410 (2006).
5. Boackle, S.A. Complement and autoimmunity. *Biomed Pharmacother* **57**, 269-273 (2003).
6. Waters, A.M. & Licht, C. aHUS caused by complement dysregulation: new therapies on the horizon. *Pediatr Nephrol* **26**, 41-57 (2011).
7. Hirt-Minkowski, P., Dickenmann, M. & Schifferli, J.A. Atypical hemolytic uremic syndrome: update on the complement system and what is new. *Nephron Clin Pract* **114**, c219-235 (2010).
8. Meri, S. Loss of Self-Control in the Complement System and Innate Autoreactivity. *Ann NY Acad Sci* **1109**, 93-105 (2007).
9. Ricklin, D. & Lambris, J.D. Complement-targeted therapeutics. *Nat Biotechnol* **25**, 1265-1275 (2007).
10. Arlaud, G.J*., et al.* Structural biology of the C1 complex of complement unveils the mechanisms of its activation and proteolytic activity. *Mol Immunol* **39**, 383-394 (2002).
11. Sepp, A*., et al.* Covalent binding properties of the human complement protein C4 and hydrolysis rate of the internal thioester upon activation. *Protein Sci* **2**, 706-716 (1993).
12. Law, S.K. & Dodds, A.W. The internal thioester and the covalent binding properties of the complement proteins C3 and C4. *Protein Sci* **6**, 263-274 (1997).
13. Muller-Eberhard, H.J., Polley, M.J. & Calcott, M.A. Formation and functional significance of a molecular complex derived from the second and the fourth component of human complement. *J Exp Med* **125**, 359-380 (1967).

14. Matsushita, M. & Fujita, T. Ficolins and the lectin complement pathway. *Immunol Rev* **180**, 78-85 (2001).
15. Matsushita, M., Endo, Y., Hamasaki, N. & Fujita, T. Activation of the lectin complement pathway by ficolins. *Int Immunopharmacol* **1**, 359-363 (2001).
16. Gadjeva, M., Thiel, S. & Jensenius, J.C. The mannan-binding-lectin pathway of the innate immune response. *Curr Opin Immunol* **13**, 74-78 (2001).
17. Vorup-Jensen, T., Jensenius, J.C. & Thiel, S. MASP-2, the C3 convertase generating protease of the MBLectin complement activating pathway. *Immunobiology* **199**, 348-357 (1998).
18. Xu, Y., Narayana, S.V.L. & Volanakis, J.E. Structural biology of the alternative pathway convertase. *Immunological Reviews* **180**, 123-135 (2001).
19. Muller-Eberhard, H.J. & Gotze, O. C3 proactivator convertase and its mode of action. *J Exp Med* **135**, 1003-1008 (1972).
20. Fishelson, Z., Pangburn, M.K. & Muller-Eberhard, H.J. Characterization of the initial C3 convertase of the alternative pathway of human complement. *J Immunol* **132**, 1430-1434 (1984).
21. Pangburn, M., and Muller-Eberhard, H.J. The C3 convertase of the alternative pathway of human complement: Enzymic properties of the bimolecular proteinase. *Biochem. J.* **235**, 723-730 (1986).
22. Janssen, B.J*., et al.* Structures of complement component C3 provide insights into the function and evolution of immunity. *Nature* **437**, 505-511 (2005).
23. Janssen, B.J., Christodoulidou, A., McCarthy, A., Lambris, J.D. & Gros, P. Structure of C3b reveals conformational changes that underlie complement activity. *Nature* **444**, 213-216 (2006).
24. Wiesmann, C*., et al.* Structure of C3b in complex with CRIg gives insights into regulation of complement activation. *Nature* **444**, 217-220 (2006).
25. Gros, P., Milder, F.J. & Janssen, B.J.C. Complement driven by conformational changes. *Nat Rev Immunol* **8**, 48-58 (2008).
26. Lambris, J.D. The multifunctional role of C3, the third component of complement. *Immunol Today* **9**, 387-393 (1988).
27. Lambris, J.D. & Muller-Eberhard, H.J. The multifunctional role of C3: structural analysis of its interactions with physiological ligands. *Mol Immunol* **23**, 1237-1242 (1986).
28. Pryzdial, E.L. & Isenman, D.E. Alternative complement pathway activation fragment Ba binds to C3b. Evidence that formation of the factor B-C3b complex involves two discrete points of contact. *J. Biol. Chem.* **262**, 1519-1525 (1987).
29. Hourcade, D.E., Wagner, L.M. & Oglesby, T.J. Analysis of the Short Consensus Repeats of Human Complement Factor B by Site-directed Mutagenesis. *J. Biol. Chem.* **270**, 19716-19722 (1995).
30. Harris, C.L., Abbott, R.J.M., Smith, R.A., Morgan, B.P. & Lea, S.M. Molecular Dissection of Interactions between Components of the Alternative Pathway of Complement and Decay Accelerating Factor (CD55). *J. Biol. Chem.* **280**, 2569-2578 (2005).
31. Pangburn, M.K. & Rawal, N. Structure and function of complement C5 convertase enzymes. *Biochem. Soc. Trans.* **30**,

1006-1010 (2002).

32. Rawal, M.K.P.a.N. Structure and function of complement C5 convertase enzymes. *Biochemical Society Transactions* (2002).

33. Hourcade, D.E., Mitchell, L.M. & Oglesby, T.J. Mutations of the Type A Domain of Complement Factor B That Promote High-Affinity C3b-Binding. *J Immunol* **162**, 2906-2911 (1999).

34. Fishelson, Z. & Muller-Eberhard, H.J. C3 convertase of human complement: enhanced formation and stability of the enzyme generated with nickel instead of magnesium. *J Immunol* **129**, 2603-2607 (1982).

35. Milder, F.J*., et al.* Structure of Complement Component C2a: Implications for Convertase Formation and Substrate Binding. *Structure* **14**, 1587-1597 (2006).

36. Milder, F.J*., et al.* Factor B structure provides insights into activation of the central protease of the complement system. *Nat Struct Mol Biol* **14**, 224-228 (2007).

37. Janssen, B.J*., et al.* Insights into complement convertase formation based on the structure of the factor B-cobra venom factor complex. *EMBO J* **28**, 2469-2478 (2009).

38. Kondos, S.C*., et al.* The structure and function of mammalian membrane-attack complex/perforin-like proteins. *Tissue Antigens* **76**, 341-351 (2010).

39. Zipfel, P.F. & Skerka, C. Complement regulators and inhibitory proteins. *Nat Rev Immunol* **9**, 729-740 (2009).

40. Rodriguez de Cordoba, S., Diaz-Guillen, M.A. & Heine-Suner, D. An integrated map of the human regulator of complement activation (RCA) gene cluster on 1q32. *Mol Immunol* **36**, 803-808 (1999).

41. Nilsson, U.R. & Muller-Eberhard, H.J. Isolation of b1F-globulin from human serum, and its characterisation as the fifth component of complement. *J Exp Med* **122**, 277-290 (1965).

42. Lambris, J.D. & Muller-Eberhard, H.J. Isolation and characterization of a 33,000-dalton fragment of complement Factor B with catalytic and C3b binding activity. *J. Biol. Chem.* **259**, 12685-12690 (1984).

43. Kuhn, S. & Zipfel, P.F. Mapping of the domains required for decay acceleration activity of the human factor H-like protein 1 and factor H. *Eur J Immunol* **26**, 2383-2387 (1996).

44. Gordon, D.L., Kaufman, R.M., Blackmore, T.K., Kwong, J. & Lublin, D.M. Identification of complement regulatory domains in human factor H. *J Immunol* **155**, 348-356 (1995).

45. Discipio, R.G. The binding of human complement proteins C5, factor B, beta 1H and properdin to complement fragment C3b on zymosan. *Biochem. J. (1981) 199,485-496* **199**, 485-496 (1981).

46. Blackmore, T.K., Sadlon, T.A., Ward, H.M., Lublin, D.M. & Gordon, D.L. Identification of a heparin binding domain in the seventh short consensus repeat of complement factor H. *J Immunol* **157**, 5422-5427 (1996).

47. Prosser, B.E*., et al.* Structural basis for complement factor H linked age-related macular degeneration. *J. Exp. Med.* **204**, 2277-2283 (2007).

48. Schmidt, C.Q*., et al.* A new map of glycosaminoglycan and C3b binding sites on factor H. *J Immunol* **181**, 2610-2619 (2008).

49. Bhattacharjee, A., Lehtinen, M.J., Kajander, T., Goldman, A. & Jokiranta, T.S. Both domain 19 and domain 20 of factor H are involved in binding to complement C3b and C3d. *Mol Immunol* (2010).

50. Kajander, T.*, et al.* Dual interaction of factor H with C3d and glycosaminoglycans in host-nonhost discrimination by complement. *Proc Natl Acad Sci USA* (2011).

51. Morgan, H.P.*, et al.* Structural basis for engagement by complement factor H of C3b on a self surface. *Nat Struct Mol Biol* **18**, 463-470 (2011).

52. Pangburn, M.K.*, et al.* Polyanion-induced self-association of complement factor H. *J Immunol* **182**, 1061-1068 (2009).

53. DiScipio, R.G. Ultrastructures and interactions of complement factors H and I. *J Immunol* **149**, 2592-2599 (1992).

54. Aslam, M. & Perkins, S.J. Folded-back solution structure of monomeric factor H of human complement by synchrotron X-ray and neutron scattering, analytical ultracentrifugation and constrained molecular modelling. *Journal of Molecular Biology* **309**, 1117-1138 (2001).

55. Hocking, H.G.*, et al.* Structure of the N-terminal region of complement factor H and conformational implications of disease-linked sequence variations. *J. Biol. Chem.*, M709587200 (2008).

56. Wu, J.*, et al.* Structure of complement fragment C3b-factor H and implications for host protection by complement regulators. *Nat Immunol* **10**, 728-733 (2009).

57. Schmidt, C.Q.*, et al.* The central portion of factor H (modules 10-15) is compact and contains a structurally deviant CCP module. *J Mol Biol* **395**, 105-122 (2010).

58. Barlow, P.N.*, et al.* Solution Structure of a Pair of Complement Modules by Nuclear Magnetic Resonance. *Journal of Molecular Biology* **232**, 268-284 (1993).

59. Herbert, A.P., Uhrin, D., Lyon, M., Pangburn, M.K. & Barlow, P.N. Disease-associated Sequence Variations Congregate in a Polyanion Recognition Patch on Human Factor H Revealed in Three-dimensional Structure. *J. Biol. Chem.* **281**, 16512-16520 (2006).

60. Jokiranta, T.S.*, et al.* Structure of complement factor H carboxyl-terminus reveals molecular basis of atypical haemolytic uremic syndrome. *EMBO J* **25**, 1784-1794 (2006).

61. Lublin, D.M.*, et al.* Molecular cloning and chromosomal localization of human membrane cofactor protein (MCP). Evidence for inclusion in the multigene family of complement-regulatory proteins. *J Exp Med* **168**, 181-194 (1988).

62. Seya, T., Turner, J.R. & Atkinson, J.P. Purification and characterization of a membrane protein (gp45-70) that is a cofactor for cleavage of C3b and C4b. *J Exp Med* **163**, 837-855 (1986).

63. Adams, E.M., Brown, M.C., Nunge, M., Krych, M. & Atkinson, J.P. Contribution of the repeating domains of membrane cofactor protein (CD46) of the complement system to ligand binding and cofactor activity. *J Immunol* **147**, 3005-3011 (1991).

64. Dorig, R.E., Marcil, A., Chopra, A. & Richardson, C.D. The human CD46 molecule is a receptor for measles virus (Edmonston strain). *Cell* **75**, 295-305 (1993).

65. Dhiman, N., Jacobson, R.M. & Poland, G.A. Measles virus receptors: SLAM and CD46. *Rev Med Virol* **14**, 217-229 (2004).

66. Gaggar, A., Shayakhmetov, D.M. & Lieber, A. CD46 is a cellular receptor for group B adenoviruses. *Nat Med* **9**, 1408-1412 (2003).

67. Kallstrom, H.*, et al.* Attachment of Neisseria gonorrhoeae to the cellular pilus receptor CD46: identification of domains important for bacterial adherence. *Cell Microbiol* **3**, 133-143 (2001).

68. Tang, H. & Mori, Y. Human herpesvirus-6 entry into host cells. *Future Microbiol* **5**, 1015-1023 (2010).

69. Manchester, M.*, et al.* Measles virus recognizes its receptor, CD46, via two distinct binding domains within SCR1-2. *Virology* **233**, 174-184 (1997).

70. Gaggar, A., Shayakhmetov, D.M., Liszewski, M.K., Atkinson, J.P. & Lieber, A. Localization of Regions in CD46 That Interact with Adenovirus. *J. Virol.* **79**, 7503-7513 (2005).

71. Persson, B.D.*, et al.* Adenovirus type 11 binding alters the conformation of its receptor CD46. *Nat Struct Mol Biol* **14**, 164-166 (2007).

72. Santiago, C., Celma, M.L., Stehle, T. & Casasnovas, J.M. Structure of the measles virus hemagglutinin bound to the CD46 receptor. *Nat Struct Mol Biol* **17**, 124-129 (2010).

73. Fujita, T., Inoue, T., Ogawa, K., Iida, K. & Tamura, N. The mechanism of action of decay-accelerating factor (DAF). DAF inhibits the assembly of C3 convertases by dissociating C2a and Bb. *J Exp Med* **166**, 1221-1228 (1987).

74. Brodbeck, W.G., Liu, D., Sperry, J., Mold, C. & Medof, M.E. Localization of classical and alternative pathway regulatory activity within the decay-accelerating factor. *J Immunol* **156**, 2528-2533 (1996).

75. Harris, C.L., Pettigrew, D.M., Lea, S.M. & Morgan, B.P. Decay-Accelerating Factor Must Bind Both Components of the Complement Alternative Pathway C3 Convertase to Mediate Efficient Decay. *J Immunol* **178**, 352-359 (2007).

76. Lukacik, P.*, et al.* Complement regulation at the molecular level: The structure of decay-accelerating factor. *Proceedings of the National Academy of Sciences* **101**, 1279-1284 (2004).

77. Medof, M.E., Iida, K., Mold, C. & Nussenzweig, V. Unique role of the complement receptor CR1 in the degradation of C3b associated with immune complexes. *J Exp Med* **156**, 1739-1754 (1982).

78. Krych-Goldberg, M.*, et al.* Decay Accelerating Activity of Complement Receptor Type 1 (CD35). TWO ACTIVE SITES ARE REQUIRED FOR DISSOCIATING C5 CONVERTASES. *J. Biol. Chem.* **274**, 31160-31168 (1999).

79. Krych-Goldberg, M. & Atkinson, J.P. Structure-function relationships of complement receptor type 1. *Immunol Rev* **180**, 112-122 (2001).

80. Krych, M., Hauhart, R. & Atkinson, J.P. Structure-Function Analysis of the Active Sites of Complement Receptor Type 1. *J. Biol. Chem.* **273**, 8623-8629 (1998).

81. Krych, M.*, et al.* Analysis of the functional domains of complement receptor type 1 (C3b/C4b receptor; CD35) by substitution mutagenesis. *J. Biol. Chem.* **269**, 13273-13278 (1994).

82. Sahu, A., Isaacs, S.N., Soulika, A.M. & Lambris, J.D. Interaction of Vaccinia Virus Complement Control Protein with

Human Complement Proteins: Factor I-Mediated Degradation of C3b to iC3b1 Inactivates the Alternative Complement Pathway. *J Immunol* **160**, 5596-5604 (1998).

83. Tsiftsoglou, S.A. & Sim, R.B. Human Complement Factor I Does Not Require Cofactors for Cleavage of Synthetic Substrates. *J Immunol* **173**, 367-375 (2004).
84. Chamberlain, D., Ullman, C.G. & Perkins, S.J. Possible Arrangement of the Five Domains in Human Complement Factor I As Determined by a Combination of X-ray and Neutron Scattering and Homology Modeling. *Biochemistry* **37**, 13918-13929 (1998).
85. Roversi, P.*, et al.* Structural basis for complement factor I control and its disease-associated sequence polymorphisms. *Proc Natl Acad Sci USA* **108**, 12839-12844 (2011).
86. Pickering, M.C. & Cook, H.T. Translational Mini-Review Series on Complement Factor H: Renal diseases associated with complement factor H: novel insights from humans and animals. *Clinical & Experimental Immunology* **151**, 210-230 (2008).
87. Pechtl, I.C., Kavanagh, D., McIntosh, N., Harris, C.L. & Barlow, P.N. Disease-associated N-terminal complement factor H mutations perturb cofactor and decay-accelerating activities. *J Biol Chem* **286**, 11082-11090 (2011).
88. Lehtinen, M.J., Rops, A.L., Isenman, D.E., van der Vlag, J. & Jokiranta, T.S. Mutations of factor H impair regulation of surface-bound C3b by three mechanisms in atypical hemolytic uremic syndrome. *J Biol Chem* **284**, 15650-15658 (2009).
89. Jozsi, M.*, et al.* Factor H autoantibodies in atypical hemolytic uremic syndrome correlate with CFHR1/CFHR3 deficiency. *Blood* **111**, 1512-1514 (2008).
90. Richards, A.*, et al.* Implications of the initial mutations in membrane cofactor protein (MCP; CD46) leading to atypical hemolytic uremic syndrome. *Mol Immunol* **44**, 111-122 (2007).
91. Abrera-Abeleda, M.A.*, et al.* Variations in the complement regulatory genes factor H (CFH) and factor H related 5 (CFHR5) are associated with membranoproliferative glomerulonephritis type II (dense deposit disease). *J Med Genet* **43**, 582-589 (2006).
92. Licht, C.*, et al.* Deletion of Lys224 in regulatory domain 4 of Factor H reveals a novel pathomechanism for dense deposit disease (MPGN II). *Kidney Int* **70**, 42-50 (2006).
93. Saunders, R.E.*, et al.* The interactive Factor H-atypical hemolytic uremic syndrome mutation database and website: update and integration of membrane cofactor protein and Factor I mutations with structural models. *Hum Mutat* **28**, 222-234 (2007).
94. Klein, R.J.*, et al.* Complement factor H polymorphism in age-related macular degeneration. *Science* **308**, 385-389 (2005).
95. Edwards, A.O.*, et al.* Complement factor H polymorphism and age-related macular degeneration. *Science* **308**, 421-424 (2005).
96. Lambris, J.D., Ricklin, D. & Geisbrecht, B.V. Complement evasion by human pathogens. *Nat Rev Micro* **6**, 132-142

(2008).

97. Rooijakkers, S.H., van Kessel, K.P. & van Strijp, J.A. Staphylococcal innate immune evasion. *Trends Microbiol* **13**, 596-601 (2005).

98. Serruto, D., Rappuoli, R., Scarselli, M., Gros, P. & van Strijp, J.A. Molecular mechanisms of complement evasion: learning from staphylococci and meningococci. *Nat Rev Microbiol* **8**, 393-399 (2010).

99. Laarman, A., Milder, F., van Strijp, J. & Rooijakkers, S. Complement inhibition by gram-positive pathogens: molecular mechanisms and therapeutic implications. *J Mol Med (Berl)* **88**, 115-120 (2010).

100. Favoreel, H.W., Van de Walle, G.R., Nauwynck, H.J. & Pensaert, M.B. Virus complement evasion strategies. *J Gen Virol* **84**, 1-15 (2003).

101. Schneider, M.C.*, et al.* Neisseria meningitidis recruits factor H using protein mimicry of host carbohydrates. *Nature* **458**, 890-893 (2009).

102. Kotwal, G.J. & Moss, B. Vaccinia virus encodes a secretory polypeptide structurally related to complement control proteins. *Nature* **335**, 176-178 (1988).

103. Mullick, J., Bernet, J., Singh, A.K., Lambris, J.D. & Sahu, A. Kaposi's Sarcoma-Associated Herpesvirus (Human Herpesvirus 8) Open Reading Frame 4 Protein (Kaposica) Is a Functional Homolog of Complement Control Proteins. *J. Virol.* **77**, 3878-3881 (2003).

104. Mullick, J.*, et al.* Identification of functional domains in kaposica, the complement control protein homolog of Kaposi's sarcoma-associated herpesvirus (human herpesvirus 8). *J Virol* **79**, 5850-5856 (2005).

105. Dunlop, L.R., Oehlberg, K.A., Reid, J.J., Avci, D. & Rosengard, A.M. Variola virus immune evasion proteins. *Microbes Infect* **5**, 1049-1056 (2003).

106. Marsh, M. & Helenius, A. Virus entry: open sesame. *Cell* **124**, 729-740 (2006).

107. Rooijakkers, S.H.*, et al.* Immune evasion by a staphylococcal complement inhibitor that acts on C3 convertases. *Nat Immunol* **6**, 920-927 (2005).

108. Rooijakkers, S.H.M.*, et al.* Staphylococcal Complement Inhibitor: Structure and Active Sites. *J Immunol* **179**, 2989-2998 (2007).

109. Jongerius, I.*, et al.* Staphylococcal complement evasion by various convertase-blocking molecules. *J Exp Med* **204**, 2461-2471 (2007).

110. Hammel, M.*, et al.* A structural basis for complement inhibition by Staphylococcus aureus. *Nat Immunol* **8**, 430-437 (2007).

111. Hammel, M.*, et al.* Characterization of Ehp, a secreted complement inhibitory protein from Staphylococcus aureus. *J Biol Chem* **282**, 30051-30061 (2007).

112. Ricklin, D., Ricklin-Lichtsteiner, S.K., Markiewski, M.M., Geisbrecht, B.V. & Lambris, J.D. Cutting edge: members of the Staphylococcus aureus extracellular fibrinogen-binding protein family inhibit the interaction of C3d with complement receptor 2. *J Immunol* **181**, 7463-7467 (2008).

113. Rosengard, A.M., Liu, Y., Nie, Z. & Jimenez, R. Variola virus immune evasion design: expression of a highly efficient inhibitor of human complement. *Proc Natl Acad Sci USA* **99**, 8808-8813 (2002).

114. Yadav, V.N., Pyaram, K., Mullick, J. & Sahu, A. Identification of hot spots in the variola virus complement inhibitor (SPICE) for human complement regulation. *J Virol* **82**, 3283-3294 (2008).

115. Sfyroera, G., Katragadda, M., Morikis, D., Isaacs, S.N. & Lambris, J.D. Electrostatic Modeling Predicts the Activities of Orthopoxvirus Complement Control Proteins. *J Immunol* **174**, 2143-2151 (2005).

Chapter 2

Structural and functional implications of the complement convertase stabilized by a staphylococcal inhibitor

Jin Wu[1*], Suzan H M Rooijakkers[2*], Maartje Ruyken[2], Robert van Domselaar[2], Karel L Planken[3], Apostolia Tzekou[4], Daniel Ricklin[4], John D Lambris[4], Bert J C Janssen[1], Jos A G van Strijp[2] & Piet Gros[1]

1 Crystal and Structural Chemistry, Bijvoet Center for Biomolecular Research, Department of Chemistry, Faculty of Science, Utrecht University, Padualaan 8, 3584 CH Utrecht, The Netherlands.

2 Medical Microbiology, University Medical Center Utrecht, 3584 CX Utrecht, The Netherlands.

3 Van `t Hoff Laboratory for Physical and Colloid Chemistry, Utrecht University, Padualaan 8, 3584 CH Utrecht, The Netherlands.

4 Department of Pathology & Laboratory Medicine, University of Pennsylvania, 401 Stellar Chance, Philadelphia, PA 19104, USA.

* These authors contributed equally.

Nature Immunology, **10**, 721-727 (2009)

ABSTRACT

Activation of the complement system generates potent chemoattractants and leads to the opsonization of cells for immune clearance. Short-lived protease complexes cleave complement component C3 into anaphylatoxin C3a and opsonin C3b. Here we report the crystal structure of the C3 convertase formed by C3b and the protease fragment Bb, which was stabilized by the bacterial immune-evasion protein SCIN. The data suggest that the proteolytic specificity and activity depend on the formation of dimers of C3 with C3b of the convertase. SCIN blocked the formation of a productive enzyme-substrate complex. Irreversible dissociation of the complex of C3b and Bb is crucial to complement regulation and was determined by slow binding kinetics of the Mg^{2+}-adhesion site in Bb. Understanding the mechanistic basis of the central complement-activation step and microbial immune evasion strategies targeting this step will aid in the development of complement therapeutics.

INTRODUCTION

Complement is an ancient defense mechanism that evolved into a large protein-interaction network in mammals that initiates and serves innate immune functions and links innate immunity with adaptive immunity[1]. Activation of complement is critical for protection against microbial infection; however, over-activation of complement causes host tissue damage[2]. The complement system is initiated either by specific recognition of target cells in the classical and lectin pathways or spontaneously because of inherent instability of complement component C3 in the alternative pathway[3]. These pathways converge in the formation of C3 convertases, which cleave C3 into the small anaphylatoxin C3a and the large, reactive C3b that may covalently couple to target surfaces[4,5]. In the amplification loop of the alternative pathway, proenzyme factor B (FB) binds to surface-bound C3b and is cleaved by factor D (FD), which results in an active convertase complex that consists of C3b and the noncovalently bound protease fragment Bb (C3bBb). These convertases amplify C3b production near the target surface, which results in rapid opsonization of the target cell with C3b, which can then elicit B cell stimulation, phagocytosis and cell lysis[1]. Similarly, C3 convertases are formed in the classical and lectin pathways by C4 and C2, which are homologs of C3 and FB, respectively[6]. Both C3 convertases (C3bBb and C4b2a) are active only toward their natural substrate C3, with limited activity toward the homolog C5 (ref. 7). In the terminal complement pathway, the substrate specificity is

switched from C3 to C5 after association of one or more C3b molecules with the C3bBb or C4b2a complex[8, 9]. Regulation of activity is achieved by convertase assembly and disassembly, which is mediated by complement regulators[10]. For this regulation, it is essential that enzymatic activity toward C3 is expressed only by the assembled active convertases (C3bBb and C4b2a) and not by the proenzymes (FB and C2), proenzyme complexes (C3bB and C4bC2) or dissociated fragments (Bb and C2a). In addition, the convertases are meta-stable and dissociate irreversibly (with an inherent half-life of 60-90 s at 37 °C)[11]; therefore, the protease fragments Bb or C2a do not reassociate with C3b or C4b, respectively. In this way, the protease activity of the short-lived C3 convertase complexes determines opsonization of pathogens and altered host cells, which is a pivotal step in raising complement-mediated immune responses.

To resist the host immune response, pathogenic bacteria and viruses have evolved many well-defined strategies to evade the immune system. Because the complement system is a key element in antibacterial defense, many of these evasion molecules are directed against complement components. Blocking the central activation step of C3 to C3b is a principal bacterial complement-evasion strategy: streptococci secrete molecules that degrade the C3 molecule, whereas many pathogens indirectly block C3 convertases by attracting host convertase regulators to their surfaces[12]. Staphylococcal complement inhibitor (SCIN) from *Staphylococcus aureus* has been described as a bacterial protein that directly targets C3 convertases[13]. SCIN is found in 90% of *S. aureus* strains and specifically binds active convertases (C3bBb and C4b2a) on bacterial surfaces and prevents opsonization of bacteria and subsequent phagocytosis[13]. A notable characteristic of SCIN is that it stabilizes convertases on bacterial surfaces, and mutational analyses indicate that this is essential for its inhibitory function[14].

Structural studies of the C3 convertases are challenging because these complexes dissociate irreversibly and have short half-lives. Here we used SCIN to stabilize the C3 convertase of the alternative pathway (C3bBb) and to crystallize C3bBb in complex with SCIN. The structure gave insight into the inhibitory mode of SCIN and provided a structural basis for the enzymatic activity, substrate specificity and irreversible dissociation of the C3 convertases that are central to immune defense.

RESULTS

SCIN induces the formation of stable convertase dimers

First we studied whether SCIN, an inhibitor of surface-bound convertases, also binds and stabilizes soluble convertases. Using surface plasmon resonance, we found that surface-immobilized SCIN specifically bound C3bBb (generated in solution by mixture of C3b, FB and FD) and not FB, C3b or proconvertase C3bB (**Fig. 1a**). Incubation of histidine-tagged SCIN with C3b, FB and FD in solution resulted in simultaneous association of C3b and Bb with SCIN, whereas no complexes were formed in the absence of FD or FB (**Supplementary Fig. 1**).

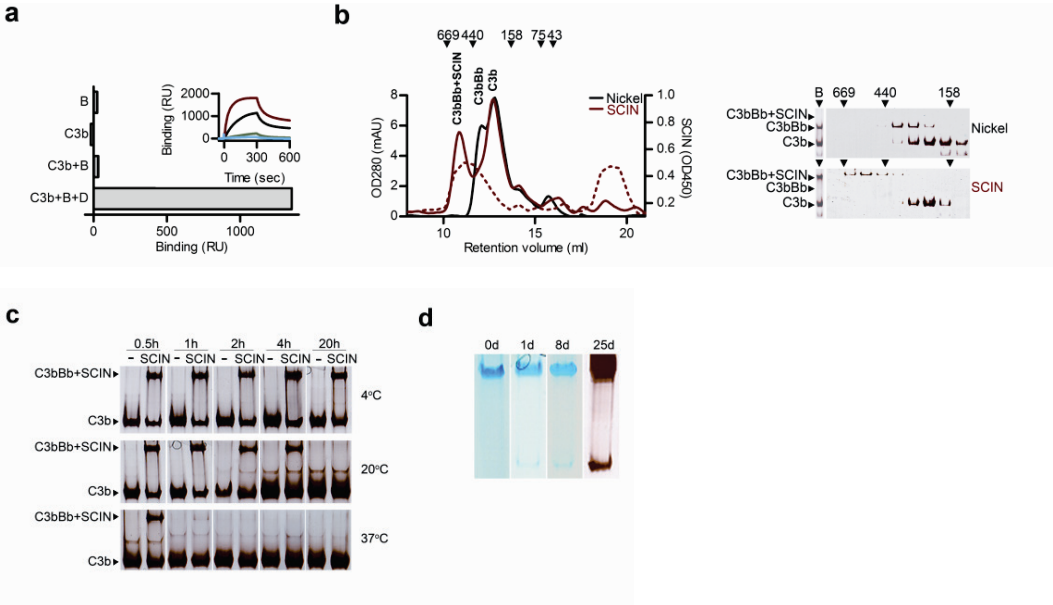

Figure 1 SCIN induces the formation of dimeric convertases. (**a**) Surface plasmon resonance analysis of the binding of soluble convertase components to surface-immobilized SCIN, showing responses at the end of injection (with all components at 100 nM). Inset, sensorgrams of injection with C3bBb, with C3b and FB at 10 nM (blue), 30 nM (green), 100 nM (black) or 300 nM (red), and FD at 100 nM. RU, resonance units. (**b**) Gel-filtration analysis (left) and native gel electrophoresis (right) of SCIN-inhibited convertases. Left, absorbance at 280 nm (A_{280}) of active convertases stabilized by Ni^{2+} (Nickel) and SCIN-inhibited convertases (SCIN). The 178-kDa peak corresponds to free C3b. Dashed red line, elution positions of SCIN determined by enzyme-linked immunosorbent assay (right axis; absorbance at 450 nm). mAU, milli-absorbance units. Right, electrophoresis of active convertase (Nickel) and SCIN-inhibited convertase (SCIN) before gel filtration (B) and of fractions eluted from the gel filtration column. (**c**) Analysis of the stability of C3b (500 nM), FB (500 nM), FD (250 nM) and SCIN (1 µM) incubated for various times (above) at 4 °C, 20 °C or 37 °C and separated by native gel electrophoresis at 4 °C. No complexes are present in the absence of SCIN (–). (**d**) Native gel electrophoresis of purified SCIN-convertase complexes after 0–8 d (left; Coomassie staining) and 25 d (far right; silver staining). Data are representative of three (**a–c**) or two (**d**) independent experiments.

SCIN inhibited convertases in solution, as C3bBb did not cleave C3 in the presence of SCIN (**Supplementary Fig. 2**). Gel-permeation chromatography of the complexes generated in the presence of SCIN showed that SCIN induced the formation of large complexes of ~500 kilodaltons (kDa), twice the size of an active convertase complex (~240 kDa; **Fig. 1b**). Immunoblot analysis and enzyme-linked immunosorbent assay showed that these complexes indeed contained C3b, Bb and SCIN (**Fig. 1b** and **Supplementary Fig. 3**). We also detected the SCIN-induced formation of large convertase complexes by native gel electrophoresis, and we used this method to analyze the stability of complexes (**Fig. 1b, c**). At 20 °C SCIN-stabilized complexes had a half-life of up to 4 h, whereas at 4 °C we noted an improvement in stability, with a half-life exceeding 20 h (**Fig. 1c**). For crystallization purposes, we optimized the stability of the complex in small-scale experiments comparing a variety of purification methods, which allowed us to generate highly stable complexes in the milligram range. We used SCIN with a histidine-tag at the amino (N) terminus to generate complexes in fluid phase that we then purified from reactants (such as FD, Ba and excess C3b and FB) with magnetic Co^{2+} beads. We used ultrafiltration to remove SCIN not in complex and to further concentrate the samples. For crystallization, we generated 10 μM complexes (approximately 5 mg/ml) that were stable over 25 d at 4 °C (**Fig. 1d**). Analytical ultracentrifugation of the purified material showed a major component of 15.2 S and a minor component of ~18 S, which probably corresponded to the SCIN-stabilized dimeric complex of ~500 kDa and a putative dimer of dimers, respectively (**Supplementary Fig. 4**). Thus, SCIN bound and blocked active convertases in solution and induced the formation of dimers of C3bBb. The stabilizing ability of SCIN allowed us to generate highly pure and stable convertase complexes.

Crystal structure of the SCIN-inhibited convertase

We used freshly prepared and purified SCIN-stabilized complexes to set up crystallization experiments at 4 °C. Crystals appeared within 1–2 d; electrophoresis showed that the crystals consisted of C3b, Bb and SCIN (**Supplementary Fig. 5**). We optimized the crystallization conditions, which resulted in a crystal that diffracted to a resolution of 3.9 Å (crystallographic statistics, **Table 1**; electron density quality, **Supplementary Fig. 6**). We solved the structure by molecular replacement with the available structures of the individual proteins present in the complex and refined it with noncrystallographic symmetry and tight geometry restraints. The final model was refined to R and R_{free} factors of 25.3% and 26.8%, respectively.

The asymmetric unit contained two complexes, each consisting of a C3bBb-SCIN dimer of 500 kDa with overall dimensions of 177×168×155 Å (**Fig. 2a**). The dimer was built of a C3b-C3b homodimer that was stabilized by bridging SCIN molecules (**Fig. 2**; complex interface analysis, **Table 2**). Each C3b molecule had a typical arrangement of 12 domains, as found in other structures of C3b[15,16], which consisted of a core formed by eight macroglobulin (MG) domains and a linker domain, a CUB domain ('complement C1r-C1s, UEGF, BMP1') and thioester-containing domain (TED) inserted between MG7 and MG8, and a carboxy (C)-terminal C345C domain (**Fig. 2b**). Two Bb molecules were positioned symmetrically on the outer edges of the C3b-C3b dimer. Bb was attached to the C-terminal C345C domain of C3b through the

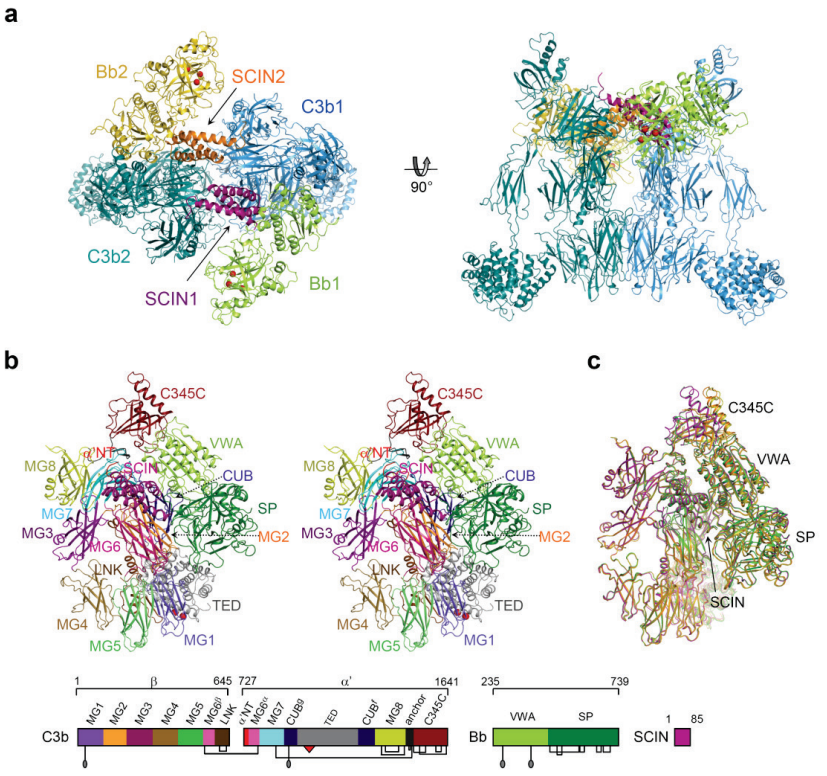

Figure 2 Crystal structure of the C3 convertase C3bBb inhibited by SCIN. (**a**) The C3bBb-SCIN dimeric complex, presented as a ribbon diagram with C3b in blue and turquoise, Bb in green and gold and SCIN in purple and orange. (**b**) 'Stereo' view of the monomeric C3bBb-SCIN extracted from the dimer, with colors indicating protein (SCIN) or protein domain (VWA and SP of Bb, and all 12 domains of C3b, with red spheres indicating thioester); below, domain composition (including disulfide bonds, glycosylation sites and thioester). α'NT, α' N-terminal tail. (**c**) Overlay of the four C3bBbSCIN complexes in the asymmetric unit (yellow, orange, green and magenta; additional details, **Supplementary Fig. 8**).

Von Willebrand factor type A (VWA) domain with the active site in the serine protease (SP) domain oriented outward.

Inhibition of C3bBb by SCIN

SCIN stabilized the convertase dimer by interacting with C3b and Bb of one convertase (with contact areas of ~1,400 Å^2 each to C3b and Bb) and with C3b of the opposing convertase (contact area of 1,800 Å^2; **Fig. 3a** and **Supplementary Fig. 7** and **Table 2**). SCIN bound the first C3b at its α'N-terminal tail and domains MG6 and MG7, whereas the binding site in the second

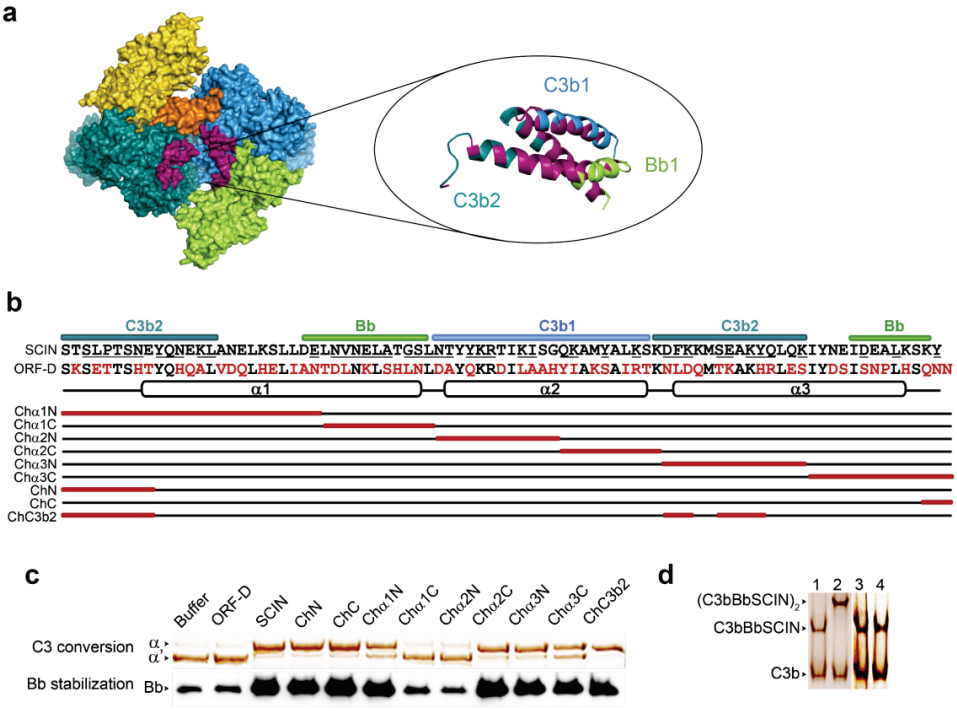

Figure 3 Inhibition of C3bBb by SCIN. (**a**) Contact sites of SCIN in the dimeric convertase with the SCIN binding pocket presented in surface representation (left) and a ribbon diagram of SCIN with colors indicating molecular contacts (right). (**b**) Amino acid sequence alignment of SCIN and the nonfunctional homolog ORF-D. Convertase contact sites in SCIN are underlined. Below, SCIN chimeras (red boxes indicate exchanged segments). (**c**) Convertase inhibition by SCIN chimeras, with C3 conversion by fluid-phase C3bBb (above) and Bb stabilization on bacterial surfaces (below). (**d**) Native gel electrophoresis of convertases in the presence of Ni^{2+} (lane 1), SCIN (lane 2), ChN (lane 3) or ChC3b2 (lane 4). Data (c,d) are representative of three independent experiments.

C3b was formed by domains MG7 and MG8. SCIN did not block the catalytic site in Bb. Instead, SCIN mainly bound the VWA domain and the VWA-SP interface of Bb (**Fig. 2b** and **Supplementary Fig. 7**). Studies of a panel of eight different chimeras of SCIN and a nonfunctional homolog have identified two segments of SCIN that are essential for activity on bacterial surfaces[14]. These segments (residues 26–36 and 37–48; exchanged in chimeras Chα1C and Chα2N, respectively) coincided with most of the contact sites for Bb and C3b of one convertase enzyme (**Fig. 3b**). We retested the same eight mutants and found that residues 26-48 were also critical for blocking C3 conversion by convertases in solution, which confirmed the observed arrangement in the crystal (**Fig. 3c**). Next, we addressed the importance of the formation of convertase dimers in the inhibition by SCIN. Two SCIN chimeras with altered C3b dimer-formation contact sites (ChN and ChC3b2) yielded stable but monomeric C3bBb-SCIN complexes (**Fig. 3d**). Moreover, these two chimeras still inhibited convertase activity in solution and stabilized convertases on bacteria (**Fig. 3c**). These data confirmed the existence of a dimer-formation site as observed in the complex but demonstrated that the formation of convertase dimers was not essential for the inhibitory activity of SCIN. We therefore conclude that SCIN probably inhibits monomeric convertases either by blocking substrate binding or by preventing critical movements required for the formation of active enzyme-substrate complexes.

Architecture of the C3 convertase

In the SCIN-stabilized complex, we noted a loose arrangement of the C3 convertase C3bBb in which Bb seemed to 'dangle' from the tip of the C3b structure. Bb contacted the C-terminal C345C domain of C3b through its VWA domain. We found no contacts between the SP domain of Bb and C3b. This arrangement of C3bBb in the inhibited complex was consistent with published three-dimensional electron microscopy reconstructions of C3bB and C3bBb at a resolution of 27 Å (ref. 17). Most notably, the C-terminal asparagine residue at position 1641 (Asn1641) of C3b chelated the Mg^{2+} bound to the metal-ion dependent adhesion site (MIDAS) formed by three loops (βA-α1, α3-α4 and βD-α5) of the VWA domain of Bb[18,19] (**Fig. 4a,b**). This arrangement is in full agreement with mutagenesis data on the critical importance of the MIDAS for convertase activity[20, 21]. The three loops of the MIDAS contributed to the C3b-Bb interface; two of these (βA-α1 and βD-α5) have been shown to be critical for convertase stability[22] (**Fig. 4b**). In addition, helix α6 of the VWA domain of Bb was near to the α' N-terminal tail of C3b (**Fig. 4b**). Published data support the possible existence of a putative secondary interaction site that may be disrupted by SCIN, as substitution of an alanine residue

for the asparagine residue at position 415 (N415A) in VWA helix α6 of FB yields convertases that are more prone to dissociation by complement regulators[23]. As for C3b, the interface was formed by loops of residues 1515–1520, 1547–1556 and the C-terminal tail (residues 1634–1641) in the C345C domain (**Fig. 4b**). Variation in the C345C orientation (**Supplementary Fig. 8**) indicated weak interactions of C345C with the α3-α4 loop of VWA that resulted in buried surface areas that ranged from 600 Å^2 to 1,200 Å^2 (**Table 2**). These variations are in agreement with published data showing a limited effect of substitution in the α3-α4 loop on convertase stability[22] (**Fig. 4b**).

The SCIN-stabilized C3bBb complex allowed us to study the effects of complex formation on the conformations of C3b and the proteolytic fragment Bb. The domain arrangement of C3b in the complex (**Supplementary Fig. 9**) was similar to that of other C3b structures[15, 16]; variations in the C345C and CUB-TED domains are common and indicate inherent flexibility of C3b. The structure of the Bb fragment in the C3 convertase was similar to that of free Bb[24], which is very different from that of the full-length proenzyme FB[25] (**Fig. 4c** and **Supplementary Fig. 10**). The MIDAS arrangement in C3bBb suggested a typical high-affinity ligand-binding configuration,

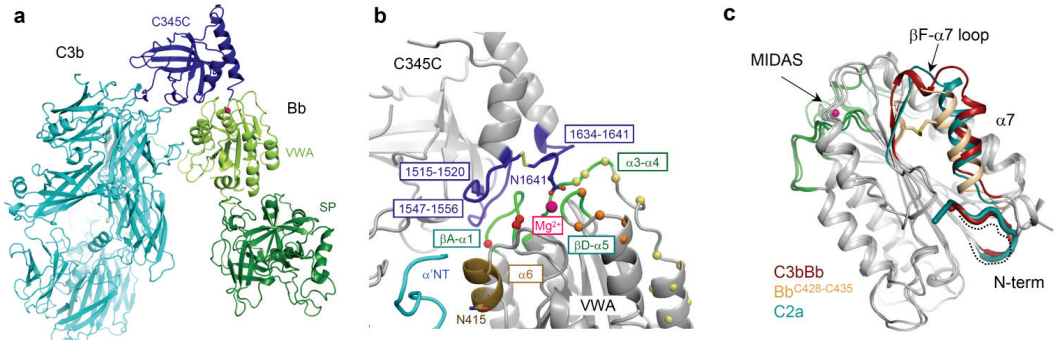

Figure 4 The C3bBb structure derived from the C3bBb-SCIN complex. (**a**) C3bBb complex, presented as a ribbon diagram with C3b in light and dark blue, Bb in light and dark green and Mg^{2+} as a pink sphere. (**b**) The C345C-VWA interface between C3b and Bb with the contact regions in blue (for the C345C domain of C3b) or green (for the VWA domain of Bb) and the disulfide bond of Cys1515-Cys1639 in C345C domain in a stick diagram. The residues substituted in FB chimeras are spheres (red, βA-α1 loop; beige, α3-α4 loop and α4 helix; orange, βD-α5 loop), based on reference 22. (**c**) Overlay of VWA domains of Bb in complex with C3b, Bb(C428-C435) (Protein Data Bank accession code 1RRK)[24] and C2a (Protein Data Bank accession code 2I6Q)[26], showing the position of helix α7 and the nascent N terminus. The MIDAS loop βA-α1, α3-α4 and βD-α5 are green; the N terminus of Bb (Cys428-Cys435) is missing (dashed line).

similar to the structures of free Bb and C2a[24, 26] and activated integrin Iα domains[27] (**Supplementary Fig. 10**); however, the low resolution of the diffraction data did not allow detailed interpretation. The nascent N-terminal tail of Bb and the VWA helix α7, which are putatively conformationally coupled to the MIDAS, adopted positions as in free C2a[26] (**Fig. 4c**). The published structure of free Bb is in part distorted, because the construct lacks the seven N-terminal residues and has an introduced disulfide bridge (Cys428-Cys435) that distorts helix α7 (ref. 24; **Fig. 4c**). Nevertheless, the VWA-SP orientations in bound versus free Bb differed by only 10°, which indicates limited overall effects of these distortions at the VWA-SP interface. Moreover, SCIN interacted with Bb at the VWA-SP interface; these interactions did not have an apparent effect on the VWA and SP conformations. In contrast, the VWA-SP orientations in C2a and C3bBb differed by 28°, which is possibly an inherent difference between Bb and C2a (**Supplementary Fig. 10a**,**b**). Overall, the conformation of the components C3b and Bb in the convertase complex are similar to those of the isolated C3b and Bb proteins.

Implications for enzymatic activity and specificity

The active site in the SP domain in C3bBb showed a typical catalytic serine-histidine-aspartic acid triad and oxyanion hole. The oxyanion-hole loop (residues 672–674), however, was distorted because of a peptide flip in all structures of FB, Bb and its homolog C2a, except for one covalently inhibited Bb structure[24, 26, 28] (**Supplementary Fig. 10d**). In the present low-resolution structure, no conformational changes were apparent in the SP domains of FB, Bb and C3bBb that would affect the catalytic site (**Supplementary Fig. 10e**), which would indicate that binding of C3b does not allosterically induce the catalytic activity of the protease fragment Bb.

C3b is probably critical in binding of the substrate C3 to the C3 convertase C3bBb; such an ‘exosite’ would explain the greater activity for the natural substrate C3 relative to that of five-amino acid peptides (with Michaelis constants of 6 μM (ref. 27) and 210-3,000 μM (ref. 29), respectively; plasma concentration of C3, ~5 μM). We noted a dimeric convertase complex that consisted of two opposing convertases created by the formation of C3b homodimers (**Fig. 2a**). The C3b dimer-formation face coincided with binding sites for the inhibitors compstatin[30], CRIg[16] and antibody S77 (ref. 31), which block the binding of substrate to the C3 convertase. In the dimeric crystal structure the C3b-C3b interface was formed by the MG4-MG5 domains of the C3b molecules (with buried surface areas of ~1,900–2,800 Å^2; **Fig. 5a**). We generated a hypothetical enzyme-substrate (C3bBb-C3) complex by superposing the substrate C3 onto C3b

based on the MG4-5 domains, with the observation that the arrangements of the MG1-6 domains (which form the β-ring) are strongly conserved between C3 and C3b (**Fig. 5b** and **Supplementary Fig. 11a**). In the resulting C3bBb-C3 model the catalytic site of C3bBb was oriented toward but positioned 30 Å away from the scissile loop of the substrate C3 (**Fig. 5b**). Furthermore, the homologous convertase C4b2a is expected to bind substrate C3 through the corresponding side of C4b, resulting in a similar C4b-C3 interface. The sequence alignment of the MG4-MG5 domains of C3, C4 and C5 indicated that many amino acid residues at the interaction site were conserved between C3 and C4 (ref 32; **Supplementary Fig. 11b**). C5, however, differed both in amino acid sequence and in the domain-domain orientation of MG4-MG5; which may explain the weak interaction of C5 with C3b and poor cleavage of C5 by

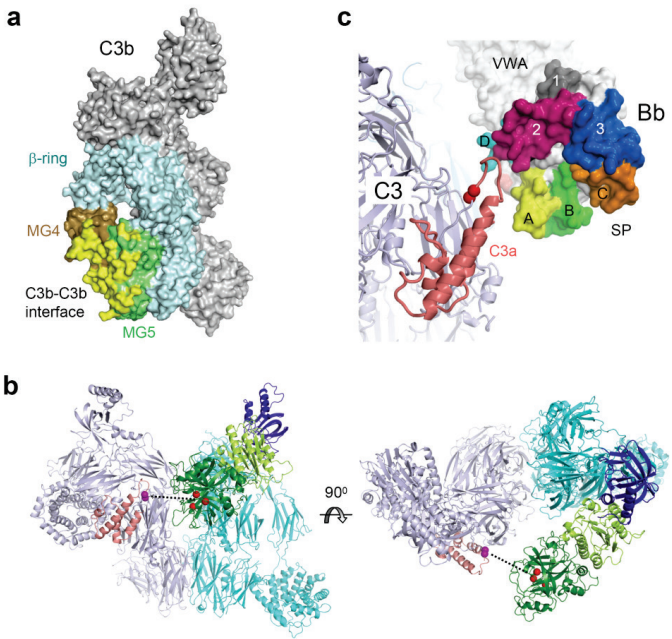

Figure 5 The C3b-C3b interface and substrate-binding model. (**a**) Surface representation of C3b with the C3b-C3b dimer interface (yellow), which is formed by domains MG4 (brown) and MG5 (green) of the β-ring of C3b (MG1-MG6; cyan). (**b**) Model of the enzyme-substrate complex (C3bBb-C3), constructed by superimposition of C3 (Protein Data Bank accession code: 2A73)[32] on the MG4-MG5 domains of the dimeric C3b molecule in the complex. Colors for C3bBb are as in **Figure 4a**; red spheres indicate the catalytic triad of Bb. The substrate C3 is gray, with the anaphylatoxin domain (C3a) highlighted in coral and the scissile bond (S726-R727) indicated by magenta spheres. The dashed line indicates the distance (~30 Å) between the catalytic site and the scissile loop. (**c**) Relative orientation of the C3a domain of C3 (substrate) and the surface loops of the SP domain of Bb forming the substrate-binding groove.

the C3bBb complex[33,34] (**Supplementary Fig. 11a**). These data indicated that the extreme specificity of the C3 convertase is possibly obtained by the formation of quasi-homodimers of C3 with C3b of the alternative pathway convertase (C3bBb) and a similar association of C3 to the evolutionary related C4b of the classical and lectin pathways convertase (C4b2a).

Positioning Bb of the C3bBb complex in place relative to the substrate C3 in the C3bBb-C3 model yielded a putative docking of the scissile loop into the active site of the SP domain in a productive (N-to-C) orientation (**Fig. 5c**). The observed orientation of the SP domain was consistent with the predicted orientation based on the crystal structure of C2a[26], with the extended surface loops (unique to the chymotrypsin-like SP domains of Bb and C2a) folding along the anaphylatoxin domain of C3. Two possible concurrent effects may overcome the 30-Å gap between the catalytic site and the scissile loop and result into an enzymatically active complex. First, the large positional variation of the C345C domain in various C3b structures (**Supplementary Fig. 9**) suggests that the flexibility in C345C orientation may be used to swing Bb into place for proteolysis. Second, the observed C3b-C3b interface in the inhibited complex probably represents the product release state C3bBb-C3b. Substrate binding putatively involves a larger area of C3 that includes the domains MG3 and MG6-MG8 at the same side as MG4-MG5, and hence closes part of the gap between the substrate and the enzymatic complex. The differences in domain orientations of MG3, MG7 and MG8 (15°, 36° and 61°; respectively) in C3 (ref. 32) versus C3b[15, 16] yield distinct shape complementarities and electrostatic surface potentials that could differentiate substrate binding from product release (**Supplementary Fig. 12**). SCIN possibly blocks both processes; it prevents swinging of Bb, and it may block a tighter C3b-C3 interface. In conclusion, the data suggest that the specific proteolytic activity of the C3bBb complexes is determined by the highly specific binding of the substrate through the 'exosite' located on the ligand C3b.

Intrinsic control of convertase activity

The C3 convertase (C3bBb) dissociates irreversibly, which is critical in controlling complement activation[35]. However, it is unclear what prevents the reassociation of Bb and C3b. Structural comparison of C3bBb with free Bb[24] and C3b[15,16] suggested that dissociation does not induce large conformational changes. Both free Bb[24] (as well as the isolated VWA domain[36]) and probably bound Bb have a MIDAS configuration that corresponds to the open, high-affinity state found in activated, ligand-binding integrin Iα domains[27]. The possibility of putative changes in

the helix α7 and the N-terminal tail of the VWA domain of Bb from the bound state to the dissociated state[5,24] was not supported by the available structural data (**Fig. 4c** and **Supplementary Fig. 10**). Surface plasmon resonance data show that the proenzyme FB and C3b associate and dissociate in a two-step process in Mg^{2+}-containing buffer with one fast kinetic phase and one slow kinetic phase that differ by orders of magnitude[37]. Here, we extended that analysis by measuring the binding of FB to C3b in the absence of Mg^{2+} (to exclude the possibility of binding of the Bb fragment) and the interaction of fragment Ba with C3b (**Supplementary Fig. 13**). Our data confirmed that Ba directly binds to C3b in a Mg^{2+}-independent way[37,38] and showed that binding of FB in the absence of Mg^{2+} shifted toward a kinetic profile similar to that of Ba. We therefore conclude that the fast on-off phase in the C3b-FB interaction is Mg^{2+} independent and can be attributed to initial contacts through the Ba segment. This result indicates that the Bb segment of FB associates and dissociates slowly. These data collectively indicate that the MIDAS and helix α7 configuration in Bb establishes a stable ligand-binding site in the open configuration with slow association and dissociation kinetics, which is responsible for the intrinsic control of the convertase activity, the half-life and irreversible dissociation.

DISCUSSION

Here we have shed important new light on the structure of the inherently instable bimolecular C3 convertase (C3bBb), which is the central protease complex of the complement system, by demonstrating the dimeric structure of C3bBb stabilized by SCIN from *S. aureus*. The structure answered crucial questions related to convertase specificity and function relevant to understanding regulation of innate immunity. Furthermore it showed in detail how bacteria may evade the immune system, which is important for understanding bacterial pathogenesis at the molecular level.

For the protection of host cells, complement activation is strictly regulated. Regulation occurs mainly at the level of C3 convertases, because the enzyme is a short-lived complex that cannot reassociate after dissociation. This first structure of C3bBb indicated that the conformation of Bb in the convertase complex is similar to that of Bb in its isolated form. Binding studies showed that Bb cannot rebind to C3b, because it has lost its fast association binding site for C3b, which is the Ba segment. Another critical aspect of complement regulation is that the C3 convertase enzyme is highly specific for C3 and does not or can hardly activate other proteins, such as the

homologous C4 or C5. The presented structure of convertases in dimer formation indicates that C3b of the enzyme complex (C3bBb) forms a dimer with its substrate C3 and provides an 'exosite' that determines the enzyme specificity.

On the basis of our results, we present a model for the activation of C3 by convertases. Surface-bound C3bBb binds the substrate C3 by forming a quasi-homodimer with C3b. Because Bb is bound to the flexible C345C domain in C3b, it can swing toward the substrate and cleave the scissile bond in C3. The C3a domain will be released, and conformational changes in C3b will induce its release from the enzyme complex. After diffusion C3b may bind covalently to hydroxyl groups on the target surface through its reactive acyl-imidazole moiety[4]. Covalent binding to the surface without diffusion may generate $C3b_2Bb$ complexes with C5-convertase activity; this would explain the apparent discrepancy that formation of the C5 convertase depends on the binding of one C3b molecule[8] or multiple C3b molecules[9] to the C3 convertase complex. However, the precise arrangement of the multimolecular enzyme complex that leads to the binding and cleavage of C5 is unclear.

From an immune-evasion point of view, it is now understood that many amino acids in SCIN are involved in the formation of the dimeric inhibited convertase. In fluid phase, SCIN strongly binds to one convertase (C3bBb) and forms a bridge to the other convertase by binding C3b. By itself, the formation of convertase dimers could be an efficient convertase-inhibitory strategy, by preventing substrate binding. By altering the dimer-formation site in SCIN, we have shown that a monomeric SCIN-convertase is still an inhibited and stable complex. Thus, even if dimers cannot form on a bacterial surface, SCIN will block the C3bBb enzyme directly. Because we found a strong correlation between enzyme stability and inhibition by SCIN, we believe that SCIN prevents the swinging of Bb by fixing Bb on C3b. The dimeric nature of the convertase will contribute to complex stability and steric hindrance of the interactions of complement receptors with the stabilized convertase on the surface of the bacterium.

Although we can mimic these processes with purified components in solution, complement activation normally occurs on surfaces like those of bacteria. SCIN is a secreted bacterial molecule and has been shown to bind back to the surface as soon as active convertases are formed[13]. The secreted versus membrane-bound character of SCIN is critical in allowing this small molecule to fit in the narrow pocket of convertase components and to bind quickly to randomly distributed convertases at the bacterial surface. The similar activity of SCIN mutants on surface-bound and

fluid-phase convertases suggests that the soluble complex is indeed representative of a surface-bound convertase. SCIN is an immunogenic bacterial protein and therefore is not suitable as an anti-inflammatory drug for humans. Nevertheless, the structure of the SCIN convertase provides insight into a unique and effective convertase-modulation strategy that evolved in a bacterial pathogen.

In summary, our data have provided insights into the molecular mechanisms that underlie the central, amplification step of the complement system that leads to the opsonization of pathogens and altered host cells. These insights are essential for understanding the regulatory mechanisms of complement activation and the wide range of evasion strategies that can be used by pathogenic microorganisms. Both the structure and understanding of the convertase-inhibitory strategy provide crucial insights for the future development of complement inhibitors.

METHODS

Protein expression and purification. C3 was purified from freshly isolated human plasma and C3b was generated as described[39]. After informed consent was provided by the donor, plasma was obtained at the University Medical Center Utrecht according to a study protocol approved by the medical ethics committee of the University Medical Center Utrecht. The preparation of recombinant SCIN and chimeric mutants has been described[14]. SCIN protein with an N-terminal six-histidine tag was prepared by overlap-extension PCR. In the ChC3b2 mutant, residues 1–13, 59–61, 64–65 and 67–68 were exchanged with corresponding residues of ORF-D. Plasma-purified FB and commercially obtained FD (Calbiochem) were used for Biacore, gel-filtration and small-scale experiments. For large-scale experiments in crystallization trials, recombinant FB and FD were used. Human FB fused to a N-terminal histidine tag containing a tobacco-etch virus protease cleavage site was expressed in human embryonic kidney 293S GnTI$^-$ (HEK293ES) cells to allow homogeneous N-linked glycosylation[40]. FB was purified by metal-affinity chromatography as described[25] and the histidine tag was removed by TEV protease cleavage and a second column passage on Ni-NTA Superflow beads (Qiagen). Finally, FB was purified by size-exclusion chromatography. Human FD was expressed without a tag in HEK293-EBNA cells (HEK293 cells that express Epstein-Bar virus nuclear antigen). Secreted FD was purified by cation-exchange and size-exclusion chromatography. Ba with a six-histidine tag at the N terminus was recombinantly expressed in a pQE30-M15 *Escherichia coli* expression system (Qiagen) and was purified from the inclusion bodies with a Ni-NTA Superflow column. After refolding, it was subjected to anion-exchange chromatography on a MonoQ1010 column.

Binding convertase to immobilized SCIN. CM5 sensor chips were immobilized with SCIN (2,526 resonance units) or CHIPS (3,372 resonance units; negative control)[41] by standard amine-coupling chemistry in 10 mM

sodium acetate, pH 5. Purified C3b, FB and FD were passed over the surface at a flow rate of 30 µl/min in HEPES-buffered saline (HBS)-Mg (20 mM HEPES, 140 mM NaCl, 5 mM $MgCl_2$ and 0.05% (vol/vol) Tween, pH 7.4); association and dissociation were both monitored for 300 s. Surfaces were regenerated with 0.1 M citric acid, 1 M NaCl and 1 mM EDTA, pH 5. Immobilization and binding experiments were done at 25 °C with a Biacore 2000.

Gel filtration and native gel electrophoresis. C3b (2 µM), FB (2 µM) and FD (1 µM, Calbiochem) were incubated for 1 h at 4 °C in the presence of SCIN (4 µM) or $NiCl_2$ (2.5 mM) in HBS-Mg and were separated on a Superdex-200 GL 10-mm × 300-mm column equilibrated with ice-cold HBS-Mg. The column was calibrated with the HMW Calibration kit (GE Healthcare) containing thyroglobulin (669 kDa), ferritin (440 kDa), aldolase (158 kDa), conalbumin (75 kDa) and ovalbumin (43 kDa). Alternatively, complexes were separated by native gel electrophoresis (7.5 %) at 4 °C and were visualized by silver staining. C3 and FB were detected by immunoblot analysis[13]. SCIN was detected by enzyme-linked immunosorbent assay with mouse antibody to SCIN (anti-SCIN; 1C9) as a capturing antibody and biotinylated mouse anti-SCIN (2F4) for detection (both prepared 'in house')[13]; binding was visualized with peroxidase-conjugated streptavidin and tetramethyl benzidine substrate.

Purification of SCIN-inhibited convertases for crystallization. C3b (0.5 µM), recombinant FB (1 µM), recombinant FD (0.5 µM) and histidine-tagged SCIN (2 µM) were incubated for 1 h at 4 °C in 20 ml HBS-Mg. SCIN complexes were purified by incubation for 1 h at 4 °C with 1.2 g magnetic cobalt beads (Dynabeads Talon, Invitrogen). Beads were washed with HBS-Mg and complexes were eluted with 500 mM imidazole in 10 mM Tris, 40 mM NaCl and 5 mM $MgCl_2$, pH 8 (2 ml). For removal of SCIN not in complex, complexes were washed with 200 ml buffer in a 100-kDa filter centricon device (Millipore); in a final centrifugation step, complexes were concentrated to ~5 mg/ml of purified complexes.

Analytical ultracentrifugation. A purified sample of the 500 kDa complex consisting of C3b, Bb and SCIN in 10 mM Tris pH 8.0, 40 mM NaCl and 0.05% (vol/vol) Tween was used for a sedimentation-velocity experiment in an Optima XL-A analytical ultracentrifuge (Beckman Coulter). The sample, contained in a standard 12-mm Epon charcoal-filled centerpiece with quartz windows, was diluted to obtain an absorbance of ~0.9 against a 'demi-water' reference, through a 12-mm path length at 229 nm for optimization of the signal/noise ratio. The sedimentation velocity run was done at 116,400g (An-50 Ti rotor) and 9.0°C ± 0.3 °C during 2.5 h in which 140 scans were recorded at a radial step size of 30 µm (data available at the UltraScan Van `t Hoff Laboratory Information Management System database as ExpDataID 74). A relative low angular velocity was chosen to retain sufficient shape information based on diffusion. Sedimentation velocity data were analyzed by enhanced van Holde-Weischet analysis[42] (UltraScan[43]) after subtraction of the time-invariant noise, which was determined in a two-dimensional spectrum analysis[44] (UltraScan). Sedimentation coefficients predicted from theory were calculated for the subunits with the assumption that they were spherical, prolate ellipsoidal and oblate ellipsoidal, and with buffer density and viscosity, as well as partial specific volumes calculated from the amino acid sequences (UltraScan[43]), accounted for (**Supplementary Fig. 4d**). For the last two shapes, an arbitrary axial or

aspect ratio of 6 was taken. On the basis of sedimentation-velocity simulations (UltraScan), the dimeric complex $(C3bBb\text{-}SCIN)_2$ has a predicted sedimentation coefficient between 10 S and 20 S ($1\ S \equiv 1\times10^{-13}$ s).

Crystallization, data collection and structure determination. Freshly purified SCIN-stabilized complexes were set up for crystallization trials by hanging-drop vapor diffusion at 4 °C. Crystals appeared overnight and grew within 2 weeks to a typical size of 300×100×40 μm^3 in many conditions. Over 100 crystals were screened at European Synchrotron Radiation Facility beamline (ID14-EH14). Most crystals diffracted between 4 Å and 5 Å, only one crystal diffracted at a resolution of better than 4 Å. A complete data set was collected from this crystal, which diffracted to resolution of 3.9 Å. This crystal was grown in the condition of 75 mM sodium-potassium tartrate, 8.0% (wt/vol) PEG 3350 and 50 mM Bis-Tris propane, pH 6.5. The crystal was in space group $P2_1$ (a = 228.6 Å, b = 121.5 Å, c = 280.8 Å, α = 90°, β = 91.6°, and γ = 90°). The data set was integrated and scaled with the programs MOSFLM and Scala[45]. The asymmetric unit contained four C3bBb-SCIN complexes arranged as two dimers. The structure was solved by molecular replacement with the PHASER program[46] with the isolated structures of C3c (2A74)[32], C3b (2I07)[15], Bb (1RRK)[24] and SCIN (2QFF)[14] as the initial search models (Protein Data Bank accession codes in parentheses). The automatic searches for the CUB, TED and C345C domains of C3b and SCIN in PHASER yielded only two copies of each domain or protein. The missing parts were placed manually by superposition and were adjusted by rigid-body refinement in PHASER to obtain a complete model. One C3b molecule lacked density for its TED because of disorder; occupancies were set to 0.0 for this domain. The C3b molecule in this copy (copy 4) had a weaker density than C3b in other copies (**Supplementary Fig. 6**). The model was rebuilt with the Crystallographic Object-Oriented Toolkit system[47], and refinement was done with PHENIX software[48]. Tight fourfold noncrystallographic symmetry restraints were used for the following domains or molecules: MG1, MG2, MG3, MG4, MG5, MG6, linker, α' N-terminal tail and MG7, MG8, CUB of C3b; VWA and SP of Bb and SCIN. Tight threefold noncrystallographic symmetry restraints were used for TEDs in copies of 1-3. Twofold noncrystallographic symmetry restraints were used for C345C domains (copies of 1 and 3 as a group and copies of 2 and 4 as a group). The final R_{work} and R_{free} values were 25.3% and 26.8%, respectively.

Convertase inhibition assays. C3 (250 nM), C3b (50 nM), FB (500 nM), FD (500 nM) and SCIN chimeras (2 μM) were incubated for 10 min at 20 °C in HBS-Mg, and C3 conversion was analyzed by SDS-PAGE in reducing conditions. Convertase stabilization on bacteria was done as described[14]. HBS-Mg-EGTA instead of HBS-Mg^{2+}-Ca^{2+} was used for induction of only the alternative pathway.

Kinetic analysis of FB and Ba interaction with C3b. Kinetics were profiled by surface plasmon resonance (Biacore 2000) at 25 °C. C3b was biotinylated at its thioester moiety and captured on a streptavidin-coated sensor chip. FB (63 nM - 2 μM) was injected for 3 min at a flow rate of 30 μl/min and dissociation was monitored for 5 min. The surface was regenerated with 2 M NaCl and 0.2 M sodium carbonate pH 9.0 for 30 s each. Fragment Ba (40 nM - 40 μM) was injected for 1 min at a flow rate of 30 μl/min with a dissociation phase of 2 min and a short regeneration pulse (20 s) of 1 M NaCl. All binding experiments were repeated in running buffer (10 mM HEPES,

pH 7.4, 150 nM NaCl and 0.005% (vol/vol) Tween-20) containing either 1 mM $MgCl_2$ or 3 mM EDTA. Signals from an untreated streptavidin surface and an ensemble of buffer blank injections were subtracted from the binding signals. Data were processed with Scrubber (BioLogic Software), and CLAMP software[49] was used for kinetic analysis.

Accession code. Protein Data Bank: Coordinates and structure factors, 2WIN.

Table 1 Data collection and refinement statistics.

	3.9-Å
Data collection	
Space group	$P2_1$
Cell dimensions	
a, *b*, *c* (Å)	228.6, 121.5, 280.8
α, β, γ (°)	90, 91.6, 90
Resolution (Å)	40-3.9 (4.11-3.9)*
R_{merge} (%)	12.8 (69.0)
$I/\sigma I$	10.4 (1.8)
Completeness (%)	97.6 (92.0)
Redundancy	3.5 (3.4)
Refinement	
Resolution (Å)	39.8-3.9
No. reflections	137476
R_{work} / R_{free} (%)	25.3 / 26.8
No. atoms	679989
Protein	67266
Ligand/ion	723
Water	
B-factors (Å^2)	
Protein	158
Ligand/ion	208
Water	
R.m.s deviations	
Bond lengths (Å)	0.002
Bond angles (°)	0.519

Table 2 Analysis of the interfaces between molecules in complexes.

Interface		Buried area (Å)
C3b1	C3b2	2832
C3b3	C3b4	1860
C3b3	Bb3	1215
C3b1	Bb1	1174
C3b2	Bb2	622
C3b4	Bb4	636
C3b3	SCIN3	1457
C3b1	SCIN1	1441
C3b2	SCIN2	1406
C3b4	SCIN4	1404
Bb3	SCIN3	1423
Bb2	SCIN2	1412
Bb1	SCIN1	1401
Bb4	SCIN4	1394
C3b4	SCIN3	1817
C3b3	SCIN4	1813
C3b1	SCIN2	1800
C3b2	SCIN1	1800

ACKNOWLEDGMENTS

We thank R. Romijn for help with mammalian protein expression; M. Otten and M. Daha for doing hemolytic assays; P. Lenting for help with Biacore analyses; the European Synchrotron Radiation Facility for synchrotron radiation facilities; and beamline scientists of the European Synchrotron Radiation Facility and the European Molecular Biology Laboratory for assistance. Supported by the Councils for Medical Sciences and Chemical Sciences of the Netherlands Organization for Scientific Research (S.H.M.R.,J.A.G.v.S. and P.G.) and the US National Institutes of Health (J.D.L. and P.G.).

REFERENCES

1. Carroll, M.C. The complement system in regulation of adaptive immunity. *Nat Immunol* **5**, 981-986 (2004).
2. Mollnes, T.E., Song, W.C. & Lambris, J.D. Complement in inflammatory tissue damage and disease. *Trends Immunol* **23**, 61-64 (2002).
3. Duncan, R.C., Wijeyewickrema, L.C. & Pike, R.N. The initiating proteases of the complement system: controlling the cleavage. *Biochimie* **90**, 387-395 (2008).
4. Law, S.K. & Dodds, A.W. The internal thioester and the covalent binding properties of the complement proteins C3 and C4. *Protein Sci* **6**, 263-274 (1997).
5. Gros, P., Milder, F.J. & Janssen, B.J. Complement driven by conformational changes. *Nat Rev Immunol* **8**, 48-58 (2008).
6. Kerr, M.A. The human complement system: assembly of the classical pathway C3 convertase. *Biochem J* **189**, 173-181 (1980).
7. Rawal, N. & Pangburn, M.K. C5 convertase of the alternative pathway of complement. Kinetic analysis of the free and surface-bound forms of the enzyme. *J Biol Chem* **273**, 16828-16835 (1998).
8. Kinoshita, T. *et al.* C5 convertase of the alternative complement pathway: covalent linkage between two C3b molecules within the trimolecular complex enzyme. *J Immunol* **141**, 3895-3901 (1988).
9. Rawal, N. & Pangburn, M.K. Structure/function of C5 convertases of complement. *Int Immunopharmacol* **1**, 415-422 (2001).
10. Kirkitadze, M.D. & Barlow, P.N. Structure and flexibility of the multiple domain proteins that regulate complement activation. *Immunol Rev* **180**, 146-161 (2001).
11. Pangburn, M.K. & Muller-Eberhard, H.J. The C3 convertase of the alternative pathway of human complement. Enzymic properties of the bimolecular proteinase. *Biochem J* **235**, 723-730 (1986).
12. Lambris, J.D., Ricklin, D. & Geisbrecht, B.V. Complement evasion by human pathogens. *Nat Rev Microbiol* **6**, 132-142 (2008).
13. Rooijakkers, S.H. *et al.* Immune evasion by a staphylococcal complement inhibitor that acts on C3 convertases. *Nat Immunol* **6**, 920-927 (2005).
14. Rooijakkers, S.H. *et al.* Staphylococcal complement inhibitor: structure and active sites. *J Immunol* **179**, 2989-2998 (2007).
15. Janssen, B.J., Christodoulidou, A., McCarthy, A., Lambris, J.D. & Gros, P. Structure of C3b reveals conformational changes that underlie complement activity. *Nature* **444**, 213-216 (2006).
16. Wiesmann, C. *et al.* Structure of C3b in complex with CRIg gives insights into regulation of complement activation. *Nature* **444**, 217-220 (2006).
17. Torreira, E., Tortajada, A., Montes, T., de Córdoba, S.R. & Llorca, O. 3D structure of the C3bB complex provides insights into the activation and regulation of the complement alternative pathway convertase. *Proceedings of the National Academy of Sciences* **106**, 882-887 (2009).

18. Muller-Eberhard, H.J. & Gotze, O. C3 proactivator convertase and its mode of action. *J Exp Med* **135**, 1003-1008 (1972).
19. Fishelson, Z., Pangburn, M.K. & Muller-Eberhard, H.J. C3 convertase of the alternative complement pathway. Demonstration of an active, stable C3b, Bb (Ni) complex. *J Biol Chem* **258**, 7411-7415 (1983).
20. Horiuchi, T., Macon, K.J., Engler, J.A. & Volanakis, J.E. Site-directed mutagenesis of the region around Cys-241 of complement component C2. Evidence for a C4b binding site. *J Immunol* **147**, 584-589 (1991).
21. Hourcade, D.E., Mitchell, L.M. & Oglesby, T.J. Mutations of the type A domain of complement factor B that promote high-affinity C3b-binding. *J Immunol* **162**, 2906-2911 (1999).
22. Tuckwell, D.S., Xu, Y., Newham, P., Humphries, M.J. & Volanakis, J.E. Surface Loops Adjacent to the Cation-Binding Site of the Complement Factor B von Willebrand Factor Type A Module Determine C3b Binding Specificity. *Biochemistry* **36**, 6605-6613 (1997).
23. Hourcade, D.E., Mitchell, L., Kuttner-Kondo, L.A., Atkinson, J.P. & Medof, M.E. Decay-accelerating factor (DAF), complement receptor 1 (CR1), and factor H dissociate the complement AP C3 convertase (C3bBb) via sites on the type A domain of Bb. *J Biol Chem* **277**, 1107-1112 (2002).
24. Ponnuraj, K. *et al.* Structural analysis of engineered Bb fragment of complement factor B: insights into the activation mechanism of the alternative pathway C3-convertase. *Molecular cell* **14**, 17-28 (2004).
25. Milder, F.J. *et al.* Factor B structure provides insights into activation of the central protease of the complement system. *Nat Struct Mol Biol* **14**, 224-228 (2007).
26. Milder, F.J. *et al.* Structure of complement component C2A: implications for convertase formation and substrate binding. *Structure* **14**, 1587-1597 (2006).
27. Luo, B.H., Carman, C.V. & Springer, T.A. Structural basis of integrin regulation and signaling. *Annu Rev Immunol* **25**, 619-647 (2007).
28. Krishnan, V., Xu, Y., Macon, K., Volanakis, J.E. & Narayana, S.V. The crystal structure of C2a, the catalytic fragment of classical pathway C3 and C5 convertase of human complement. *J Mol Biol* **367**, 224-233 (2007).
29. Kam, C.M. *et al.* Human complement proteins D, C2, and B. Active site mapping with peptide thioester substrates. *J Biol Chem* **262**, 3444-3451 (1987).
30. Janssen, B.J., Halff, E.F., Lambris, J.D. & Gros, P. Structure of compstatin in complex with complement component C3c reveals a new mechanism of complement inhibition. *J Biol Chem* **282**, 29241-29247 (2007).
31. Katschke, K.J., Jr. *et al.* Structural and Functional Analysis of a C3b-specific Antibody That Selectively Inhibits the Alternative Pathway of Complement. *J Biol Chem* **284**, 10473-10479 (2009).
32. Janssen, B.J. *et al.* Structures of complement component C3 provide insights into the function and evolution of immunity. *Nature* **437**, 505-511 (2005).
33. Fredslund, F. *et al.* Structure of and influence of a tick complement inhibitor on human complement component 5. *Nat Immunol* **9**, 753-760 (2008).

34. Rawal, N. & Pangburn, M. Formation of high-affinity C5 convertases of the alternative pathway of complement. *J Immunol* **166**, 2635-2642 (2001).

35. Hourcade, D.E., Mitchell, L.M. & Medof, M.E. Decay acceleration of the complement alternative pathway C3 convertase. *Immunopharmacology* **42**, 167-173 (1999).

36. Bhattacharya, A.A., Lupher, M.L., Jr., Staunton, D.E. & Liddington, R.C. Crystal structure of the A domain from complement factor B reveals an integrin-like open conformation. *Structure* **12**, 371-378 (2004).

37. Harris, C.L., Abbott, R.J., Smith, R.A., Morgan, B.P. & Lea, S.M. Molecular dissection of interactions between components of the alternative pathway of complement and decay accelerating factor (CD55). *The Journal of biological chemistry* **280**, 2569-2578 (2005).

38. Pryzdial, E.L. & Isenman, D.E. Alternative complement pathway activation fragment Ba binds to C3b. Evidence that formation of the factor B-C3b complex involves two discrete points of contact. *J Biol Chem* **262**, 1519-1525 (1987).

39. Lambris, J.D., Dobson, N.J. & Ross, G.D. Release of endogenous C3b inactivator from lymphocytes in response to triggering membrane receptors for beta 1H globulin. *J. Exp. Med.* **152**, 1625-1644 (1980).

40. Reeves, P.J., Callewaert, N., Contreras, R. & Khorana, H.G. Structure and function in rhodopsin: high-level expression of rhodopsin with restricted and homogeneous N-glycosylation by a tetracycline-inducible N-acetylglucosaminyltransferase I-negative HEK293S stable mammalian cell line. *Proc Natl Acad Sci USA* **99**, 13419-13424 (2002).

41. de Haas, C.J. *et al.* Chemotaxis inhibitory protein of Staphylococcus aureus, a bacterial antiinflammatory agent. *The Journal of experimental medicine* **199**, 687-695 (2004).

42. Demeler, B. & van Holde, K.E. Sedimentation Velocity Analysis of Highly Heterogeneous Systems. *Analytical Biochemistry* **335**, 279-288 (2004).

43. Demeler, B. in *Analytical Ultracentrifugation: Techniques and Methods*. (eds. D.J. Scott, S.E. Harding & A.J. Rowe) 210-230 (Royal Society of Chemistry, Cambridge; 2005).

44. Brookes, E. & Demeler, B. Parallel Computational Techniques for the Analysis of Sedimentation Velocity Experiments in UltraScan. *Colloid and Polymer Science* **286**, 139-148 (2008).

45. Evans, P. Scaling and assessment of data quality. *Acta Crystallographica Section D* **62**, 72-82 (2006).

46. McCoy, A.J. *et al.* Phaser crystallographic software. *Journal of Applied Crystallography* **40**, 658-674 (2007).

47. Emsley, P. & Cowtan, K. Coot: model-building tools for molecular graphics. *Acta Crystallogr D Biol Crystallogr* **60**, 2126-2132 (2004).

48. Adams, P.D. *et al.* PHENIX: building new software for automated crystallographic structure determination. *Acta Crystallogr D Biol Crystallogr* **58**, 1948-1954 (2002).

49. Myszka, D.G. & Morton, T.A. CLAMP: a biosensor kinetic data analysis program. *Trends Biochem Sci* **23**, 149-150 (1998).

Chapter 3

Structure of C3b-factor H and implications for host protection by complement regulators

Jin Wu[1], You-Qiang Wu[2], Daniel Ricklin[2], Bert J.C. Janssen[1], John D. Lambris[2] and Piet Gros[1]

1 Crystal and Structural Chemistry, Bijvoet Center for Biomolecular Research, Department of Chemistry, Faculty of Science, Utrecht University, Padualaan 8, 3584 CH Utrecht, The Netherlands.
2 Department of Pathology & Laboratory Medicine, University of Pennsylvania, 401 Stellar Chance, Philadelphia, PA 19104, USA.

Nature Immunology, **10**, 728-733 (2009)

ABSTRACT

Factor H (FH) is an abundant regulator of complement activation and protects host cells from self-attack by complement. Here we provide insight into the regulatory activity of FH by solving the crystal structure of the first four domains of FH in complex with its target, complement fragment C3b. FH interacted with multiple domains of C3b, covering a large, extended surface area. The structure indicated that FH destabilizes the C3 convertase by competition and electrostatic repulsion and that FH enables proteolytic degradation of C3b by providing a binding platform for protease factor I while stabilizing the overall domain arrangement of C3b. Our results offer general models for complement regulation and provide structural explanations for disease-related mutations in the genes encoding both FH and C3b.

INTRODUCTION

The efficacy of the complement-mediated immune response relies on a delicate balance between activation and regulation. Although continuous generation of the strong opsonin complement fragment C3b by the alternative pathway allows rapid reaction to foreign or abnormal cells, its indiscriminate deposition may potentially cause host tissue damage. Host cells are therefore protected by proteins of the regulator of complement activation (RCA) family, which either impair the generation of new C3b by accelerating the decay of the C3 convertases or act as cofactor for factor I (FI) in degrading existing C3b[1, 2]. In addition to cell surface–bound RCA proteins such as decay accelerating factor (DAF; also called CD55), membrane cofactor protein (MCP; also called CD46) and complement receptor 1 (CR1; also called CD35), the soluble and highly abundant regulator factor H (FH) offers an additional layer of protection, as it controls the steady-state alternative pathway activation in circulation. Furthermore, FH may be recruited to host membranes by recognizing and binding self components, such as glycosaminoglycans, and thereby may prevent the opsonization of host tissue with low surface expression of RCA[1,3].

The importance of FH in maintaining a well-balanced immune response is reflected by the increasing number of diseases found to have strong association with mutations and polymorphisms in the gene encoding FH, as found in age-related macular degeneration (AMD), atypical hemolytic uremic syndrome (aHUS) and membranoproliferative glomerulonephritis type II (MPGN-II)[4,5]. Several pathogenic microorganisms evade attack of the complement cascade by expressing

structural homologs of FH or by recruiting host FH to their surfaces via FH-binding proteins[6,7]. Owing to their vital function in immune modulation, therapeutic targeting of FH as well as other RCA proteins is considered important for the treatment of diseases associated with abnormal or loss of complement control[8,9].

FH is formed by a linear string of complement control protein (CCP) domains that consist of about 60 residues and are common to all RCA proteins[1]. The first four domains (CCP1–CCP4) of FH are necessary and sufficient for regulation of complement in the fluid phase, whereas host cell specificity is determined by domains CCP5– CCP20 of FH[1,10,11]. Despite a wealth of functional and structural data on the CCP domains of various complement regulators, understanding of the two molecular mechanisms that protect host cells, referred to as 'decay-acceleration activity' and 'cofactor activity', still remains limited.

Here we provide insight into the mechanisms of host protection against complement activation by presenting the crystal structure of the four functional domains of FH (CCP1–CCP4) in complex with C3b. By combining our structural model with biochemical and biophysical data as well as with findings from previous mutational studies, we are able to delineate individual processes and correlate disease-related mutations with functional consequences. Furthermore, our findings allow us to extrapolate these results to other members of the RCA family and to develop a more general model for complement regulation.

RESULTS

Crystal structure of C3b–in complex with FH domains 1–4

For this study, we expressed the amino (N)-terminal four CCP domains (amino acid residues 1–246) of FH (called 'FH(1–4)' here), which are known to mediate both of the regulatory activities of FH[10] (**Fig. 1a**). This recombinant FH(1–4) bound C3b with an affinity of 11 μM (measured as the dissociation constant; Fig. 1b,c) and was functionally active *in vitro* in terms of both decay-acceleration and cofactor activity (**Fig. 1d,e**). We crystallized the complex of C3b-FH(1–4) and determined the structure to a resolution of 2.7 Å (**Fig. 2** and **Table 1**). The structure showed a large and discontinuous interface between FH(1–4) and C3b that stretched over a distance of 100 Å and buried a surface area of about 4,500 Å 2 (**Fig. 2a**). Despite the putative flexibility between individual CCP domains of FH, FH(1–4) bound to C3b showed only small differences in domain

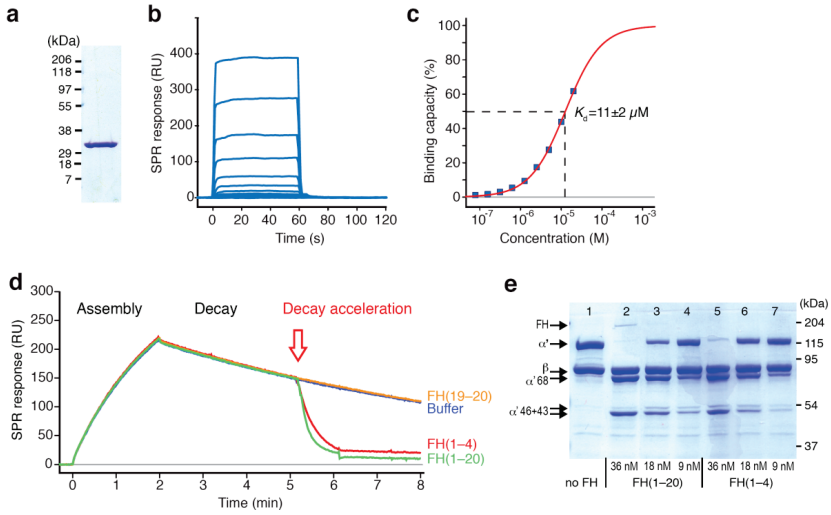

Figure 1 Characterization of recombinant FH(1–4). (**a**) Purity of FH(1–4), as assessed by SDS-PAGE (4–15% gradient gel; reducing conditions; Coomassie blue staining). Data are representative of more than five experiments with various conditions. (**b,c**) Direct binding of soluble FH(1–4) to surface-bound C3b. Injection of the FH fragment (0.08–20 μM) leads to the formation of a short-lived 1:1 complex with C3b (**b**) with a binding affinity (dissociation constant (K_d)) of 11 ± 2 μM (**c**). SPR, surface plasmon resonance. Data are representative of five experiments with different surface densities of C3b (3,000–7,000 resonance units (RU)). (**d**) Decay-acceleration activity of FH(1–4) and full-length FH (FH(1–20)) when injected onto surface-based C3 convertase (C3bBb); (additional details and control injections, **Supplementary Fig. 9**). Data are representative of three independent experiments. (**e**) Cofactor activity of FH(1–4) and FH, assessed by incubation of C3b with FI and increasing amounts of either FH(1–4) or FH(1–20), leading to the generation of iC3b, as indicated by degradation of the α' chain to three fragments of 43, 46 and 68 kDa (α' 43, α' 46 and α' 68, respectively; left margin). Data are representative of more than five individual experiments.

orientations compared with the nuclear magnetic resonance (NMR) structures of CCP1–CCP2 and CCP2–CCP3 (ref. 12). The tilt angle between CCP1 and CCP2 was altered by about 10°, which led to closer proximity of CCP1 to C3b (**Fig. 2b** and **Table 2**). There was a kink between CCP3 and CCP4 that was responsible for the overall L-shaped appearance of FH(1–4), which is consistent with small-angle X-ray-scattering data of CCP1–CCP5 of FH[13]. The structure of C3b showed its typical arrangement of 12 domains formed by the β chain (amino acid residues 1–645) and the α' chain (amino acid residues 727–1641)[14,15,] obtained after proteolytic activation of the native C3 (Fig. 2). The core of the structure was formed by eight macroglobulin (MG) domains and a linker domain. Inserted between MG7 and MG8 were a CUB domain ('complement C1r-C1s, UEGF,

BMP1') and a thioester-containing domain (TED), which allows covalent attachment to target surfaces. The carboxyl (C) terminus was extended by a C345C domain, which is common to complement components C3, C4 and C5. We found two differences in domain orientations in C3b-FH(1–4) versus unbound C3b: the C-terminal C345C domain was repositioned, which we attributed to differences in crystal packing, and the CUB domain and TED were rotated by about 12° (refs. 14,15; **Fig. 2b** and **Supplementary Figs. 1** and **2**). The change in CUB and TED was probably due to interactions with FH(1–4); however, variations in CUB-TED positioning have been reported for other structures of C3b[14,15] (**Fig. 2b** and **Supplementary Fig. 1**).

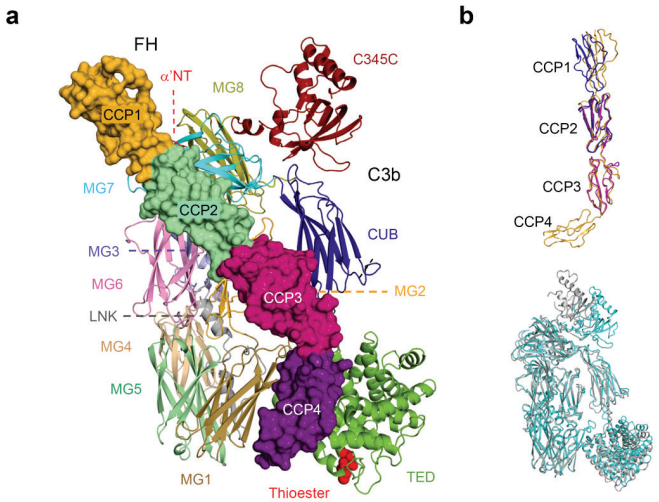

Figure 2 Structure of C3b in complex with FH(1–4). (**a**) Overall structure of the C3b-FH(1–4) complex. C3b is presented as a 'ribbon' and FH is presented as surface representations; red spheres indicate thioesters. (**b**) Top, FH(1–4) in complex (orange) with NMR structures of CCP1–CCP2 (blue) and CCP2–CCP3 (magenta)[12]; bottom, C3b in complex with FH(1–4) (cyan) and free C3b (gray)[14]. Diagrams were generated with the PyMOL molecular visualization system.

The C3b-FH(1–4) interface consisted of four contact regions spanning the length of FH(1–4) (**Fig. 3** and **Table 3**). The bottom half of CCP1 and the CCP1–CCP2 linker attached through hydrophobic interactions and salt bridges to the acidic α' N-terminal (α' NT) region (amino acid residues 727–746) and the MG7 domain in C3b. Antibody binding to MG7–MG8 inhibited the interaction of C3b with both FH(1–4) and full-length FH[16] (**Supplementary Fig. 3**), which confirms that the α' NT and MG7 region is a primary binding site for FH[17,18]. The second main binding site involved a patch of conserved hydrophobic residues surrounded by hydrophilic residues on CCP2 that interacted with MG6 of C3b (**Fig. 2a** and **Supplementary Figs. 4** and **5**). At

the third site, CCP3 contacted residues of both the α'-chain and β-chain of C3b and bridged MG2 and CUB, which contains the three scissile bonds that are cleaved by FI. Notably, the hypervariable loop of CCP3 of FH (amino acid residues 139–145) that was disordered in the published NMR structure[12] was ordered in the C3b-FH(1–4) complex and interacted with the CUB domain of C3b. At the fourth and final site, CCP4 formed another bridge between MG1 and TED, which we confirmed by blocking experiments with a TED-specific antibody (**Supplementary Fig. 3**). The arrangement of the α' NT, MG7, CUB and TED domains are known to change considerably during the conversion of C3 to C3b[14,15,19,20], which explains the specificity of FH for C3b rather than C3. In summary, the complex showed an extensive interface that involved many domains of C3b and all domains of FH(1–4), a result that is supported by the binding studies reported here (**Fig. 1b,c** and **Supplementary Fig. 4**) and in published reports[16–18].

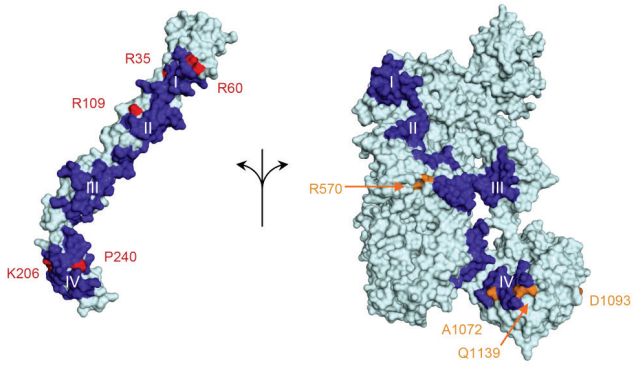

Figure 3 Mapping of FH and C3 mutants on the complex structure. Molecules are presented in surface representation with FH(1–4) on the left and C3b on the right. The four contact regions (I–IV) between FH(1–4) and C3b are in blue, with substitutions linked to AMD, MPGN-II and aHUS in red (for FH mutants) or orange (for C3b mutants).

Structural basis of decay-acceleration activity

The ability of FH(1–4) to dissociate the protease fragment (Bb) from the alternative pathway C3 convertase complex (C3b–Bb; **Fig. 1d**) suggested competition for the same binding region on C3b. We therefore compared the structure of C3b-FH(1–4) with that of the convertase stabilized by the staphylococcal inhibitor SCIN[21] (**Fig. 4a**) by superimposing the β-chains of the C3b molecules of both complexes. The superposition showed a large steric clash between CCP1– CCP2 of FH(1–4) and the Bb fragment of the convertase. The N-linked glycan at the asparagine residue at position

260 (Asn260) in Bb contributed to the observed clash (**Supplementary Fig. 6**). In agreement with that finding, deletion of this glycan by the substitution N260D renders the convertase less sensitive to decay-acceleration[22]. In addition to steric hindrance, the complementary surfaces of FH and Bb were both negatively charged (**Fig. 4b**), which indicates that electrostatic repulsion contributed to the destabilization of the C3bBb complex. These results indicate a functional role for CCP1–CCP2 in displacing Bb and a supportive role for CCP3–CCP4 in binding to C3b.

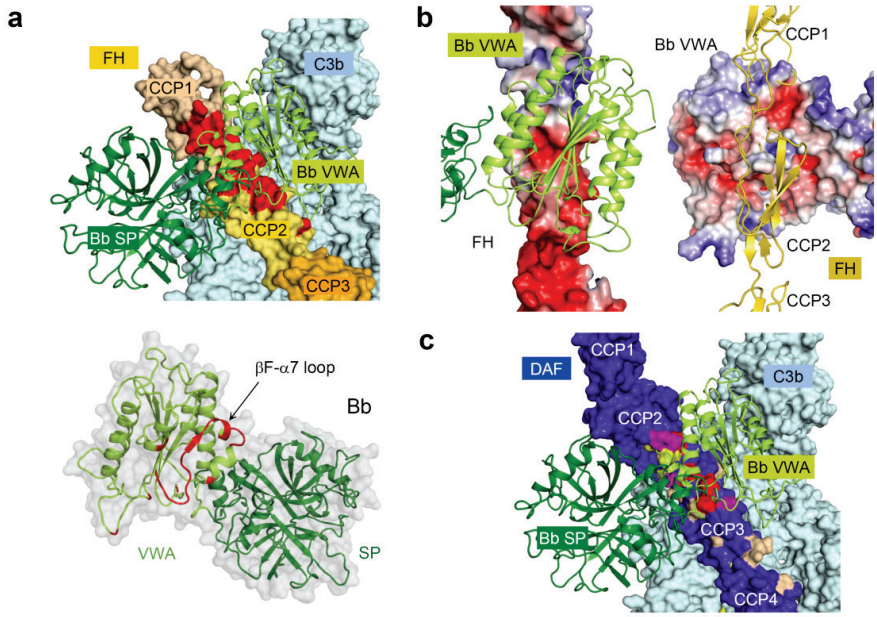

Figure 4 Structural basis of decay-acceleration activity. (**a**) Overlay of the C3b-FH and C3bBb complexes[21] (top) with C3b (light cyan) and CCP1–CCP3 of FH (beige, yellow-orange and orange, respectively) in surface representation and Bb in ribbon representation (light green, VWA domain; dark green, serine protease (SP) domain); the red surface area indicates the region where FH and Bb overlap (atomic distances of less than 2 Å). Below, overlap region (red) in Bb (Bb is rotated by 180° relative to the diagram above). (**b**) Electrostatic surface potential of FH and ribbon representation of Bb (left) and vice versa (right) in the regions facing each other. Potential contours are presented on a scale from $-5\ k_BTe_c^{-1}$ (red) to $+5\ k_BTe_c^{-1}$ (blue), where k_B is the Boltzmann constant, T is absolute temperature and e_c is elementary charge. (**c**) Superposition of CCP2–CCP4 of DAF[23] onto CCP1–CCP3 of FH, presented as in a. Colors of DAF substitutions indicate the degree of functional interference, from minor (beige), medium (yellow) and severe (magenta) to complete abortion (red) of decay-acceleration by DAF[24].

To propose a general model of decay-acceleration, we compared our data with the structure and

mutagenesis data of DAF[23,24]. Overlay of the functional CCP2–CCP3 domains of DAF onto CCP1–CCP2 of FH showed that DAF had similar residues at the C3b contact sites (**Supplementary Fig. 5**). Moreover, residues critical for DAF activity, which are located in the CCP2–CCP3 linker and on the CCP3 surface, faced Bb in the C3bBb complex[24] (**Fig. 4c**). Similar to the binding of FH, the proposed binding mode of DAF resulted in steric overlap with Bb. However, the critical residues on DAF facing Bb in the C3bBb complex were mainly hydrophobic and not negatively charged, as in the case of FH (**Fig. 4b,c** and **Supplementary Fig. 5**). The hydrophobic patch on DAF faced the βF-α7 loop of the von Willebrand factor A (VWA) domain in Bb (**Fig. 4a,c**). This section of the VWA domain was hidden in the proenzyme FB, which possibly explains why DAF binds Bb but hardly binds full-length FB[25]. Interaction of DAF with this loop may induce a low affinity state of the metal ion–dependent adhesion site in Bb and thereby disrupt the C3bBb complex, similar to the allostery in integrin I domains[26]. However, the structural observations do not readily explain the effects of substitutions at Lys298 and Tyr338 in FB on the decay-acceleration activity of DAF, CR1 and FH[22,27]. It is possible that these substitutions in the VWA domain, distal from the RCA-interaction side, may affect the allosteric mechanism.

Implications for cofactor activity

FH supported two of three possible cleavages in the CUB domain of C3b by FI (between Arg1281 and Ser1282 and between Arg1298 and Ser1299) that yield the inactive iC3b species[28] (**Fig. 1e**). The crystal structure showed that CCP2–CCP3 of FH bound to C3b adjacent to the CUB domain (**Figs. 2a** and **5a**), with the hypervariable loop of CCP3 directly contacting the CUB domain[10] (**Fig. 5**). Cleavage site Arg1281-Ser1282 was well exposed, whereas Arg1298-Ser1299 was occluded in the complex (**Fig. 5b**), which confirms the idea that Arg1281-Ser1282 is cleaved first and suggests that cleavage of Arg1298-Ser1299 requires conformational changes. The strong influence of ionicity on the binding of FI indicates that polar interactions are important for this interaction[29]. CCP1–CCP3 of FH indeed showed several conserved and charged patches on its surface (**Fig. 5a** and **Supplementary Fig. 7**), which may be involved in the binding of FI. For the FH homolog vaccinia virus complement control protein (VCP), CCP2 has been shown to have a dominant function in complement inhibition. Substitution of four residues in CCP2 markedly enhances cofactor activity, although it only moderately increases the affinity of VCP for C3b[30]. The equivalent residues in FH (Gln101, Ile106, Asp112 and Asp119) were fully exposed and were adjacent to conserved patches (**Fig. 5a**), which suggests involvement of these four residues in the binding of FI. Furthermore, studies of cobra venom factor have indicated that the C345C domain of

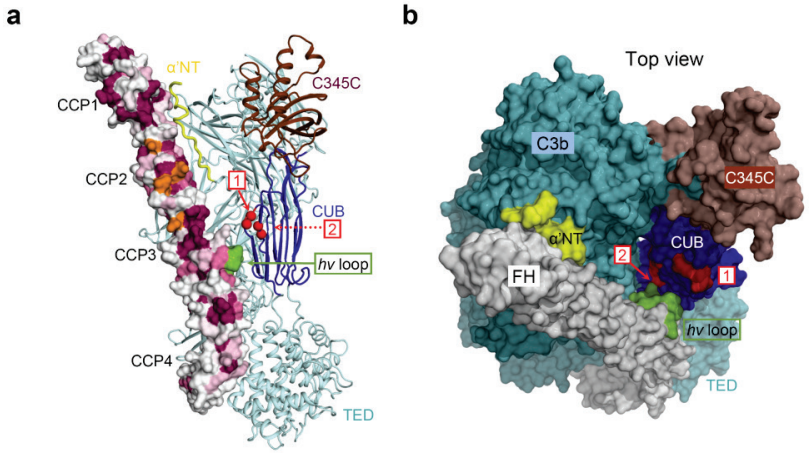

Figure 5 Structural implications of cofactor activity. (**a**) Sites of FI binding and cleavage. FH is presented in surface representation; colors indicate residue conservation with mutational data from ref. 30. Residues with the conservation scores of less than 5 are white; substitutions in VCP that enhance FI binding are orange; the hypervariable loop (HV loop) of CCP3 is green. C3b is cyan, with the CUB (blue), α'NT (yellow) and C345C (dark red) domains highlighted and the first and second scissile bonds in the CUB domain indicated by red spheres (conservation scale and corresponding colors, **Supplementary Fig. 4**). (**b**) Surface representation of the complex from the top view. Colors of the domains and FI cleavage sites are as in **a**; FH domains are gray.

C3b may contribute to this interaction[31]. These data suggest that FI binds the C3b-FH complex at the area formed by CCP1–CCP3 of FH and by C345C and CUB of C3b (**Supplementary Fig. 7**). In addition to providing a platform for FI, FH may have a second function in cofactor activity; we hypothesize that the bridge formed by CCP4 between TED and the core of C3b may maintain the position of TED while the connecting CUB domain undergoes further cleavage. This suggested function is supported by disease-related mutations in the sequence encoding CCP4 of FH[32,33] and in the sequence encoding TED of C3b[34], which indicates functional importance for interactions of RCA proteins with TED.

Mapping of disease-related mutations

The complex structure provided a structural basis for understanding the effects of six disease-related mutations that can be found in the sequence encoding domains CCP1– CCP4 of FH. In a first step, we examined two substitutions (R60G and P204L) and one deletion (K206Δ) located directly at the C3b-FH(1–4) interface (**Fig. 3**). In case of the aHUS-related mutant R60G[35], a salt

bridge between the guanidium group of Arg60 in CCP1 of FH and the acidic Asp732 of α'NT in C3b was lost by the substitution (**Supplementary Fig. 8a**). In CCP4 of FH, the backbone amide of Lys206 formed a hydrogen bond with the carboxylate of Glu1138 in TED, whereas the lysine side chain formed an intramolecular salt bridge with the carboxylate of Glu213 (**Supplementary Fig. 8b**). The MPGN-II-associated deletion of this residue probably considerably alters the local structure in CCP4, which would explain the diminished binding to C3b and loss of regulatory functions of FH[32]. In the aHUS-related mutant P240L[33], the *cis*-peptide conformation of Pro240 is probably essential for the binding of CCP4 in a pocket formed by both MG1 and TED of C3b (**Supplementary Fig. 8c**), and its substitution may directly affect the C3b-FH interaction. The remaining three substitutions (V44I, R35H and R109L) were not located at the C3b-FH interface (**Supplementary Fig. 8d,e**). The V44I mutant is not only associated with AMD and MPGN-II (refs. 36, 37) but also has been shown to have a strong association with polypodial choroidal vasculopathy[38]. Val44 is part of the hydrophobic core of the CCP1 domain and may therefore affect domain stability. Indeed, NMR studies have demonstrated an effect on the thermal stability of V44I, whereas only subtle structural differences could be detected between wild-type and mutant proteins[12]. Arg35 of the aHUS-related substitution R35H[33] was solvent exposed and was located on the bottom part of CCP1 opposite the C3b-interaction surface (**Supplementary Fig. 8d**). Although few structural rearrangements have been reported for the R35H mutant[12], its localization on the putative FIinteraction face of FH may affect binding to FI. The substitution R109L has been found in two patients with MPGN-II (ref. 39). As the hydrophobic portion of the arginine side chain was buried in the hydrophobic core of the CCP2 domain packing against the conserved Trp116 residue (**Supplementary Fig. 8e**), this substitution possibly affects the folding or stability of the CCP2 domain.

Many aHUS-linked mutations have also been described for the gene encoding C3 (ref. 34); they have large effects on C3b-MCP binding and smaller effects on C3b-FH binding. Substitutions R570Q or R570W, A1072V and Q1139K were all located at the C3b-FH interface (**Fig. 3**) and decreased the binding of FH by 10–50% (ref. 34). For R570Q and R570W, the replacement of Arg570 may lead to a loss of electrostatic interactions (at a distance of 4 Å) with Glu98 of FH (**Supplementary Fig. 8f**). In the A1072V mutant, the bulkier side chain of valine may sterically hinder interactions with Tyr225 of FH (**Supplementary Fig. 8g**) and diminish C3b-FH binding. Substitution Q1139K introduces a positive charge that possibly leads to a salt bridge between Lys1139 and the preceding Asp1138 (**Supplementary Fig. 8h**) and probably modifies interactions with FH. Other substitutions in TED, such as D1093N (**Fig. 3**), may not be connected with FH(1–4)

but instead may be connected with the secondary C3b binding site at CCP19–CCP20 (ref. 11).

DISCUSSION

Tight regulation of the complement response on host cells and in the circulation is critical for providing selectivity against foreign cells and preventing complement-mediated tissue damage. Given their essential function in immune response and the increasing number of diseases with known or suspected involvement of complement regulators, detailed knowledge about the underlying molecular processes is very much desired. Our data are important in this context, as they have yielded a structure of C3b in complex with a complement regulator. Our results not only provide insight into the function of the most abundant regulator, FH, but also allow us to develop more general models of complement regulation. In agreement with published observations[10], the N-terminal 4 of 20 CCP domains of FH were functionally sufficient and showed both decay-acceleration and cofactor activity. FH(1–4) bound C3b in an extended configuration, which resulted in a long contact interface that covered the entire flank of C3b. The interface involved all four N-terminal CCP domains of FH and many domains of C3b, including α' NT, MG1, MG2, MG6, MG7, CUB and TED. Despite this large interface, the binding affinity of the two molecules was rather low, with a dissociation constant of 11 μM. This result is in agreement with a published study comparing the binding affinities of several FH fragments to C3b and is in a range similar to that of FH(19–20) but much weaker than that of full-length FH[11].

The structure of the C3b-FH(1–4) complex provides a molecular basis for understanding the two regulatory mechanisms, decay-acceleration activity and cofactor activity, by which proteins of the RCA family protect host cells. On the basis of structural comparisons of C3b-FH(1–4) and C3bBb[21], we conclude that decay-acceleration is mediated mainly by the first two N-terminal CCP domains of FH, which bind the α' NT and MG2 and MG6–MG7 domains of C3b. These domains probably dislocate the Bb protease fragment by electrostatic repulsion and steric hindrance from the convertase. The conserved location of functional residues in the homologous domains CCP2–CCP3 of DAF suggests that similar displacement effects are also involved in case of this regulator[24]. Nevertheless, DAF and FH may differ in their precise mechanisms of dislocating Bb from C3b, as direct interaction with Bb has been reported for DAF but not for FH[25]. We therefore hypothesize that DAF interacts with the βF-α7 loop of the VWA domain in Bb and hence induces a low-affinity conformation of the metal ion–dependent adhesion site that mediates binding of Bb to the C terminus of C3b. More structural data, such as C3b-DAF and DAF-Bb complexes, are

needed to understand the differences in the precise mechanisms of DAF and FH.

Our data further suggest that the cofactor activity of FH in the conversion of C3b to the inactive iC3b species is based on two essential mechanisms. First, FH provides a contact interface for the initial binding of the protease FI to the C3b-regulator complex and brings it into close proximity to the CUB domain of C3b. The four N-terminal CCP domains of FH bind along the CUB domain of C3b. This structural arrangement suggests that FI may bind CCP1–CCP3 of FH and C345C of C3b, a proposal that is supported by VCP mutagenesis data[30] and studies of cobra venom factor chimeras[31]. Although FI is reported to bind directly yet weakly to C3b in the absence of FH, the binding affinity substantially increases after the addition of FH[29]. The newly formed extended binding site between FH and C3b probably considerably improves the FI binding affinity and, as a consequence, the cleavage rate. Secondly, FH enables the sequential cleavage of C3b through stabilization of the TED-CUB arrangement relative to the core of the C3b molecule. We have shown that domain CCP4 bridges the TED and MG1 domains of C3b and we argue that these interactions keep TED in place during cleavage by FI. In contrast to FH, MCP does not bind to the α'NT region of C3b, which explains its lack of decay-acceleration activity[17,18]. The cofactor activity of MCP, in contrast, may be mediated in a way similar to that of FH. Binding experiments analyzing disease-related mutations have indicated that MCP also binds C3b through MG6 and TED[34]. Several of the C3 mutants that showed much less C3b-MCP binding have substitutions such as R570Q, R570W, A1072V and Q1139K that are all at the C3b-FH interface[34]. However, the exact binding arrangement is probably different for the two regulators, as the C3b-binding site in domain CCP4 of MCP, as derived from mutagenesis studies[40], does not coincide fully with the corresponding site in CCP4 of FH.

FH has experienced increasing interest in biomedical sciences during the past decade as it has become evident that mutations and polymorphisms of the gene encoding this regulator are strongly associated with diseases such as aHUS, AMD and MPGN-II (refs. 33,34). In AMD, mutation of the gene encoding FH is even considered the most consistent genetic risk factor[41]. Although some effects may be attributed to altered binding of glycosaminoglycan or changes in the secondary C3b binding site on CCP19–CCP20, other substitutions are located in CCP1–CCP4 and were therefore mapped on the C3b-FH(1–4) structure. Our analysis indicates that disruption of specific contacts (such as salt bridges) or the induction of local conformational changes may substantially alter the C3b-FH interface. The specific yet rather weak interaction between C3b and FH(1–4) may be essential for fast and selective complement regulation but also makes FH prone to functional

interference by even small modifications in its sequence. The substitutions described, therefore, probably weaken the affinity, which may lead to a loss of regulatory activity and, finally, to apparent disease states.

In conclusion, our structural data provide an important framework for understanding the two key molecular mechanisms of host protection by RCA proteins: decay-acceleration activity and cofactor activity. We have also offered a basis for explaining the functional consequences of individual substitutions related to dysfunctional complement regulation and associated diseases. Thus, our study may pave the way for the development of therapeutics directed at modulating complement activation.

METHODS

Protein expression and purification. C3 was isolated from human plasma. After informed consent was provided by the donor, plasma was obtained at the University Medical Center Utrecht according to a study protocol approved by the medical ethics committee of the University Medical Center Utrecht. C3b was generated by limited trypsin treatment of C3 as describedwith some modifications[19,42]. 1 mg/ml purified C3 was treated with 1% (w/w enzyme/substrate) trypsin for 2 min at 37 °C in phosphate buffered saline (PBS). 5% (w/w inhibitor/substrate) soybean trypsin inhibitor was added to stop the reaction and the protein sample was transferred on ice immediately, followed by treatment with 20 mM iodoacetamide for 30 min. The C3b sample was diluted 1:1 with 25 mM Tris, 50 mM NaCl, pH 8.0 and loaded on a Mono-Q HR 5/5 (1 ml) column, equilibrated in 25 mM Tris, 100 mM NaCl, pH 8.0, and eluted with a linear gradient of 100-300 mM NaCl over 30 column volumes. The fractions containing C3b were pooled, concentrated and further purified by a Superdex 200 HR 10/30 column. The purified C3b sample was dialyzed against 10 mM Tris, 50 mM NaCl, pH 7.4, concentrated to 30 mg/ml, and stored at -80 ºC. The purity of C3b was verified using SDS-PAGE. The DNA fragment encoding human FH domains CCP1–CCP4 (residues 1–246) was amplified by PCR from the full-length CFH clone and was ligated into the pSecTag2 B vector (Invitrogen). Recombinant FH(1–4), which contains a c-Myc tag and sixhistidine tag at its C terminus, was expressed in human embryonic kidney HEK293T cells with plasmids with polyethenimine (linear, ~ 25 kDa; Polysciences) and was incubated in Hybridoma-SFM (Gibco-Invitrogen) containing 1% (vol/vol) FBS (HyClone). Medium was collected 4 d after transfection and was concentrated before protein purification. FH(1–4) was purified by metalaffinity chromatography (Ni-NTA Superflow; Qiagen) and was eluted with 200 mM imidazole in PBS, pH 8.0. All protein-containing fractions were pooled and were dialyzed against 10 mM phosphate buffer, pH 7.4, and were further purified by ion-exchange chromatography with a Resource Q column (GE Healthcare BioSciences) with a linear gradient of 0–300 mM NaCl over 30 column volumes. Purified FH(1–4) was dialyzed against 10 mM Tris, 50mM NaCl, pH 7.4 and was concentrated to 1.7 mg/ml before crystallization. The purity of FH(1–4) was verified by SDS-PAGE.

Crystallization, data collection and structure determination. Purified C3b (30 mg/ml) and FH(1–4) (1.7 mg/ml) were mixed at a molar ratio of 1:1 to a final concentration 8.5 mg/ml (40 μM) of the complex. C3b-FH(1–4) was crystallized in 7.0% (wt/vol) PEG 3,350 and 70 mM ammonium acetate, pH 7.1, by hanging-drop vapor diffusion at 18 °C. Crystals appeared after 2 d and grew within 5 d to a typical size of 200 × 100 × 60 μm. Crystals were soaked for several minutes in reservoir solution supplemented with 20% (vol/vol) glycerol and then were 'flash-cooled' in liquid nitrogen. Crystals belong to space group $P2_12_12$ (a = 223.4, b = 84.9, c = 128.8 Å), and the best crystal diffracted to a resolution of 2.7-Å at European Synchrotron Radiation Facility beamline ID14-EH4. Diffraction data were integrated and scaled with the programs MOSFLM and Scala[43]. The structure of C3b-FH(1–4) was determined by molecular replacement with the program PHASER[44]. First, the β-chain (residues 1–642) of C3c (Protein Data Bank accession code 2A74)[19] was placed, followed by the stepwise addition of the TED, CUB and α'NT, MG7-MG8 domains from C3b (Protein Data Bank accession code 2I07)[14]. The initial models for the individual CCP domains of FH were generated by the program Chainsaw[45] with structures of CCP2 of human β_2-glycoprotein I (Protein Data Bank accession code 1QUB; residues 63–121)[46] and CCP4 of DAF (Protein Data Bank accession code 1H03; residues 130–191)[23] as templates. The CCP2 and CCP3 domains of FH were found, but molecular replacement searches of domains CCP1 and CCP4 initially failed. The C345C domain of C3b was then successfully placed with the C345C domain from the C3c structure (residues 1496–1641) as search model. The Chainsaw model for the fourth CCP domain of FH was placed manually with the Crystallographic Object-Oriented Toolkit[47], based on an *Fo-Fc* (observed structure factor – calculated structure factor) difference map and subsequently refined as a rigid body in PHASER. After several rounds of refinement and model building with the Crystallographic Object-Oriented Toolkit, the bottom part of CCP1 (20 of 65 residues in total) could be built manually. The complete CCP1 derived from the NMR structure of CCP1–CCP2 of FH (Protein Data Bank accession code 2RLP; residues 2–64)[12] was then placed by superposition and rigid-body refinement in PHASER to obtain the complete model. The model was refined with the macromolecular refinement program REFMAC[48] and the PHENIX software suite[49]. The final model, consisting of 1,536 residues of C3b and 244 residues of FH(1–4), had R_{work} and R_{free} values of 21.7% and 25.2%, respectively.

Binding-affinity assay. Surface plasmon resonance was used to determine the binding affinity of soluble FH(1–4) for C3b immobilized specifically by its thioester. All surface plasmon resonance (SPR) studies were performed on a Biacore 2000 instrument (GE Healthcare Corp., Piscataway, NJ) at 25 ºC. Binding signals were processed and evaluated using Scrubber (version 2; BioLogic Software Pty. Ltd., Campbell, Australia). The direct binding of FH(1-4) to C3b was assessed by capturing thioester-specifically biotinylated C3b (30 μg ml^{-1}) to a streptavidin-coated sensor chip (SA chip; GE Healthcare) at various surface densities (3,000-7,000 resonance units; RU) and injecting a twofold dilution series of recombinant FH(1-4) (20-0.02 μM) for 1 min. at a flow rate of 20 μl min^{-1} in 10 mM PBS-T pH 7.4 (10 mM sodium phosphate, 150 mM NaCl, 0.005% Tween-20). Owing to the rapid dissociation rate, no regeneration was required between injections. A blank streptavidin surface was used as a reference and an ensemble of buffer blank injections was subtracted from the data sets to eliminate injection artifacts[49]. The apparent equilibrium dissociation constant (K_D) was calculated as an average of six data

sets by plotting the steady state signals of FH(1-4) injections against the concentration and fitting individual data sets to a single-binding-site model.

Complement decay-acceleration activity and cofactor activity. The decay acceleration activity of the alternative pathway of complement activation was assessed by surface plasmon resonance. On-chip formation and decay of the C3 convertase were assessed by injection of an equimolar mixture of factor B and factor D (100 nM each) on immobilized C3b for 2 min at a flow rate of 10 µl/min in HEPES-buffered saline–Mg^{2+} buffer (10 mM HEPES, 150 mM NaCl, 0.005% (vol/vol) Tween-20 and 1 mM $MgCl_2$, pH 7.4). After an undisturbed decay phase of 3 min, 200 nM FH(1–20), FH (1–4), FH(19–20) or a buffer control was injected for 1 min and the decrease in baseline after injection was evaluated. For removal of residual interactants, the surface was regenerated with 1 µM FH(1–4) and 1 M NaCl. Values for binding signals of the FH fragments with C3b (in absence of the convertase) were subtracted from the data set for visualization of the pure decay acceleration. The cofactor activity of FH(1–4) was tested with a published protocol[50]. Human C3b (4 µg; 1.14 µM) and human factor I (10 ng; 8 nM) were incubated for 1 h at 37 °C with various amounts (9, 18, 36 nM) of FH(1–20) or FH(1–4) in PBS buffer in a final volume of 20 µl. Reactions were stopped by the addition of SDS-PAGE loading buffer and samples were analyzed by 10% SDS-PAGE.

Antibody competition assay. The ability of anti-C3c or anti-C3d mAbs to block the binding of FH fragments to C3b was investigated by SPR using a Biotin CAPture sensor chip (prototype kit; GE Healthcare Corp.) and PBS-T as running buffer. Streptavidin was loaded on the chip surface by injecting a conjugate solution (50 µg/ml) for 5 min at 2 µl/min on all four flow cells. Biotinylated C3b (30 µg/ml; 5 min) was then injected on two of the streptavidin-coated flow cells, resulting in surface densities of 2,500-3,000 RU. All surfaces were stabilized by three consecutive 30 s injections of 1 M NaCl and equilibrated for 10 min. A buffer blank (control) or 10 µg/ml of mAb 311 (anti-C3d)[16] or mAb C3-9 (anti-C3c)[16] were injected on a single C3b surface for 5 min to form the corresponding mAb-C3b complex. 1 µM recombinant FH(1-4) and FH(19-20) were each injected for 1 min at 20 µl/min, and their differential signal intensities were compared between the mAb-C3b complexes and the C3b control surface. A plain streptavidin-coated flow cell served as a reference. Buffer blank injections before and after each FH fragment sample were subtracted for compensating injection artifacts and drifting baselines on the mAb-C3b complex surfaces. At the end of each injection cycle, captured streptavidin was removed by injecting a regeneration solution (6 M guanidine-HCl in 0.25 M NaOH) for 2 min, and the chip was equilibrated in running buffer for 5 min. mAb 311 and C3-9 were kindly provided by J. Tamerius (Cytotech) and C.E. Hack (Central Laboratory of the Netherlands Red Cross Blood Transfusion Service, The Netherlands), respectively.

Table 1 Data collection and refinement statistics.

	2.7-Å
Data collection	
Space group	$P2_12_12$
Cell dimensions	
a, *b*, *c* (Å)	223.5, 84.9, 128.8
Resolution (Å)	67-2.7 (2.85-2.7)
R_{merge} (%)	11.3% (60.8%)
$I/\sigma i$	8.3 (1.9)
Completeness (%)	99.7 (100)
Redundancy	3.7 (3.8)
Refinement statistics	
Resolution (Å)	64.5-2.7
Reflections	67,893
R_{work}/ R_{free} (%)	21.7 / 25.2
Atoms	14,442
Protein	14,081
Ligand/ion	189
Water	172
B-factors (Å^2)	
Protein	68.2
Ligand/ion	106.7
Water	48.2
r.m.s.d	
Bond lengths (Å)	0.002
Bond angles (°)	0.446

Table 2 Structural comparison of FH(1-4) with NMR structures of FH(1-2) and FH(2-3).
Superposition of FH(1-4) from the C3b-FH(1-4) complex and NMR structures of FH (1-2) and FH (2-3)12 based on the CCP2 domains (see **Fig. 2b**, top). The values of domain translation and rotation were calculated using SUPERPOSE in the CCP4 package[51].

	FH(1-2) (pdb code: 2RLP)		FH(2-3) (pdb code: 2RLQ)	
	Translation (Å)	Rotation (°)	Translation (Å)	Rotation (°)
CCP1	3.5	9.3	--	--
CCP3	--	--	3.2	9.5
	Rmsd (Cα) (Å)			
CCP2	1.3		1.1	

Table 3 Analysis of the interfaces between C3b and FH(1-4).
All values are calculated by PISA (www.ebi.ac.uk/msd-srv/prot_int). The buried area is calculated as difference in total accessible surface areas of isolated and interfacing structures. $^{i}N_{res}$ indicates the number of residues at the interface. The N_{HB} and N_{SB} indicate the number of potential hydrogen bonds and salt bridges across the interface, respectively. $\Delta^{i}G$ indicates the solvation free energy gain upon formation of the interface. $\Delta^{i}G$ P-value indicates the P-value of the observed solvation free energy gain.

Interface		Buried area (Å)	$^{i}N_{res}$		N_{HB}	N_{SB}	$\Delta^{i}G$ Kcal/mol	$\Delta^{i}G$ P-value
			C3b	FH				
C3b	FH(1-4)	4485	79	68	21	8	-4.1	0.609
C3b	CCP1	838	15	9	6	1	-0.4	0.539
C3b	CCP2	1009	22	18	1	1	-2.6	0.575
C3b	CCP3	1239	24	20	7	4	-2.8	0.440
C3b	CCP4	1472	24	21	7	2	-1.0	0.635

ACKNOWLEDGMENTS

We thank the European Synchrotron Radiation Facility for synchrotron radiation facilities; beamline scientists of the European Synchrotron Radiation Facility and the European Molecular Biology Laboratory for assistance; M. Pangburn (University of Texas at Tyler) for the CFH clone; P. Barlow (University of Edinburgh) for FH(19–20) protein; and M.A. Hadders for critical reading of the manuscript and comments. Supported by the Council for Chemical Sciences of the Netherlands Organization for Scientific Research (P.G.) and the US National Institutes of

Health (J.D.L.).

REFERENCES

1. Schmidt, C.Q., Herbert, A.P., Hocking, H.G., Uhrin, D. & Barlow, P.N. Translational Mini-Review Series on Complement Factor H: Structural and functional correlations for factor H. *Clinical & Experimental Immunology* **151**, 14-24 (2008).
2. Liszewski, M.K., Farries, T.C., Lublin, D.M., Rooney, I.A. & Atkinson, J.P. Control of the complement system. *Adv Immunol* **61**, 201-283 (1996).
3. Prosser, B.E. *et al.* Structural basis for complement factor H linked age-related macular degeneration. *J. Exp. Med.* **204**, 2277-2283 (2007).
4. Meri, S. Loss of self-control in the complement system and innate autoreactivity. *Ann N Y Acad Sci* **1109**, 93-105 (2007).
5. de Cordoba, S.R. & de Jorge, E.G. Translational mini-review series on complement factor H: genetics and disease associations of human complement factor H. *Clin Exp Immunol* **151**, 1-13 (2008).
6. Lambris, J.D., Ricklin, D. & Geisbrecht, B.V. Complement evasion by human pathogens. *Nat Rev Microbiol* **6**, 132-142 (2008).
7. Schneider, M.C. *et al.* Neisseria meningitidis recruits factor H using protein mimicry of host carbohydrates. *Nature* **458**, 890-893(2009).
8. Ricklin, D. & Lambris, J.D. Complement-targeted therapeutics. *Nat Biotechnol* **25**, 1265-1275 (2007).
9. Noris, M. & Remuzzi, G. Translational Mini-Review Series on Complement Factor H: Therapies of renal diseases associated with complement factor H abnormalities: atypical haemolytic uraemic syndrome and membranoproliferative glomerulonephritis. *Clinical & Experimental Immunology* **151**, 199-209 (2008).
10. Gordon, D.L., Kaufman, R.M., Blackmore, T.K., Kwong, J. & Lublin, D.M. Identification of complement regulatory domains in human factor H. *J Immunol* **155**, 348-356 (1995).
11. Schmidt, C.Q. *et al.* A new map of glycosaminoglycan and C3b binding sites on factor H. *J Immunol* **181**, 2610-2619 (2008).
12. Hocking, H.G. *et al.* Structure of the N-terminal region of complement factor H and conformational implications of disease-linked sequence variations. *J Biol Chem* **283**, 9475-9487 (2008).
13. Okemefuna, A.I. *et al.* The regulatory SCR-1/5 and cell surface-binding SCR-16/20 fragments of factor H reveal partially folded-back solution structures and different self-associative properties. *J Mol Biol* **375**, 80-101 (2008).
14. Janssen, B.J., Christodoulidou, A., McCarthy, A., Lambris, J.D. & Gros, P. Structure of C3b reveals conformational changes that underlie complement activity. *Nature* **444**, 213-216 (2006).

15. Wiesmann, C. *et al.* Structure of C3b in complex with CRIg gives insights into regulation of complement activation. *Nature* **444**, 217-220 (2006).
16. Becherer, J.D., Alsenz, J., Esparza, I., Hack, C.E. & Lambris, J.D. Segment spanning residues 727-768 of the complement C3 sequence contains a neoantigenic site and accommodates the binding of CR1, factor H, and factor B. *Biochemistry* **31**, 1787-1794 (1992).
17. Lambris, J.D. *et al.* Dissection of CR1, factor H, membrane cofactor protein, and factor B binding and functional sites in the third complement component. *J Immunol* **156**, 4821-4832 (1996).
18. Oran, A.E. & Isenman, D.E. Identification of residues within the 727-767 segment of human complement component C3 important for its interaction with factor H and with complement receptor 1 (CR1, CD35). *J Biol Chem* **274**, 5120-5130 (1999).
19. Janssen, B.J. *et al.* Structures of complement component C3 provide insights into the function and evolution of immunity. *Nature* **437**, 505-511 (2005).
20. Gros, P., Milder, F.J. & Janssen, B.J. Complement driven by conformational changes. *Nat Rev Immunol* **8**, 48-58 (2008).
21. Rooijakkers, S.H.M. *et al.* Structural and functional implications of the complement convertase stabilized by a staphylococcal inhibitor. *Nat. Immunol.* advance online publication, doi:10.1038/ni.1756 (7 June 2009).
22. Hourcade, D.E., Mitchell, L., Kuttner-Kondo, L.A., Atkinson, J.P. & Medof, M.E. Decay-accelerating factor (DAF), complement receptor 1 (CR1), and factor H dissociate the complement AP C3 convertase (C3bBb) via sites on the type A domain of Bb. *J Biol Chem* **277**, 1107-1112 (2002).
23. Lukacik, P. *et al.* Complement regulation at the molecular level: the structure of decay-accelerating factor. *Proc Natl Acad Sci USA* **101**, 1279-1284 (2004).
24. Kuttner-Kondo, L. *et al.* Structure-based mapping of DAF active site residues that accelerate the decay of C3 convertases. *J Biol Chem* **282**, 18552-18562 (2007).
25. Harris, C.L., Abbott, R.J., Smith, R.A., Morgan, B.P. & Lea, S.M. Molecular dissection of interactions between components of the alternative pathway of complement and decay accelerating factor (CD55). *J Biol Chem* **280**, 2569-2578 (2005).
26. Luo, B.H., Carman, C.V. & Springer, T.A. Structural basis of integrin regulation and signaling. *Annu Rev Immunol* **25**, 619-647 (2007).
27. Goicoechea de Jorge, E. *et al.* Gain-of-function mutations in complement factor B are associated with atypical hemolytic uremic syndrome. *Proc Natl Acad Sci USA* **104**, 240-245 (2007).
28. Sahu, A., Isaacs, S.N., Soulika, A.M. & Lambris, J.D. Interaction of vaccinia virus complement control protein with human complement proteins: factor I-mediated degradation of C3b to iC3b1 inactivates the alternative complement pathway. *J Immunol* **160**, 5596-5604 (1998).
29. DiScipio, R.G. Ultrastructures and interactions of complement factors H and I. *J Immunol* **149**, 2592-2599 (1992).

30. Yadav, V.N., Pyaram, K., Mullick, J. & Sahu, A. Identification of hot spots in the variola virus complement inhibitor (SPICE) for human complement regulation. *J Virol* **82**, 3283-3294 (2008).

31. Fritzinger, D.C. *et al.* Functional characterization of human C3/cobra venom factor hybrid proteins for therapeutic complement depletion. *Developmental & Comparative Immunology* **33**, 105-116 (2009).

32. Licht, C. *et al.* Deletion of Lys224 in regulatory domain 4 of Factor H reveals a novel pathomechanism for dense deposit disease (MPGN II). *Kidney Int* **70**, 42-50 (2006).

33. Saunders, R.E., Goodship, T.H., Zipfel, P.F. & Perkins, S.J. An interactive web database of factor H-associated hemolytic uremic syndrome mutations: insights into the structural consequences of disease-associated mutations. *Hum Mutat* **27**, 21-30 (2006).

34. Fremeaux-Bacchi, V. *et al.* Mutations in complement C3 predispose to development of atypical hemolytic uremic syndrome. *Blood* **112**, 4948-4952 (2008).

35. Caprioli, J. *et al.* Complement factor H mutations and gene polymorphisms in haemolytic uraemic syndrome: the C-257T, the A2089G and the G2881T polymorphisms are strongly associated with the disease. *Hum Mol Genet* **12**, 3385-3395 (2003).

36. Hageman, G.S. *et al.* A common haplotype in the complement regulatory gene factor H (HF1/CFH) predisposes individuals to age-related macular degeneration. *Proc Natl Acad Sci USA* **102**, 7227-7232 (2005).

37. Abrera-Abeleda, M.A. *et al.* Variations in the complement regulatory genes factor H (CFH) and factor H related 5 (CFHR5) are associated with membranoproliferative glomerulonephritis type II (dense deposit disease). *J Med Genet* **43**, 582-589 (2006).

38. Kondo, N., Honda, S., Kuno, S. & Negi, A. Coding variant I62V in the complement factor H gene is strongly associated with polypoidal choroidal vasculopathy. *Ophthalmology* **116**, 304-310 (2009).

39. Dragon-Durey, M.A. *et al.* Heterozygous and homozygous factor h deficiencies associated with hemolytic uremic syndrome or membranoproliferative glomerulonephritis: report and genetic analysis of 16 cases. *J Am Soc Nephrol* **15**, 787-795 (2004).

40. Liszewski, M.K. *et al.* Dissecting sites important for complement regulatory activity in membrane cofactor protein (MCP; CD46). *J. Biol. Chem.* **275**, 37692–37701 (2000).

41. Coleman, H.R., Chan, C.C., Ferris, F.L.III & Chew, E.Y. Age-related macular degeneration. *Lancet* **372**, 1835-1845 (2008).

42. Lambris, J.D., Dobson, N.J. & Ross, G.D. Release of endogenous C3b inactivator from lymphocytes in response to triggering membrane receptors for beta 1H globulin. *J. Exp. Med.* **152**, 1625-1644 (1980).

43. Evans, P. Scaling and assessment of data quality. *Acta Crystallographica Section D* **62**, 72-82 (2006).

44. McCoy, A.J. *et al.* Phaser crystallographic software. *Journal of Applied Crystallography* **40**, 658-674 (2007).

45. Stein, N. CHAINSAW: a program for mutating pdb files used as templates in molecular replacement. *Journal of Applied Crystallography* **41**, 641-643 (2008).

46. Bouma, B. *et al.* Adhesion mechanism of human β_2-glycoprotein I to phospholipids based on its crystal structure. *EMBO J* **18**, 5166-5174 (1999).

47. Emsley, P. & Cowtan, K. Coot: model-building tools for molecular graphics. *Acta Crystallogr D Biol Crystallogr* **60**, 2126-2132 (2004).

48. Winn, M.D., Murshudov, G.N. & Papiz, M.Z. Macromolecular TLS refinement in REFMAC at moderate resolutions. *Methods Enzymol* **374**, 300-321 (2003).

49. Adams, P.D. *et al.* PHENIX: building new software for automated crystallographic structure determination. *Acta Crystallogr D Biol Crystallogr* **58**, 1948-1954 (2002).

50. Alsenz, J., Lambris, J.D., Schulz, T.F. & Dierich, M.P. Localization of the complement-component-C3b-binding site and the cofactor activity for factor I in the 38kDa tryptic fragment of factor H. *Biochem J* **224**, 389-398 (1984).

51. The CCP4 suite: programs for protein crystallography. *Acta Crystallogr D BiolCrystallogr,* **50**, 760-763. (1994)

52. Nagar, B., Jones, R.G., Diefenbach, R.J., Isenman, D.E., Rini, J.M. X-ray crystal structure of C3d: a C3 fragment and ligand for complement receptor 2. *Science*, **280**, 1277-1281 (1998).

53. Nishida, N., Walz, T. & Springer, T.A. Structural transitions of complement component C3 and its activation products. *Proc Natl Acad Sci USA* **103**, 19737-19742 (2006).

54. Landau, M., Mayrose, I., Rosenberg, Y., Glaser, F., Martz, E., Pupko, T. and Ben-Tal, N. ConSurf 2005: the projection of evolutionary conservation scores of residues on protein structures. *Nucleic Acids Res*, **33**, W299-302 (2005).

Chapter 4

Structures of C3b-MCP and C3b-SPICE reveal molecular modularity underlying complement regulator structure and function

Jin Wu[1], Daniel Ricklin[2], Georgia Sfyroera[2], Apostolia Tzekou[2], John D. Lambris[2] and Piet Gros[1]

1 Crystal and Structural Chemistry, Bijvoet Center for Biomolecular Research, Dept. Chemistry, Faculty of Science, Utrecht University, Padualaan 8, 3584 CH Utrecht, The Netherlands.
2 Department of Pathology & Laboratory Medicine, University of Pennsylvania, Philadelphia, Pennsylvania, PA 19104, USA.

Manuscript in preparation

ABSTRACT

The human body protects itself from self-attack by complement by expressing regulators of complement activation (RCA) that bind to opsonins (C3b, C4b) via strings of four complement control protein (CCP) domains, and prevent amplification on host cells. Since mutations in RCA are associated with diseases and orthopox viruses produce RCA mimics for evading immune response, insights into structural determinants of regulatory activities are crucial. Here we describe crystal structures of C3b in complex with a human regulator (membrane cofactor protein; MCP) and a viral homologue (smallpox inhibitor of complement enzymes; SPICE) at 2.4 and 2.6-Å resolution, respectively. In contrast to the known complex of C3b-factor H (FH), only CCP3-4 rather than all four domains were involved in MCP binding to C3b, with CCP4 interacting distinctly between the two regulators. Conversely, CCP1-3 of SPICE bound in a similar fashion as FH, while CCP4 more resembled MCP yet was only weakly associated to C3b. Our structural and biochemical data therefore indicate a high degree of modularity and diversity that define the regulatory functions of RCA and their mimics.

INTRODUCTION

The complement system of the mammalian immune defense efficiently recognizes and clears microbial intruders and apoptotic host cells from blood and interstitial fluids[1-2]. This system is initiated *via* three main routes (classical, lectin, and alternative pathway) that can be either antibody-mediated, through direct recognition of pathogen-associated molecular patterns, or by a low level of spontaneous hydrolysis of the central complement component C3. Activation of all pathways leads to the formation of enzymatic complexes, the so-called C3 convertases (C3bBb in the alternative pathway or C4b2a in the classical and lectin pathways), which cleave C3 into its active fragments C3a and C3b. The C3b molecules bind covalently to cell surfaces via their exposed thioester moiety and act as opsonins[3], but also facilitate amplification of the complement response by forming additional convertase complexes and converting a large number of C3 molecules into C3b. Upon activation, opsonization of targeted particles can lead to pro0inflammatory signaling, attraction and stimulation of immune cells, phagocytosis *via* complement receptors, and cell lysis by the membrane attack complex[4].

Complement activation and amplification by the alternative pathway are in principle non-specific

and, hence, give rise to potential injury by self-attack of host cells and tissue. Thus, complement activation needs to be tightly controlled, and improper regulation often leads to clinical conditions such as ischemia-reperfusion injury during heart attack or stroke, as well as various inflammatory, immune, or degenerative diseases[5-6]. An important family of regulators, the so-called 'regulators of complement activation' (RCA), is formed by a group of soluble and membrane-attached proteins that suppress the complement-amplification loop. The regulators stop the opsonization with C3b either by dissociating the C3 convertases, and preventing their re-formation, by blocking binding of factor B to C3b (referred to as decay-acceleration activity) or by mediating the degradation of C3b and C4b by the protease factor I (referred to as cofactor activity)[7]. The soluble regulators factor H (FH) in the alternative pathway and C4b-binding protein (C4bp) in the classical pathway discriminate "self" from "non-self" by recognizing molecular patterns on host cells and keep solution activation in check[8-9]. The other members of the RCA family, i.e. membrane-cofactor protein (MCP, CD46), complement receptor 1 (CR1, CD35) and decay-accelerating factor (DAF, CD55) are membrane-bound, either through a trans-membrane helix or glycosylphosphatidylinositol anchor, and inhibit complement activation directly on the host-cell surfaces where they are expressed[10]. All RCA proteins consist of strings, varying in length from 4 to 35 copies, of a distinctive module known as complement-control protein (CCP) domain (also referred to as short-consensus repeat or Sushi domain). Each CCP domain consists of ~60 amino acids and forms a rod-like structure that is build up from a main three-stranded and small two-stranded anti-parallel β-sheet stabilized by two disulfide bridges and contains an invariant tryptophan residue with highly conserved prolines and bulky hydrophobic residues, such as phenylalanine and tyrosine[11]. Despite those structural similarities between RCA proteins, previous studies have suggested that the binding modes of individual CCP domains between different regulators can be highly distinct and may thereby define the functional pattern. In addition, deficiencies and dysfunctions of complement regulators have been strongly associated with renal diseases such as atypical haemolytic uraemic syndrome (aHUS) or membranoproliferative glomerulonephritis (MPGN-II) (also known as dense deposit disease (DDD)), and ocular diseases like age-related macular degeneration (AMD)[12-13]. Moreover, many aHUS-associated polymorphisms and mutations were found both in RCA proteins and in the central complement components C3 and factor B[14], suggesting an essential role of a proportionate level of complement activation in tissue protection. Detailed structural insight into RCA complexes with their targets (C3b and C4b) is therefore critical for understanding the role of regulators in health and disease.

The complement regulator MCP is a trans-membrane protein that is widely expressed on human cells[15]. MCP only has cofactor activity yet is a potent complement inhibitor of all three pathways by binding to both C3b and C4b[16]. Both C3b-MCP and C4b-MCP allow binding of factor I, which cleaves C3b or C4b at two sites present in their respective 'complement C1r/C1s, UEGF, BMP1' (CUB) domains. MCP contains four CCP domains at the N-terminus followed by a serine/threonine-rich stretch, a trans-membrane region and a short cytoplasmic tail[17]. Truncated constructs of MCP showed that the first domain (CCP1) is not required for C3b binding or cofactor activity, whereas CCP2 only has a minor effect on C3b binding but is necessary for its cofactor activity. Importantly, both CCP3 and CCP4 are essential for C3b binding and cofactor activity of MCP[18].

Because complement exerts a primary immune response to microbial invasion, many pathogens developed RCA-related strategies to evade complement activation. Bacteria like *Neisseria meningitidis* and *Borrelia burgdorferi* express surface proteins that recruit host FH to their surface[19-20]. On the other hand, many orthopox viruses encode soluble proteins, which are secreted by virus-infected cells and structurally and functionally mimic human RCA. The highly virulent variola virus, for example, secretes a protein called smallpox inhibitor of complement enzymes (SPICE), consists of four CCP domains and is a potent complement regulator with both decay-acceleration and cofactor activity[21]. SPICE consists of 244 amino acids and has ~33% and ~26% sequence identity with human MCP and the N-terminal four CCP domains of human FH, FH(1-4), respectively[22]. SPICE is highly homologous to the vaccinia virus complement control protein (VCP); the two proteins differ by only 11 amino-acid residues in domains 2 to 4 (CCP2-4). SPICE is ~100-fold stronger than VCP in cofactor activity. Mutagenesis studies showed that four residues (Tyr98, Tyr103, Lys108, and Lys120 in SPICE *versus* His98, Ser103, Glu108 and Glu120 in VCP) located in CCP2 account for the activity enhancement of SPICE[23]. Among them, K120E contributes most to the difference in activity, suggesting the importance of charged interactions[23-24]. Phylogenetic analysis, as well as the structural and functional homology, suggests that the viral and human complement regulators most likely evolved from a common ancestor[25].

A first insight into the interaction between RCA proteins and complement activation fragments was provided by the crystal structure of C3b in complex with domains CCP1-4 of FH, referred to as C3b-FH(1-4). This structure revealed an extensive contact area between C3b and the regulator, which involved multiple domains of C3b and all four N-terminal domains of FH[26]. Structure comparison of C3b-FH(1-4) with C3bBb derived from an inhibitor-stabilized convertase dimer,

$(C3bBb\text{-}SCIN)_2$ (ref. 27), combined with structure-based sequence alignment and mutagenesis data of DAF[28], suggested that FH domains CCP1-2 are directly involved in decay acceleration and that domains CCP3-4 have a supportive role in binding FH(1-4) to C3b. Cofactor activity requires the first three domains, CCP1-3, of FH; whereas, the first four CCP1-4 domains show cofactor activity comparable to full-length of FH[26,29]. FH only binds to C3b but not C4b, yet shows both cofactor and decay-acceleration activities towards the alternative pathway convertase. While MCP binds to and mediates the degradation of both C3b and C4b, it lacks any decay acceleration function. SPICE, on the other hand, exerts cofactor activity to C3b and C4b, but only interferes with the decay of the C4b2a convertase. Mutations in the NH_2-terminal segment of α'-chain (α'NT) of C3b resulted in impaired interaction and cofactor activity of FH and CR1, which is in agreement with the interactions observed between CCP1-2 of FH and α'NT region of C3b in the C3b-FH(1-4) crystal structure[26,30-31]. In contrast, mutations in α'NT region do not have an effect on C3b binding and cofactor activity of MCP[31-32]. Moreover, mutations in CCP4 of MCP indicated that the binding of this domain is inconsistent with the binding mode observed for FH CCP4 in the crystal structure of the C3b-FH(1-4) complex[33]. These data would suggest that MCP binds C3b in a different way than FH. SPICE, and particular its fourth domain, is in sequence more similar to MCP than FH (SPICE CCP4 has 38% sequence identity to MCP and 31% to FH) nevertheless it has both decay accelerating and cofactor activities as does FH. We determined the crystal structures of C3b in complex with MCP and SPICE to characterize the similarities and differences in C3b-regulator interactions and the structural requirement for cofactor and decay-accelerating activities. Analysis of the structural information and functional data highlights the critical element of complement regulatory activities and helps to explain the variable binding and activities for these homologous proteins.

RESULTS AND DISCUSSION

Structure determinations of C3b-MCP and C3b-SPICE

MCP could be produced at high purity from both bacterial (*E. coli*) and mammalian (HEK293) expression systems for crystallization and functional studies, respectively. Whereas expression in *E. coli* did not result in N-glycosylation at any of the 3 known sites, this construct is active in cofactor activity assay (**Supplementary Fig. 1a**). When evaluated for C3b binding by surface plasmon resonance (SPR), the *E.coli*-derived MCP showed high affinity with a K_D value of 350 nM (**Supplementary Figs. 2a** and **2b**). This affinity obtained with enzymatically deposited C3b is

in a similar range as recently published SPR data for the interaction of soluble MCP to randomly immobilized C3b (K_D ~1 µM)[34]. Importantly, MCP produced in mammalian cells showed a highly comparable activity profile (**Supplementary Fig. 1b**); thereby confirming that glycosylation does not essentially contribute to C3b binding. Crystals could be obtained after mixing C3b and MCP in a 1:1 molar ratio to a concentration of 8 mg/ml. Diffraction data was collected to 2.4-Å resolution and the structure was solved by molecular replacement (for data and model statistics see **Table 1**).

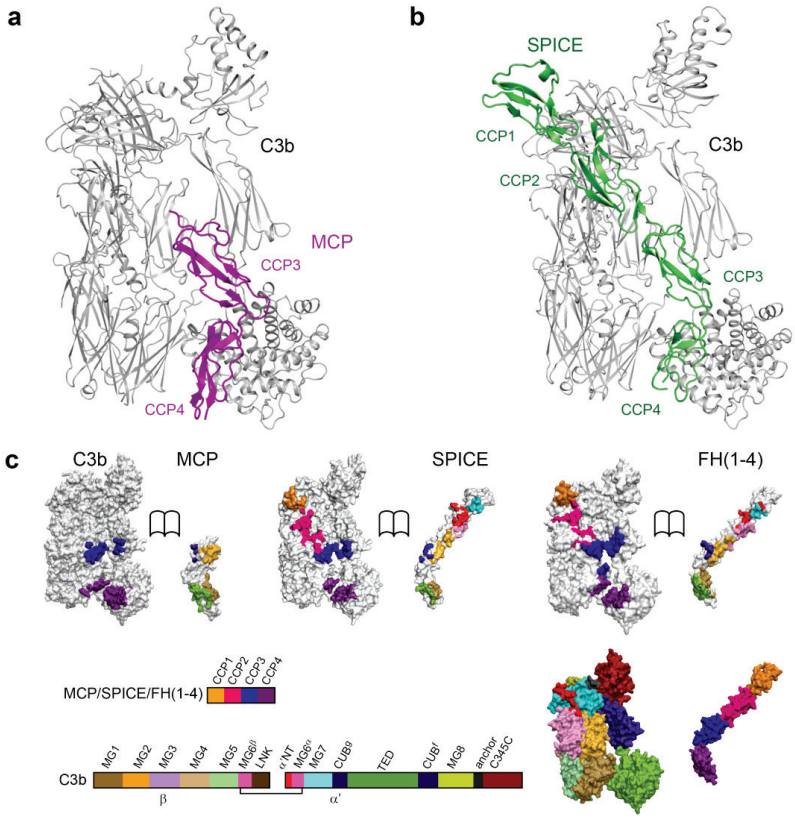

Figure 1 Structure of C3b-MCP and C3b-SPICE. Crystal structures of the C3b-MCP (**a**) and C3b-SPICE (b) complexes are shown in cartoon representation. Both MCP (pink) and SPICE (green) form a similar, extended interface with C3b (gray). (**c**) Opened view of the footprint of each complex interface. C3b and regulator domains are colored according to the color scheme depicted below. A schematic surface representation of the domain organization of regulators and C3b corresponding to this color scheme is shown at the bottom right.

The final model contains all domains of C3b but only domains CCP3 and 4 of MCP (**Fig. 1a**); discontinuous density was observed for the C-terminal tail of domain CCP2, but was insufficient

to model any residues of CCP2 (**Supplementary Fig. 3b**). Finally, no density was present for CCP1 of MCP. The missing density for CCP1-2 is likely due to lack of interactions, which causes disorder in domain positioning.

Similar to MCP, SPICE could be successfully expressed and refolded from *E. coli* with high purity. Recombinant SPICE showed an affinity of 1.2 μM affinity to C3b (**Supplementary Figs. 2a** and **2b**) when measured under the same conditions as MCP. Whereas no binding data for C3b under physiological buffer conditions are available in the case of SPICE, previous studies in low salt buffer also indicated a stronger binding of MCP when compared with SPICE, yet the K_D difference observed here is much smaller[35]. On the other hand, SPICE bound much stronger to C3b than recombinant FH(1-4)[26]. Mixing of C3b and SPICE in 1:1 molar ratio to a concentration of 8 mg/ml again yielded crystals that contained both components. The structure of C3b in complex with SPICE was determined to 2.6-Å resolution (for data and model statistics see **Table 1**). In contrast to the complex with MCP; all four CCP domains were visible in the electron density map in the case SPICE; however CCP4 was poorly defined (**Supplementary Fig. 3d**). We choose to include the fourth CCP domain in the model for sake of completeness and have set the occupancy of residues in CCP4 domain to zero.

C3b offers a common preformed site for regulator binding

Both the C3b-MCP and C3b-SPICE complexes show C3b in a highly similar manner that observed in previously reported structures of C3b alone and in complex with other ligands [Refs]; therein, C3b is built by two chains, β (res. 1-645) and α' (res. 727-1,641), forming a ring-like core structure that consists of six macroglobulin (MG1-6) and a linker (LNK) domain, with domains MG7 and MG8 located above, CUB and the thioester-containing domain (TED) alongside the ring-like core, and the C-terminal C345C domain on top (**Fig. 1c**). This arrangement of C3b is obtained upon removal of the anaphylatoxin domain (res. 650-726) from C3, which induces large conformational changes in the structure[23,24]. These changes activate and expose the thioester for covalent attachment to target particles. Relocation of α'NT, MG7-8, CUB and TED domains are critical for forming the extended binding platform for the regulators[23].

As evident by the so-far resolved co-crystal structures of RCA proteins, MCP, SPICE and FH(1-4) share a common binding site on C3b (**Fig. 1c** and **Supplementary Fig. 4c**). Whereas the contact areas overlap fully between C3b-SPICE and C3b-FH(1-4), C3b-MCP utilizes only the bottom half

of the binding site consistent with the absence of CCP1-2 domains of MCP in the model. The extended binding site on C3b is formed by MG1-2 and MG6 of the ring-like core structure; MG7 together with the α'NT region at the top part; and, CUB and TED. Comparison of the C3b, C3b-MCP, C3b-SPICE and C3b-FH(1-4) structures shows only small variations up to 4.5° in domain positions of MG2-3,6-8 and minor rigid-body like rotations of up to 7.6° of domains MG1,4-5 and LNK (**Supplementary Fig. 4**). MCP, SPICE and FH(1-4) bridge interactions between CUB-TED and the C3b core domains; the orientations of CUB and TED domains vary up to 6.4°. The C-terminal C345C domain in C3b-SPICE differs up to 46.8° in orientation from that in C3b-MCP and C3b-FH(1-4), while C3b-MCP and C3b-FH(1-4) differ by only 3.9° from each other. The large deviation of C345C in C3b-SPICE is likely due to crystal packing effects; C3b-MCP and C3b-FH(1-4) have a similar packing while C3b-SPICE has a different packing. Overall, our analysis with an extended panel of regulators confirms that proteolytic activation of C3 into C3b induces conformational changes that yield an arrangement of the 12 domains of C3b that exposes a preformed binding site for MCP, SPICE and FH(1-4), and potentially other members of the RCA family and their viral mimics.

C3b-MCP features a shortened contact interface harboring disease-related residues

The crystal structure of the C3b-MCP complex revealed two contact sites mediated by domains CCP3 and CCP4 of MCP and domains MG1-2, CUB and TED of C3b (**Fig. 1a** and **1c**). As described above, domains CCP1 and CCP2 of MCP appear disordered, which implies that they do not significantly interact with C3b. This observation is consistent with binding studies of MCP deletion constructs, which showed that CCP1 has no and CCP2 has little contribution to C3b binding[33].

In some parts, the arrangement of the CCP3-4 domains in C3b-MCP differs markedly from that of FH in the C3b-FH(1-4) complex (**Fig. 2a**), despite that these domains dock onto the same site of C3b. Whereas MCP domain CCP3 is tilted by 8º, the CCP4 domain is rotated by 117º around its longitudinal axis and thus uses a different face of the domain to bind C3b (**Supplementary Fig. 4d**). Importantly, a cluster of residues in CCP4 of MCP that have previously described important for C3b binding[33] indeed participates in the observed C3b-MCP interactions in the crystal structure (**Fig. 2b**); whereas, these residues would have been mapped to a region outside the binding interface when assuming a similar arrangement as in C3b-FH(1-4). The mutagenesis data and the observed interaction site are further supported by the competitive binding of the GB24 antibody to

MCP for which Phe196 and Phe208 are essential[33]. The observed domain-domain orientation for CCP3-4 in the C3b-MCP complex differs by 10º from that observed in the structure of MCP (CCP1-4) in complex with the Ad11 knob domain[38] (**Fig. 2c**). Rigid-body docking of MCP to C3b by Persson *et al.* led to a model that suggested marked CCP3-4 inter-domain adjustments in MCP upon binding to C3b[38]; the discrepancy between this predicted model and the observed crystal structure can be explained by a combination of differential orientation of CCP3 when bound to C3b and in the distinct inter-domain orientation between domains CCP3 and 4. Intriguingly, superposing MCP domains CCP1-4 from the Ad11 knob complex[38] onto CCP3-4 in the C3b-MCP structure results in an overall arrangement of MCP in which domains CCP3-4 are bound to C3b whereas CCP1-2 bend away from C3b (**Fig. 2d**). All three potential glycosylation sites of MCP, i.e. Asn49 in CCP1, Asn80 in CCP2 and Asn239 in CCP4, point away from C3b, therefore suggesting that N-glycosylation would not interfere with C3b interactions (**Fig. 2d**). This observation is supported by our binding data that show minimal differences between MCP expressed in bacterial and HEK cells (**Supplementary Fig. 1a-b**), and by previous data about retained cofactor activity in absence of glycosylation. In the docking model described above, the same side of CCP1-2 in MCP would be facing C3b as FH CCP1-2 in the C3b-FH(1-4) complex. Importantly, though, this side of CCP1 is far more negatively charged in MCP than that of CCP1 in FH(1-4) (**Supplementary Fig. 5**). The overall charge distribution together with specific amino acid differences (such as Glu63 in MCP instead of Arg65 in FH, which is likely important for binding CCP1-2 linker region to the α'NT of C3b) may very likely explain the observed reduced binding of MCP domains CCP1-2 to C3b.

Domain CCP3 of MCP interacts with MG2 and CUB of C3b, burying a surface area of ~900 Å^2. The interactions with MG2 of C3b center around Leu150 and Ala152 of MCP, which form hydrogen bonds through their main-chain atoms to Ser159 and Ser157 of C3b, respectively (**Supplementary Fig. 6a**). The side chain of Tyr149 of MCP forms a hydrogen bond with Gln163 of C3b (**Supplementary Fig. 6a**). The residue Phe141 docks against the hydrophobic pocket formed by residues Met142, Gln155 and Ser157 of C3b (**Supplementary Fig. 6b**). Finally, the acidic residue Glu143 of MCP forms a salt bridge with Arg1288 of the CUB domain in C3b, thereby stabilizing the interactions between the hyper-variable loop (residue 140-146) of CCP3 in MCP and the CUB domain of C3b (**Supplementary Fig. 6b**).

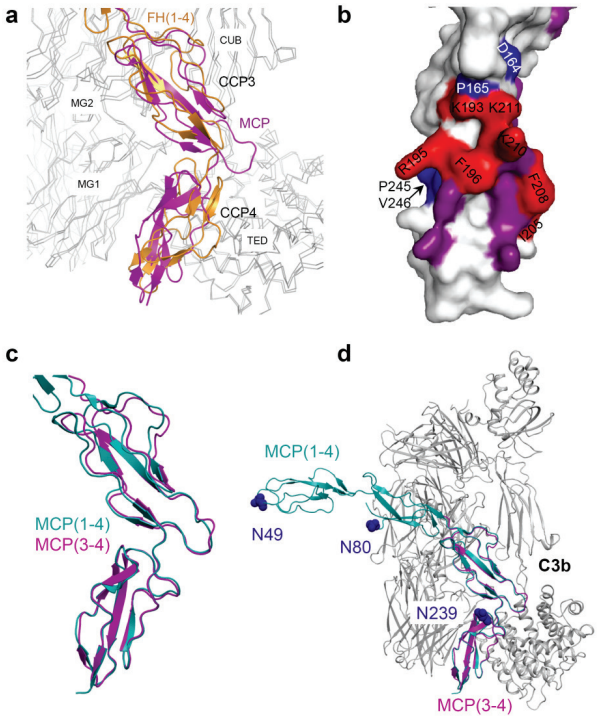

Figure 2 Structural analysis of C3b-MCP complex. (**a**) A structural comparison between C3b-FH(1-4) and C3b-MCP in the CCP3-4 region. (**b**) Mapping of the MCP residues that are important for C3b binding to the C3b-MCP complex structure. The interface is colored in purple. MCP mutants colored in red strongly affect C3b binding, while mutants colored in blue have medium effects[33]. These mutants are also at the complex interface. (**c**) Superposition of MCP(3-4) in C3b-MCP complex and MCP(1-4) in CD46-4D structure (PDB code: 3O8E). (**d**) A model of C3b-MCP(1-4) made by superposition of the C3b-MCP complex and MCP(1-4) in the CD46-4D complex based on domains of MCP CCP 3-4. Blue spheres indicate the position of N-linked glycans.

Domain CCP4 of MCP interacts with both MG1 and TED domains of C3b through a surface area of ~1500 Å^2. At the center of this interaction site are Phe196 and Phe208 of MCP; Phe196 interacts with a hydrophobic patch formed by residues of Val1068, I1073 and Ile1135 in the TED domain of C3b (**Supplementary Fig. 6c**). Lys210 of MCP CCP4 makes a salt bridge with Glu1131 in the TED domain of C3b (**Supplementary Fig. 6c**). Phe208 packs against the hydrophobic portion of Lys43 in MG1 domain of C3b (**Supplementary Fig. 6d**). The Lys43 residue in MG1 of C3b forms H-bond via its backbone nitrogen with the backbone of Gly207 of MCP CCP4 domain (**Supplementary Fig. 6d**). Analysis of this contact interface also reveals insight into the clinical significance of the C3b-MCP interaction. Three of the reported mutations and polymorphisms associated with aHUS map to this C3b-MCP interface: MCP mutations S206P and F208C, and C3b mutation A1072V (**Supplementary Fig. 6d and 7**)[14,39-40]. Whereas mutation S206A did not show a significant effect on neither C3b binding nor cofactor activity, the aHUS-associated mutant S206P has previously been shown to lead to severely reduced C3b binding and cofactor activity[33,39]. In latter case, proline may rearrange the backbone conformation and alter the local structure, causing reduced binding. Changing Phe208 to a cysteine abrogates the interaction of the

phenyl ring with the hydrophobic patch of TED, as discussed above, and thereby reduces C3b affinity. A change in C3b from Ala1072 to valine likely causes steric hindrance and hence reduced binding of both MCP and FH to C3b[14]. This reduced binding is stronger for MCP than for FH(1-4), which may be explained by the relatively larger role of CCP4 in binding to C3b for MCP than for FH(1-4).

C3b-SPICE combines shared homologies to both C3b-FH and C3b-MCP

The crystal structure of C3b-SPICE shows that SPICE domains CCP1-3 bind C3b in a highly similar manner as CCP1-3 of FH, while binding of domain CCP4 more closely resembles the orientation of CCP4 observed in C3b-MCP (**Fig. 3**). SPICE domains CCP2 and CCP3 differ in orientation only by 3 and 4º, respectively, from CCP2 and CCP3 of FH in C3b-FH(1-4). Domain CCP1, however, differs between C3b-SPICE and C3b-FH(1-4) by 19º. The weak electron density at the N-terminal 'top' side of FH CCP1 in C3b-FH(1-4) indicates flexibility in the domain orientation; only interactions between the 'bottom' C-terminal part of CCP1 and C3b are present and no additional crystal contacts are made to restrict the position of CCP1 in FH. In the case of SPICE, the density of CCP1 is well defined and the domain position is restrained by interactions at its C-terminal 'bottom' part with C3b and by crystal contacts with four neighboring C3b molecules. The CCP4 of SPICE differs in orientation from CCP4 of FH in C3b-FH(1-4) by 113º yet from CCP4 of MCP in C3b-MCP by only 5º; thus, SPICE CCP4 binds in a similar orientation as MCP CCP4. The observed CCP3-4 inter-domain orientation in C3b-SPICE differs by ~30° from the NMR structure of the closely related protein VCP[41] (**Supplementary Fig. 8**). Even though the orientation of CCP4 in C3b-SPICE could be defined by molecular replacement procedure, the resulting electron density is poorly defined (**Supplementary Fig. 2d**), which indicates that SPICE CCP4 associates very loosely with MG1 and TED of C3b. A fusion construct consisting of VCP domains CCP1-3 and MCP domain CCP4 showed increased binding affinity[42], supporting the notion that CCP4 domain of VCP and SPICE binds weaker to C3b than CCP4 of MCP.

Residues of domains CCP1-2 of SPICE show several interactions with the α'NT loop and MG7 domain of C3b (**Supplementary Fig. 6e, 6f** and **6g)**. Similar to FH, Arg65 located in the linker between CCP1 and 2 of SPICE likely plays a central role by making a hydrogen bond with the backbone of Glu737 in the α'NT loop of C3b (**Supplementary Fig. 6f** and **6j**). In addition, Arg65

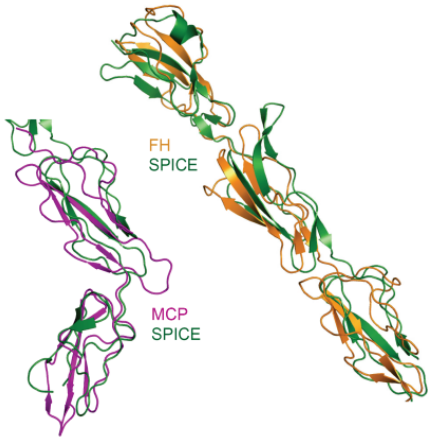

Figure 3 Structural comparison of SPICE with MCP and FH(1-4), respectively.

of SPICE forms intra-molecular contacts with the backbone atoms of residue Gly113 and may contribute to the rigidity of CCP1-2 domain interface (**Supplementary Fig. 6f**). Residues Ser69-Asp72, which form part of a β-strand in CCP2, make two salt bridges with C3b: the side chain of Arg71 with the side chain of Glu744 of C3b and Asp72 with Lys774 of C3b (**Supplementary Fig. 6g**). FH has, in part, a similar binding pattern in this region (compare **Supplementary Fig. 6g** to **6k**). The major difference is that FH contains a glycine instead of an arginine at equivalent position; in this case, Glu744 forms a hydrogen bond with the backbone of Gly71 of FH (**Supplementary Fig. 6k**).

In CCP3 two hydrogen bonds are formed by the backbones of Ser159 in MG2 of C3b and Gly150 of SPICE, and Ser157 in MG2 of C3b and Val152 of SPICE (**Supplementary Fig. 6h**). Similar interactions are also observed in C3b with MCP and FH(1-4) (**Supplementary Fig. 6a, 6h and 6l**). Whereas the hyper-variable loop (res. 141-146) is well defined in MCP and makes contacts to both MG2 and CUB domains of C3b, the density is poorly defined in the case SPICE. Nevertheless, Yadav *et al.* showed that mutating VCP Asp144 to Asn, the residue found in SPICE at this position, enhanced VCP binding to C3b 100-fold, up to a level of SPICE[23]. The previously described weaker binding of native VCP may therefore likely be explained by putative charge repulsion between VCP Asp144 and C3b Asp156 on MG2. In CCP4 only two contacts to C3b were observed in crystal structure: His189 makes a salt bridge with Glu1138 and Arg203 to Glu1134 in TED domain of C3b.

Implications for cofactor activity and decay acceleration

The crystal structures of C3b in complex with regulators MCP, SPICE and FH(1-4) display both clear common features and marked differences. SPICE and FH(1-4) share the same binding area for CCP1-3 on C3b (**Fig. 1c**). In both cases, CCP1-3 is the minimal fragment to retain cofactor activity, and the fourth CCP domain is required for the full activity[29,43]. Whereas CCP3 of MCP binds C3b in a similar position and orientation, CCP1-2 do not interact with C3b in the C3b-MCP structure and likely bend away from C3b (**Fig. 2d**). MCP and SPICE, on the other hand, share the C3b binding mode for CCP4, though CCP4 of SPICE appears only weakly bound to C3b. The orientation of CCP4 of FH is markedly different from that observed for MCP and SPICE.

Notwithstanding the structural differences, all three regulators have cofactor activity, which enable binding of the multi-domain protease factor I to the C3b-regulator complexes for cleavage of C3b at Arg1281-Ser1282 and Arg1298-Ser1299 in the CUB domain. Previous mutagenesis studies showed that four residues in CCP2 (Tyr98, Tyr103, Lys108, and Lys120) account for the activity enhancement of SPICE compared to VCP[23]; with the largest effect arising from a lysine at position 120 in SPICE instead of a glutamate in VCP[23-24]. The four residues are not located at the immediate C3b-SPICE interface, but are fully exposed in the C3b-SPICE structure (**Supplementary Fig. 9**), thereby indicating that they may affect the cofactor activity through differential binding to factor I rather than C3b. Because the equivalent residue of K120 is also a lysine (K119) in MCP, we decided to express several charge-reversed mutations (lysine to glutamate) in domains CCP2 and 3 of MCP in areas that are not involved in direct interactions with C3b. As expected, all these MCP mutants bind C3b (**Supplementary Fig. 10**). On the other hand, a fluid-phase cofactor activity assay shows that MCP mutants that include Lys119 to glutamate mutation (MCP-K119E, MCP-K110EK119E and MCP-K119EK133E) have severely reduced activity (**Supplementary Fig. 1**). Mutant MCP-K110E, which does not involve K119E, retains full activity when compared to wild-type MCP (**Supplementary Fig. 1c**). These data indicate that, in agreement with published data for SPICE, the CCP2 domain of MCP is important for cofactor activity, even though this domain is only loosely associated with C3b according to the crystallographic data. Furthermore, MCP with residues 127-134 in CCP3 substituted with the corresponding residues in DAF maintained 97% of C3b binding but lost all cofactor activity[33]. In the C3b-MCP structure, this loop is full exposed (**Fig. 4**) and is available for putative interactions

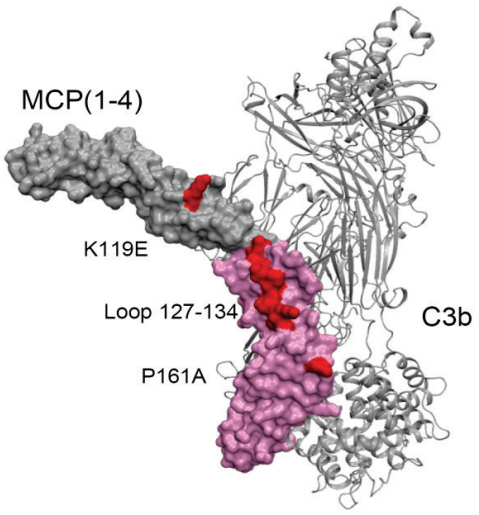

Figure 4 Implication for cofactor activity. A model of C3b-MCP(1-4) is shown in surface representation. Residue mutations that still bind to C3b but severely affect MCP cofactor activity are shown in red.

with factor I. Mutation of P161A in MCP, in a PxPxPxP motif (res. 159-165) that forms an exposed loop at the 'bottom' of CCP3 in MCP, also maintained 83% of C3b binding yet lost cofactor activity (**Fig. 4**)[33]. The double mutation D158A/P159A showed no effect on C3b binding and cofactor activity. Mutations G162A/P163A and D164A/P165A partially reduced both C3b binding and cofactor activity[33]. Asp164 makes an internal salt bridge between CCP3 and 4; putatively, the latter two double mutations affect the CCP3-4 orientation and hence result in reduced C3b binding. Thus, the available biochemical data indicates a direct role for the CCP2-3 domains in binding factor I.

The recent publication discussed two aHUS-associated mutants in CCP1 of FH: R35H and R60G. Arg60 is at C3b-FH interface, making salt bridge with Asp732 of C3b (**Supplementary Fig. 6i**). This mutant has reduced C3b binding and reduced cofactor and decay acceleration activity[30]. The other mutant R35H has comparable affinity to C3b and decreased cofactor activity, indicating CCP1 of FH may also contribute to FI binding[30]. FH has decay-acceleration activity, whereas MCP has not. Based on the structure of C3b-FH(1-4)[26] and mutagenesis data of DAF[28], it was proposed that the CCP1-2 domains of FH are responsible for decay acceleration by charge repulsion or steric hindrance with the Bb fragment in C3bBb[26]. The CCP1-2 domains of FH binds to the α'NT, MG6-7 region of C3b, whereas this is not the case in the C3b-MCP complex. This is in agreement with binding data that indicated that the α'NT of C3b is important for binding FH and CR1, regulators with decay-acceleration activity, *versus* MCP, which is a regulator without decay-acceleration activity. Binding of CCP1-2 to C3b involves several interactions (**Supplementary Fig. 6**). FH has an arginine (Arg65) in the CCP1-2 linker that makes hydrogen bonds to C3b. MCP has, instead, has a glutamic acid at the equivalent position and cannot make these interactions (**Supplementary Fig. 5**). Mutation of Lys126 to alanine or glutamic acid at the

equivalent position (i.e. in the CCP2-3 linker) in DAF leads to loss of decay acceleration[28]. Moreover, insertion of glycine residue after the CCP2-3 linker (after Lys127) also abrogates DAF activity, possibly because of additional flexibility in the CCP1-2 linker[28] or misalignment of the interactions surfaces of the molecules. Thus, the structural data of C3b-FH(1-4) *versus* C3b-MCP underscore the critical importance of CCP1-2 binding to the α'NT and MG7 domain for decay-acceleration activity.

CONCLUDING REMARKS

The structures of C3b-MCP, C3b-SPICE and C3b-FH(1-4) show that all three regulators bind to the same site on C3b. The structural data support the biochemical data that show variation in contributions among the four CCP domains to the overall binding of the various regulators. According to the three crystal structures, MCP almost entirely relies on CCP3-4 for binding to C3b, whereas SPICE depends on CCP1-3 and FH(1-4) uses all four domains for optimal binding (where CCP1 only contributes with the C-terminal 'bottom' side close to the CCP1-2 linker to C3b binding). Though poor electron density for a whole domain may be associated with limited interactions, and thus low binding affinity, the reverse may not be true, because additional crystal contacts may restrict domain positioning and thus yield good electron density. Overall, regulators with decay-acceleration activity have strong binding of CCP1-3 to C3b (equivalent to CCP2-4 in the case of DAF). This supports the hypothesis that CCP1-2 binding to α'NT and MG7 of C3b is functionally critical for dissociating fragment Bb from C3b and preventing formation of convertases by blocking the factor B binding site on C3b[26]. Cofactor activity depends critically on domains CCP2-3. We hypothesize that binding of factor I to CCP2-3 of e.g. human FH, MCP or viral SPICE, and the C345C of C3b or C4b, positions the serine protease domain towards the cleavage sites in the CUB domains. So far, no functional data are available that involves CCP4 directly in FI binding. Possibly, CCP4 contributes only to C3b binding affinity. The marked difference in CCP4 orientation of FH *versus* MCP and SPICE in binding to C3b may be related to surface recognition by domains CCP6-7 (ref. 44) or binding of CCP19-20 to the TED domain[45-46] of the soluble regulator FH. Unfortunately, no structure for C4 or C4b is available to correlate the structural data of alternative pathway inhibition with regulation of the classical and lectin pathways. Nevertheless, it is likely that the functional roles of CCP1-2 and CCP2-3 in decay-acceleration and cofactor activity, respectively, are similar in the classical and lectin pathways. However, the amino acid differences between C3b and C4b will affect the binding interactions with the regulators. Putatively, the diverse domain binding patterns are related to

regulators binding to the two different targets, C3b and C4b.

METHODS

Protein purification and crystallization. Complement component C3b was obtained by isolating C3 from fresh human plasma, followed by specific cleavage of C3 into C3b by recombinant factor B and factor D as described previously[47]. Iodoacetamide was used to block the nascent thioester for preventing dimerization of C3b[26]. Both the extracellular CCP1-4 domains of human MCP and full-length SPICE (CCP1-4) were expressed in *E. coli* and refolded from inclusion bodies according to established protocols[23]. The MCP mutants were generated by QuikChange site-directed mutagenesis and expressed in human embryonic kidney 293 cells stably expressing EBNA1 (HEK293E). Medium was harvested five days post transfection by centrifugation (15 minutes at 1,000 x g) and dialyzed in phosphate-buffered saline (PBS, pH 7.4) overnight. Sample was purified by Ni-NTA affinity chromatography and eluted with PBS buffer containing 500 mM imidazole. The protein containing fractions were collected and dialyzed against PBS buffer. The protein was further purified by size exclusion column using PBS buffer. The protein containing fractions were pooled and concentrated.

Crystallization and data collection. Purified C3b was mixed with MCP and SPICE, respectively, in a 1:1 molar ratio to a final concentration of 8.0 mg/ml. For C3b-MCP complex, the crystallization experiments were performed by vapour diffusion using a HoneyBee robot (Genomic Solutions). Sitting drops were set up by mixing 0.15 µl of complex sample with 0.24 µl of mother liquor at 18 ºC. The drops were equilibrated over a reservoir solution consisting of 100mM $(NH_4)_2$ Citrate, 7% PEG 3350, 5mM L-Glutathione and 50mM bis-tris-propane pH 6.5. The crystals appeared after 2-3 days. Crystals were harvested after one week, cryoprotected by reservoir solution supplemented with 20% ethylene glycol, and flash-frozen in liquid N_2 for data collection. For C3b-SPICE the crystallization experiments were performed by vapour diffusion using hanging drops at 18 ºC. 0.7 µl of complex sample was mixed with 0.7 µl of mother liquor containing 75 mM NH_4I and 3.5% PEG 3350. Diffraction quality crystals were obtained by microseeding with a cat's whisker from the poor quality crystals obtained from initial screens. The crystals appeared over night and continued to grow for about one week. The crystals were harvested for data collection by soaking in reservoir solution containing 18% glycerol as a cryoprotectant and flash-frozen in liquid N_2. Diffaction data for both complexes were collected at ESRF beam-line ID14-EH4 and ID29 in Grenoble, France. The data were processed by MOSFLM[48] and scaled using SCALA[49].

Structure determination and refinement. Both C3b-MCP and C3b-SPICE complexes were determined by molecular replacement using Phaser[50]. Coordinates of C3c (PDB code: 2A74)[51] and C3b-FH(1-4) (PDB code: 2WII)[26] were used as initial search models. The models were improved by manual building using COOT[52] and refined with PHENIX[53].

Cofactor activity assay. The Cofactor activity assay was performed in PBS buffer using the same protocol as

described previously[23]. In brief, 1.0 µg of purified C3b, 0.3µg of MCP or the MCP mutants were mixed with 7 ng of factor I in a total volume of 6µl. The reactions were stopped by addition of SDS-PAGE sample loading buffer containing β-mercaptoethanol. The cleavage products were analyzed by SDS-PAGE.

Table 1 Data collection and refinement statistics.

	C3b-MCP	C3b-SPICE
Data collection		
Space group	$P2_12_12$	P1
Cell dimensions		
a, b, c (Å)	232.6, 82.4, 129.9	68.9, 83.3, 127.4
α, β, γ (°)	90, 90, 90	75.0, 76.2, 68.5
Resolution (Å)	40-2.4 (2.53-2.4)	45.0-2.6 (2.74-2.6)
R_{merge}	0.072 (0.399)	0.088 (0.384)
$I/\sigma I$	12.9 (2.9)	5.8 (1.9)
Completeness (%)	99.7 (98.5)	97.4 (96.4)
Multiplicity	3.8 (3.2)	2.0 (1.9)
Refinement		
Resolution (Å)	36.4-2.4	42.4-2.6
Reflections	98,012	75,212
R_{work}/R_{free}	0.204/0.241	0.230/0.267
Number of atoms	13,772	13,828
Protein	13,015	13,506
Ligand/ion	286	146
Water	471	176
B-factors (Å^2)		
Protein	59.1	95.4
Ligand/ion	77.7	117.0
Water	50.9	71.8
R.m.s deviations		
Bond lengths (Å)	0.006	0.003
Bond angles (°)	0.890	0.592

ACKNOWLEDGEMENTS

We gratefully thank the European Synchrotron Radiation Facility (ESRF) for the provision of synchrotron radiation

facilities and beamline scientists of the ESRF and the European Molecular Biology Laboratory for assistance. The authors gratefully thank Federico Forneris for carefully reading the manuscript. This work was supported by a "Top" grant (700.54.304 to P.G.) by the Council for Chemical Sciences of the Netherlands Organization for Scientific Research (NWO-CW) and NIH grants AI68730, AI30040, AI72106 and GM62134 (to J.D.L.) and EY20633 (to J.D.L. and D.R.).

REFERENCES

1. Ricklin, D., Hajishengallis, G., Yang, K. & Lambris, J.D. Complement: a key system for immune surveillance and homeostasis. *Nat Immunol* **11**, 785-797 (2010).
2. Trouw, L.A., Blom, A.M. & Gasque, P. Role of complement and complement regulators in the removal of apoptotic cells. *Mol Immunol* **45**, 1199-1207 (2008).
3. Law, S.K. & Dodds, A.W. The internal thioester and the covalent binding properties of the complement proteins C3 and C4. *Protein Sci* **6**, 263-274 (1997).
4. Zipfel, P., Mihlan, M. & Skerka, C. The Alternative Pathway of Complement: a Pattern Recognition System. in *Current Topics in Innate Immunity* 80-92 (2007).
5. Okroj, M., Heinegard, D., Holmdahl, R. & Blom, A.M. Rheumatoid arthritis and the complement system. *Ann Med* **39**, 517-530 (2007).
6. Sjoberg, A.P., Trouw, L.A. & Blom, A.M. Complement activation and inhibition: a delicate balance. *Trends Immunol* **30**, 83-90 (2009).
7. Liszewski, M.K., Farries, T.C., Lublin, D.M., Rooney, I.A. & Atkinson, J.P. Control of the complement system. *Adv Immunol* **61**, 201-283 (1996).
8. Hellwage, J.*, et al.* Complement C3b/C3d and cell surface polyanions are recognized by overlapping binding sites on the most carboxyl-terminal domain of complement factor H. *J Immunol* **169**, 6935-6944 (2002).
9. Blom, A.M., Webb, J., Villoutreix, B.O. & Dahlback, B. A cluster of positively charged amino acids in the C4BP alpha-chain is crucial for C4b binding and factor I cofactor function. *J Biol Chem* **274**, 19237-19245 (1999).
10. Zipfel, P.F. & Skerka, C. Complement regulators and inhibitory proteins. *Nat Rev Immunol* (2009).
11. Kirkitadze, M.D. & Barlow, P.N. Structure and flexibility of the multiple domain proteins that regulate complement activation. *Immunol Rev* **180**, 146-161 (2001).
12. Meri, S. Loss of Self-Control in the Complement System and Innate Autoreactivity. *Ann NY Acad Sci* **1109**, 93-105 (2007).
13. Waters, A.M. & Licht, C. aHUS caused by complement dysregulation: new therapies on the horizon. *Pediatr Nephrol* **26**, 41-57 (2011).
14. Fremeaux-Bacchi, V.*, et al.* Mutations in complement C3 predispose to development of atypical hemolytic uremic syndrome. *Blood* **112**, 4948-4952 (2008).

15. Johnstone, R.W., Loveland, B.E. & McKenzie, I.F. Identification and quantification of complement regulator CD46 on normal human tissues. *Immunology* **79**, 341-347 (1993).
16. Seya, T. & Atkinson, J.P. Functional properties of membrane cofactor protein of complement. *Biochem J* **264**, 581-588 (1989).
17. Post, T.W.*, et al.* Membrane cofactor protein of the complement system: alternative splicing of serine/threonine/proline-rich exons and cytoplasmic tails produces multiple isoforms that correlate with protein phenotype. *J Exp Med* **174**, 93-102 (1991).
18. Adams, E.M., Brown, M.C., Nunge, M., Krych, M. & Atkinson, J.P. Contribution of the repeating domains of membrane cofactor protein (CD46) of the complement system to ligand binding and cofactor activity. *J Immunol* **147**, 3005-3011 (1991).
19. Schneider, M.C.*, et al.* Functional significance of factor H binding to Neisseria meningitidis. *J Immunol* **176**, 7566-7575 (2006).
20. Hellwage, J.*, et al.* The complement regulator factor H binds to the surface protein OspE of Borrelia burgdorferi. *J Biol Chem* **276**, 8427-8435 (2001).
21. Rosengard, A.M., Liu, Y., Nie, Z. & Jimenez, R. Variola virus immune evasion design: expression of a highly efficient inhibitor of human complement. *Proc Natl Acad Sci USA* **99**, 8808-8813 (2002).
22. Kotwal, G.J. & Moss, B. Vaccinia virus encodes a secretory polypeptide structurally related to complement control proteins. *Nature* **335**, 176-178 (1988).
23. Yadav, V.N., Pyaram, K., Mullick, J. & Sahu, A. Identification of hot spots in the variola virus complement inhibitor (SPICE) for human complement regulation. *J Virol* **82**, 3283-3294 (2008).
24. Sfyroera, G., Katragadda, M., Morikis, D., Isaacs, S.N. & Lambris, J.D. Electrostatic Modeling Predicts the Activities of Orthopoxvirus Complement Control Proteins. *J Immunol* **174**, 2143-2151 (2005).
25. Ciulla, E., Emery, A., Konz, D. & Krushkal, J. Evolutionary history of orthopoxvirus proteins similar to human complement regulators. *Gene* **355**, 40-47 (2005).
26. Wu, J.*, et al.* Structure of complement fragment C3b-factor H and implications for host protection by complement regulators. *Nat Immunol* **10**, 728-733 (2009).
27. Rooijakkers, S.H.*, et al.* Structural and functional implications of the alternative complement pathway C3 convertase stabilized by a staphylococcal inhibitor. *Nat Immunol* **10**, 721-727 (2009).
28. K.*, et al.* Structure-based mapping of DAF active site residues that accelerate the decay of C3 convertases. *J Biol Chem* **282**, 18552-18562 (2007).
29. Hocking, H.G.*, et al.* Structure of the N-terminal region of complement factor H and conformational implications of disease-linked sequence variations. *J. Biol. Chem.*, M709587200 (2008).
30. Pechtl, I.C., Kavanagh, D., McIntosh, N., Harris, C.L. & Barlow, P.N. Disease-associated N-terminal complement factor H mutations perturb cofactor and decay-accelerating activities. *J Biol Chem* **286**, 11082-11090 (2011).

31. Oran, A.E. & Isenman, D.E. Identification of residues within the 727-767 segment of human complement component C3 important for its interaction with factor H and with complement receptor 1 (CR1, CD35). *J Biol Chem* **274**, 5120-5130 (1999).
32. Lambris, J.D.*, et al.* Dissection of CR1, factor H, membrane cofactor protein, and factor B binding and functional sites in the third complement component. *J Immunol* **156**, 4821-4832 (1996).
33. Liszewski, M.K.*, et al.* Dissecting Sites Important for Complement Regulatory Activity in Membrane Cofactor Protein (MCP; CD46). *J. Biol. Chem.* **275**, 37692-37701 (2000).
34. Alcorlo, M.*, et al.* Unique structure of iC3b resolved at a resolution of 24 A by 3D-electron microscopy. *Proc Natl Acad Sci USA* **108**, 13236-13240 (2011).
35. Liszewski, M.K.*, et al.* Structure and Regulatory Profile of the Monkeypox Inhibitor of Complement: Comparison to Homologs in Vaccinia and Variola and Evidence for Dimer Formation. *J Immunol* **176**, 3725-3734 (2006).
36. Janssen, B.J., Christodoulidou, A., McCarthy, A., Lambris, J.D. & Gros, P. Structure of C3b reveals conformational changes that underlie complement activity. *Nature* **444**, 213-216 (2006).
37. Wiesmann, C.*, et al.* Structure of C3b in complex with CRIg gives insights into regulation of complement activation. *Nature* **444**, 217-220 (2006).
38. Persson, B.D.*, et al.* Structure of the extracellular portion of CD46 provides insights into its interactions with complement proteins and pathogens. *PLoS Pathog* **6**(2010).
39. Richards, A.*, et al.* Mutations in human complement regulator, membrane cofactor protein (CD46), predispose to development of familial hemolytic uremic syndrome. *Proc Natl Acad Sci USA* **100**, 12966-12971 (2003).
40. Caprioli, J.*, et al.* Genetics of HUS: the impact of MCP, CFH, and IF mutations on clinical presentation, response to treatment, and outcome. *Blood* **108**, 1267-1279 (2006).
41. Kirkitadze, M.D.*, et al.* Central modules of the vaccinia virus complement control protein are not in extensive contact. *Biochem J* **344 Pt 1**, 167-175 (1999).
42. Ahmad, M.*, et al.* Domain swapping reveals complement control protein modules critical for imparting cofactor and decay-accelerating activities in vaccinia virus complement control protein. *J Immunol* **185**, 6128-6137 (2010).
43. Mullick, J.*, et al.* Identification of Complement Regulatory Domains in Vaccinia Virus Complement Control Protein. *J. Virol.* **79**, 12382-12393 (2005).
44. Prosser, B.E.*, et al.* Structural basis for complement factor H linked age-related macular degeneration. *J. Exp. Med.* **204**, 2277-2283 (2007).
45. Kajander, T.*, et al.* Dual interaction of factor H with C3d and glycosaminoglycans in host-nonhost discrimination by complement. *Proc Natl Acad Sci USA* (2011).
46. Morgan, H.P.*, et al.* Structural basis for engagement by complement factor H of C3b on a self surface. *Nat Struct Mol Biol* **18**, 463-470 (2011).
47. Forneris, F.*, et al.* Structures of C3b in complex with factors B and D give insight into complement convertase

formation. *Science* **330**, 1816-1820 (2010).

48. Leslie, A.G.W. Recent changes to the MOSFLM package for processing film and image plate data. *Joint CCP4 + ESF-EAMCB Newsletter on Protein Crystallography* **26**(1992).

49. Evans, P. Scaling and assessment of data quality. *Acta Crystallographica Section D* **62**, 72-82 (2006).

50. McCoy, A.J.*, et al.* Phaser crystallographic software. *Journal of Applied Crystallography* **40**, 658-674 (2007).

51. Janssen, B.J.*, et al.* Structures of complement component C3 provide insights into the function and evolution of immunity. *Nature* **437**, 505-511 (2005).

52. Emsley, P. & Cowtan, K. Coot: model-building tools for molecular graphics. *Acta Crystallogr D Biol Crystallogr* **60**, 2126-2132 (2004).

53. Adams, P.D.*, et al.* PHENIX: building new software for automated crystallographic structure determination. *Acta Crystallogr D Biol Crystallogr* **58**, 1948-1954 (2002).

Chapter 5

Summarizing discussion

Complement system is an ancient branch of mammalian immune defense, which has evolved to respond rapidly to invading pathogens, leading to various immune effector functions that efficiently recognize and eliminate these pathogens in blood. This system can be activated either by specific recognition or by spontaneous activation of the central component C3. The complement pathways converge at the formation of C3 convertase, which is the central enzyme complex in the amplification loop of the complement responses. The complement system is tightly regulated at multiple levels to protect the host cells from unwanted self attacks. For such host protection to take place, a group of complement regulators known as the RCA proteins are essential, as they carefully modulate the amount of C3 convertase and major oposonins C3b molecules on host cell surface. Several mutations and polymorphisms in the genes encoding complement regulators have been identified. Growing evidence now supports the strong association between the dysfunction of complement regulation and certain kidney or ocular diseases. In this thesis, we use X-ray crystallography to determine complex structures central to complement activation and regulation. The structural knowledge in combination with functional studies, help to elucidate molecular mechanisms of biological activities, understand bacterial and viral evasion strategies, explain mutations associated with complement-mediated diseases, and make the complement cascade an intriguing target for therapeutic development.

Structural insights into C3 convertase formation

Initiation of complement cascades results in the formation of the C3 convertase, a highly specific enzyme complex that cleaves C3 into the active form C3b and generates additional C3 convertase via the "tick-over loop". The C3 convertase plays an important role in amplification of complement responses. Excess C3 convertase formation on the cell surface may lead to uncontrolled complement activation leading to cell injury or damage. To prevent that, the C3 convertase has a sophisticated self regulatory mechanism: the serine protease fragment is present in blood as the pro-enzyme prior to the convertase formation; it only has proteolytic activity when bound in the C3 convertase complex. Additionally, the C3 convertase is short-lived, which ensures an efficient but brief boost of complement amplification on the target surface. Such metastability is important for regulation of complement responses, but makes the structural study of C3 convertase challenging.

We were able to stabilize the C3 convertase using a staphylococcal inhibitor SCIN, which freezes the enzyme complex in an inactive form that no longer has proteolytic activity, but has a longer

half life. As showed in **Chapter 2**, a complex containing three components C3b, Bb and SCIN is formed in solution, which is stable for more than two weeks at 4 ℃. The complex was purified and the size of the complex was estimated by analytical ultracentrifugation. The data suggested that SCIN induces the formation of the convertase dimer with a size of approximately 500 kDa. We obtained crystals using freshly purified samples of the complex. Using X-ray crystallography, the best dataset diffracted to a resolution of 3.9 Å, which gave the first reported atomic structure of C3 convertase. The overall structure shows a dimer of C3 convertase complex bridged by two SCIN molecules. The two C3b molecules sit in the center of the dimer with two protease fragments Bb positioned symmetrically outside. SCIN has extensive contact sites with both C3b and Bb in one convertase, and with the other C3b molecule of the opposing C3 convertase.

These results allow us for the first time to describe the structure of C3 convertase in detail. The monomeric C3 convertase structure derived from the dimer complex shows a loose arrangement. The major contact site is formed by the VWA domain of protease fragment Bb and the C-terminal C345C domain of C3b. There is no contact site observed in the crystal structure between serine protease domain of Bb and the non-catalytic unit C3b. The most notable finding at the complex contact site is that the Mg^{2+} ion bound in MIDAS chelates with the carboxyl group of the asparagine residue at C-terminus of C3b. The observation explains why the previous mutagenesis studies could not identify any acidic residue in C3b as the natural ligand for chelation with the divalent ion in the MIDAS. The observed interface highlights the loops adjacent to MIDAS that directly contribute to C3b binding, which is consistent with the previous mutagenesis studies. On the other side, the interfaces on C3b site are composed by the residues in C345C domain, which is also supported by the functional studies on hybrid proteins where the residues were substituted by the corresponding residues in CVF.

Both components C3b and Bb in convertase complex shows similar domain arrangement compared to their isolated states. The most significant variation is the position of C345C domain, which shows the most diverse orientations in the C3b structures determined so far. This observation suggests the intrinsic flexibility of this domain. In the catalytic centre of the protease fragment Bb, no major changes were observed in the complex structure, which shows a typical nearly-active conformation similar to the free Bb structure and its classical pathway homolog C2a. We could not determine the precise position of each atom in the catalytic center due to the limited resolution of our dataset. Most likely, the binding regulatory domain VWA to C3b does not have an allosterical influence on the catalytic center of serine protease domain.

What determines the enzyme activity of C3 convertase? We proposed an enzyme-substrate binding model based on the intended C3b dimer interface observed in dimer complex, as this site has been shown to be important for the substrate binding of C3 convertase. In the proposed model, the SP domain of Bb is positioned in a productive orientation but is ~30 Å away to the scissile loop of the substrate C3. The flexible C345C domain may have a biological meaning by swinging the protease domain closer to its substrate. Moreover, the surface loops of SP domain is likely to be rearranged, which may provide additional contact sites, which allows the scissile loop to bind properly into the substrate pocket and induce a fully active form of the catalytic centre. This enzyme-substrate model is further supported by the recent published C5-CVF complex structure, in which the substrate C5 binds to the non-catalytic unit C3b in the convertase in a similar manner to the C3b homodimer that observed in the SCIN-convertase structure[1].

"*The characteristic unidirectionality of alternative complement pathway C3 convertase decay may simply result from the low intrinsic association of 'univalent' Bb for the C3b subunit*" as pointed out by Pryzdial and Isenman in 1987 is one of the possible explanations for spontaneous decay of C3 convertase[2]. It has been well-characterized that the irreversible dissociation of C3 convertase is an important self-regulation mechanism to keep complement activation in control. However, the molecular mechanisms of such irreversible associations are not fully understood. Now we have the first C3 convertase structure, which shows Bb in complex with its natural ligand C3b. There is no major conformational change in bound Bb compared to the isolated Bb. In both structures, the major C3b binding sites, i.e. MIDAS, are in the open conformation. Thus, if it is not due to conformational changes, what can be the reason for the spontaneous decay of the convertase? We used surface plasmon resonance to study the binding kinetic of FB to C3b in detail, which indicates that a slow association and dissociation kinetics is likely to determine the irreversible dissociation and metastability of convertase complex. Thus, the results provide further evidence that the irreversible dissociation could be determined by the binding kinetics rather than the conformational changes at complex interface.

The complex structure gives a precise detailed molecular mechanism that explains how SCIN specifically targets C3 convertase and blocks all three complement pathways. SCIN sits in between C3b and Bb and provides extensive contacts to both components. Thus, by offering additional interaction sites, SCIN stabilizes C3 convertase on the bacterial surface. SCIN blocks C3 convertase by freezing the enzyme in its inactive form so that Bb cannot reach its substrate C3.

The structure also explains the active sites of SCIN identified previously by mutagenesis studies. Based on the complex structure obtained, we were able to generate a SCIN chimera that results a monomeric stable SCIN-convertase complex in the inactive form. This result provides further motivation to elucidate the biological action of SCIN as a specific convertase inhibitor and stabilizer.

Structural insights into complement regulation

The efficient machinery in which complement fights infections and clears cellular debris requires tight regulation to avoid undesirable attacks on healthy host cells. As a consequence, mammals express various cell-surface bound and soluble complement regulators, which degrade C3b into fragments that no longer form C3 convertase and modulate the decay rate of C3 convertase to stop C3b production. These regulators has essential role in host protection thus defects in genes encoding complement regulators increase the risk of certain diseases. One evasion strategy that virus use to avoid complement activation is to produce proteins that mimic the structure and function of these host regulators; some examples of well-studied models are VCP from vaccinia virus and SPICE from smallpox.

All complement regulators consist of multiple copies of CCP domains. First, we focused on complement factor H (FH) which has 20 CCP domains. The first 4 domains of FH contain both cofactor and decay accelerating activities. We obtained the structure of FH(1-4) fragment in complex with C3b. The structure has an extensive interface formed by all four domains of FH and multiple domains of C3b. Both FH and C3b show minor differences compared to their respective isolated structures. This suggests that the binding sites are pre-formed in both components. The α'NT loop and MG7 domains of C3b have tight contracts with CCP 1 and 2 domains of FH, which significantly contribute to the complex formation. This structural observation is in agreement with the previous mutagenesis studies on α'NT region of C3b, which indicates some acidic residues have severe impact on FH binding and therefore activity.

The structural information gives molecular insights into the regulatory activity of the major alternative pathway regulator FH. FH(1-4) binds to C3b adjacent to the two FI-mediated cleavage sites, with the first site (Arg1281-Ser1282) fully exposed while the second site (Arg1298-Ser1299) is buried within the complex. This suggests that conformational changes are required after the first cleavage event. Combined with functional data, our results suggest that binding of a regulator to

C3b creates a binding platform for FI, thus explaining the presence of a cofactor protein to assist C3b processing. This model was further supported by the recent published data of the FI structure, which suggests binding of FI to the C3b-regulator complex, essential for the proteolytic activity of FI[3]. Comparing C3bFH(1-4) with C3bBb derived from the SCIN-convertase structure suggests steric clashes between the first two CCP domains of FH and Bb. Moreover, in the modeled complex proximal FH and Bb residues are negatively charged suggesting that electrostatic repulsion effect contributes to convertase decay. Recently, an atypical HUS mutant R35H in FH was shown to have severely decreased decay acceleration activity whilst retaining comparable C3b binding affinity to the wild type[4]. This provides functional data showing that residues in this region of FH influence the formation of C3 convertase. We extended the discussion on molecular mechanism of decay accelerating activity to another complement regulator DAF and analyzed the mutagenesis data of DAF. These results indicate that the functionally important residues in DAF overlap with the region in FH that clash with Bb, suggesting that FH and DAF may interfere with C3 convertase in a similar way, but the precise mechanisms may differ. The current functional and structural data give some insights into the interactions between regulators and the non-catalytic subunit of C3b. A complex structure of DAF with Bb may provide further details into the interaction pattern between this regulator and the protease fragment Bb. Comparing this with the existing complexes could reveal general mechanistic trends.

The complex provides structural explanations for understanding the functional effects of the diseases-associated mutations in both FH and C3b. We mapped these mutants on C3bFH(1-4) structure together with mutants from functional studies. Many of these mutants are at the complex interface, explaining the alternation of the complement regulatory activities. While the crystal structure of C3bFH(1-4) gives novel insights into mechanisms of complement regulation, many questions arise when we compare current structural data with functional data from various regulators and their viral homologs. Not all the data can be correlated with structural insights of C3bFH(1-4), suggesting that regulators may interact with C3b in a different way. Thus, we extended our structural study to two other complement regulators, MCP and the potent viral complement modulator SPICE. These results are discussed in **Chapter 4**.

The crystal structure of C3bMCP is determined at a resolution of 2.4 Å. Presently, this is the highest quality C3b-containing dataset. We used a construct of full length MCP, composed of four CCP domains, for the crystallization experiment. Only the positions of CCP 3 and 4 can be determined in our dataset as CCP 1 and 2 appear to be disordered so the precise positions of these

two domains cannot be determined. The disorder at the first two MCP domains is probably due to lack of interaction with C3b, which is supported by functional data that show CCP 1 and 2 make minor contributions to C3b binding[5]. The relative domain orientation between CCP3 and 4 of MCP are remarkably different from that of CCP3 and 4 of FH. Comparison of the two complex structures shows that the two regulators bind to the same sites of C3b formed by domains of MG1-2, CUB and TED. CCP3 of MCP binds to C3b in a similar way as CCP3 of FH, whereas CCP4 of MCP binds to the same site of C3b but use a completely different region of the domain for C3b interaction. The structure of C3bMCP fully supports that residues in CCP4, identified by mutagenesis studies, are important for C3b binding and this explains why we previously could not interpret these key residues based on the structural analysis of C3bFH(1-4) and primary sequence alignment.

SPICE is a potent viral complement regulator that consists of four CCP domains. The structure of SPICE in complex with C3b was determined at a resolution of 2.7 Å. The first three domains of SPICE bind to C3b in a highly similar way as FH, whereas the fourth domain binds to C3b in a similar way as MCP. SPICE differs only in 11 amino acids from its vaccinia homolog VCP, but SPICE is more than 100 times more potent than VCP in complement inhibition. Previous mutagenesis studies located 4 amino acids in CCP2 that contribute most to the increase in regulatory activity[6]. Our structure shows all four residues are fully exposed in the proposed FI binding site, suggesting SPICE offers a better FI binding platform and leading to the enhanced cofactor activity.

Taking into consideration all of the available structural information, C3b offers a common binding platform for regulators, which is preformed and composed by multiple domains of C3b. In all complexes, no major conformational changes were observed upon regulator binding. Although the orientation of CCP 3 and 4 in MCP is dramatically different from that of FH, this conformational difference is not induced by C3b binding since the full-length MCP structure shows the same bend between CCP 3 and 4 as in the complex. This suggests that the binding sites are already preformed in the unbound state. The C3bMCP and C3bSPICE structures provide further support to the putative factor I binding site formed by both C3b and regulator. Although CCP2 domain of MCP is disordered in the complex structure, this domain is required for the cofactor activity. We identified a positive charged lysine residue in CCP2 of MCP that contributes significantly to the MCP cofactor activity, indicating a direct role of CCP2 in FI binding. Regarding the decay accelerating activity, it seems that the interactions between the α'NT region of C3b and regulators are important

for the decay of the convertase. This may also explain why MCP does not have decay accelerating activity, as the binding of MCP to C3b is independent of the α'NT loop. The current data elucidate novel insights into the molecular mechanisms of decay-accelerating activity, but it also provides many questions that require further research using structural information in combination with biochemical and biophysical approaches.

REFERENCES

1. Laursen, N.S., *et al.* Substrate recognition by complement convertases revealed in the C5-cobra venom factor complex. *EMBO J* **30**, 606-616 (2011).
2. Pryzdial, E.L. & Isenman, D.E. Alternative complement pathway activation fragment Ba binds to C3b. Evidence that formation of the factor B-C3b complex involves two discrete points of contact. *J. Biol. Chem.* **262**, 1519-1525 (1987).
3. Roversi, P., *et al.* Structural basis for complement factor I control and its disease-associated sequence polymorphisms. *Proc Natl Acad Sci USA* **108**, 12839-12844 (2011).
4. Pechtl, I.C., Kavanagh, D., McIntosh, N., Harris, C.L. & Barlow, P.N. Disease-associated N-terminal complement factor H mutations perturb cofactor and decay-accelerating activities. *J Biol Chem* **286**, 11082-11090 (2011).
5. Adams, E.M., Brown, M.C., Nunge, M., Krych, M. & Atkinson, J.P. Contribution of the repeating domains of membrane cofactor protein (CD46) of the complement system to ligand binding and cofactor activity. *J Immunol* **147**, 3005-3011 (1991).
6. Yadav, V.N., Pyaram, K., Mullick, J. & Sahu, A. Identification of hot spots in the variola virus complement inhibitor (SPICE) for human complement regulation. *J Virol* **82**, 3283-3294 (2008).

Samenvatting

Het complement systeem is een oude tak van het menselijke immuunsysteem. Het immuunsysteem heeft zich ontwikkeld om snel te reageren op binnendringende ziektekiemen door deze kiemen in het bloed efficiënt te herkennen en te elimineren. Dit systeem kan door specifieke herkenning of door spontane activering van de centrale component C3 worden geactiveerd. De verschillende routes van complement activatie leiden allemaal tot vorming van de C3 convertase, het centrale enzymcomplex in de versterkingslus van de door complement gemedieerde immuunresponse.

Het complement systeem is op verschillende niveaus sterk gereguleerd om gastheercellen van de eigen weefsels tegen ongewenste aanvallen op zichzelf te beschermen. Voor een dergelijke bescherming zijn een groep van complement regulatoren, bekend als de RCA-eiwitten, essentieel, omdat deze in staat zijn de hoeveelheid C3 convertase op het celoppervlak van gastheercellen te moduleren. In de genen die coderen voor deze complement regulatoren zijn dan ook verschillende ziekte gerelateerde mutaties en polymorfismen geïdentificeerd. Een groeiende hoeveelheid bewijs ondersteunt nu een duidelijk verband tussen de disfunctie van complement regulering en bepaalde nier- of oogaandoeningen. In dit proefschrift maken we gebruik van röntgen diffractie om structuren van eiwitten en eiwitcomplexen op te lossen die van centraal belang zijn voor de activering en regulering van het complement systeem. De hieruit verworven structurele inzichten helpen om moleculaire mechanismen achter de biologische activiteit van deze complexen toe te lichten, te begrijpen hoe bacteriële en virale strategieën zijn ontwikkeld om herkenning te ontwijken en als mede om een verband te leggen tussen mutaties in deze eiwitten en ziektebeelden die geassocieerd zijn met gebrekkige regulatie van het complement systeem. De combinatie van deze kennis maakt de complement cascade een interessant doelwit voor de ontwikkeling van therapeutische toepassingen.

Initiatie van complement cascades resulteert in de vorming van de C3 convertase, een zeer specifiek enzymcomplex dat C3 splitst in de actieve vorm C3b en daardoor opnieuw C3 convertase genereert via de zogenaamde "tick-over loop". De C3 convertase speelt daardoor een belangrijke rol in de versterking van de immuunresponse. Overtollige formatie van C3 convertase op het celoppervlak kan echter leiden tot ongecontroleerde activering van het complementsysteem. Om dit te voorkomen heeft de de C3 convertase een uitgekiend zelfregulerend mechanisme: Het serine protease fragment is voorafgaand aan de vorming van de convertase als een pro-enzym in bloed aanwezig en verwerft zijn proteolytische activiteit alleen wanneer het deel uit maakt van het C3 convertase complex. Bovendien is de levensduur van de C3 convertase beperkt, wat zorgt voor

een efficiënte maar korte versterking van complement op het reactieoppervlak. Dergelijke metastabiliteit is belangrijk voor de regulering van de door complement gemedieerde immuunresponse, maar maakt structurele studies van de C3 convertase uitermate uitdagend.

Structurele inzichten in de vorming van de C3 convertase

Een door Staphylococcus aureus uitgescheiden eiwit, genaamd SCIN, stelde ons in staat om de C3 convertase te stabiliseren. SCIN is een remmer van het complementsysteem en zet het enzymcomplex in een inactieve vorm vast, waardoor deze zijn proteolytische activiteit verliest maar tegelijkertijd een langere halfwaardetijd verkrijgt. In **Hoofdstuk 2** beschrijven wij hoe wij er in slaagden een complex met de drie componenten C3b, Bb en SCIN te vormen die in oplossing langer dan twee weken stabiel is. Analytische ultracentrifugatie met het gezuiverde complex suggereerde dat SCIN de vorming van het convertase dimeer met een moleculair gewicht van ongeveer 500 kDa induceert. We verkregen kristallen met vers gezuiverde monsters van het complex en konden met behulp van röntgen diffractie de eerste structuur van de C3 convertase met een resolutie tot 3.9 Å bepalen. Uit de structuur kwam naar voren dat het gestabiliseerde C3 convertase complex bestaat uit een dimeer van C3 moleculen die worden overbrugd door twee SCIN moleculen. In het complex zitten de twee C3b moleculen in het midden van het dimeer en wijzen de Bb fragmenten van de Factor B protease symmetrisch naar buiten. SCIN gaat tal van interacties aan met C3b en Bb in een monomeer van de convertase, alsmede met het C3b monomeer van de tegengestelde C3 convertase.

De verkregen resultaten stellen ons in staat voor de eerste keer de structuur van de C3 convertase in detail te beschrijven. De van het dimeer afgeleide structuur van de monomere convertase toont een los arrangement. De belangrijkste contacten worden gevormd door het VWA domein van protease fragment Bb en het C-terminale C345C domein van C3b. In de kristalstructuur werden geen contacten tussen het serine protease domein van Bb en de niet-katalytische eenheid C3b waargenomen. De meest opvallende bevinding van het complex is dat het in de MIDAS gebondene Mg^{2+} ion door de C-terminale carboxylgroep van C3b gechelateerd worden. Deze waarneming verklaart waarom in mutagenese studies geen zuur residu in C3b als de natuurlijke ligand voor het tweewaardige ion in de MIDAS geïdentificeerd kon worden. Uit de kristalstructuur blijkt dat de aan de MIDAS aangrenzende lussen een directe bijdrage leveren aan de binding van C3b, in overeenstemming met mutagenese studies. Aan de kant van C3b wordt de interface vooral gevormd door residuen in het C345C domein. Ook deze bevinding wordt ondersteund door

functionele studies met hybride eiwitten, waarin deze residuen werden vervangen door de overeenkomstige residuen in CVF.

De twee componenten in het convertase complex, C3b en Bb, hebben een domein arrangement dat vergelijkbaar is met hun geïsoleerde toestand. De grootste verandering, tussen vrij C3b eiwit en complex zit in de positie van het C345C domein, dat echter een grote positionele variatie vertoont in alle C3b structuren die tot nu toe zijn bepaald. Dit laatste laat zien dat dit domein een grote intrinsieke flexibiliteit vertoond. Het katalytisch centrum van het protease fragment Bb heeft in het complex geen significante veranderingen ondergaan en laat de typische bijna-actieve conformatie zien die bekend is van vrij Bb en zijn 'klassieke route'-homoloog C2a. Door de relatief lage resolutie kon de precieze positie van elk individueel atoom in het katalytische centrum van Bb niet bepaald worden. Echter, naar alle waarschijnlijkheid heeft de binding van het VWA domein aan C3b geen allosterische gevolgen voor het katalytische centrum in het serine protease domein.

Wat bepaald de enzymatische activiteit van de C3 convertase? We stellen een enzym-substraat model voor dat gebaseerd is op de C3b dimeer interface zoals dat is bepaald in het complex. Van dit eiwit oppervlak is al aangetoond dat het belangrijks is voor substraat binding aan de C3 convertase. In het voorgestelde model bevindt het serine protease domein van Bb zich in een productieve orientatie maar is wel ~30 Å verwijderd van de knip-plek in het substraat, C3. De flexibiliteit van het C345C domein zou hier een functie kunnen hebben, doordat een beweging van het C345C domein het serine protease domein dichter bij zijn substraat zou kunnen brengen. Daar komt bij dat delen van het oppervlak van het serine protease domein zich waarschijnlijk heroriënteren. Hierdoor zijn extra contactpunten met het substraat mogelijk die ervoor kunnen zorgen dat de knip-plek goed in de substraat-bindingsplaats kan binden en daar de volledige actieve conformatie van het katalytische centrum kan induceren. Dit enzym-substraat model wordt verder ondersteund door de recent gepubliceerde structuur van het C5-CVF complex. In deze structuur bindt C5 aan de niet-katalytische C3b homoloog, CVF, in een oriëntatie die vergelijkbaar is met die van de C3b-homodimeer uit het SCIN-convertase complex[1].

In 1987 stelden Pryzdial an Isenman dat het karakteristieke eenrichtingsverkeer van de alternatieve route richting uiteenvallen van de C3 convertase simpelweg het gevolg zou kunnen zijn van een lage intrinsieke associatie van 'enkelvoudig' Bb aan C3b . Dit is één van de mogelijke verklaringen voor het spontane uiteenvallen van de C3 convertase[2]. Het onomkeerbare uiteenvallen van de C3

convertase is een welbekend mechanisme van zelfregulering dat ongewenste complement activatie voorkomt. Echter het moleculaire mechanisme achter deze onomkeerbare dissociatie wordt niet geheel begrepen. Hier presenteren we de eerste C3 convertase structuur dat Bb laat zien in complex met zijn natuurlijk ligand C3b. Er is geen grote conformatie verandering in gebonden Bb ten opzichte van de vrije structuur. In beide gevallen zijn de belangrijkste C3b bindingsplekken, zoals de MIDAS, in de open conformatie. Dus als er geen conformatie veranderingen zijn, wat is dan de reden voor het spontane uiteenvallen van de convertase? We gebruikten een techniek genaamd 'surface plasmon resonance' om de bindingskinetiek van factor B aan C3b in detail te bestuderen. Deze proeven lieten zien dat een langzame associatie en dissociatie kinetiek het onomkeerbare uiteenvallen en de 'metastabiliteit' van het convertase complex kunnen verklaren. Samenvattend leveren deze resultaten aanvullend bewijs dat het onomkeerbare uiteenvallen van de convertase wordt bepaald door de bindingkinetiek en niet door conformatie veranderingen aan het bindingsoppervlak.

De kristal structuur van het SCIN-convertase complex heeft geresulteerd in het gedetaileerde begrip van het moleculaire mechanisme dat verklaard waarom SCIN specifiek de C3 convertase tot doelwit heeft en hiermee alle drie de complement routes blokkeert. SCIN zit gebonden tussen C3b en Bb en heeft uitgebreide contacten met beide eiwitten. Door de vorming van deze extra interactieplekken stabiliseert SCIN de C3 convertase op het bacteriële oppervlak. SCIN remt de C3 convertase door deze te bevriezen in een inactieve conformatie, zodat Bb niet bij zijn substraat, C3, kan komen. De structuur biedt ook een verklaring voor de functionele regio's van SCIN die in eerdere mutagenese studies zijn geïdentificeerd. Op basis van de strcutuur van het SCIN-complex hebben we een chimeer SCIN-eiwit ontworpen dat zorgt voor een stabiel monomeer SCIN-convertase complex in een niet-actieve conformatie. Deze resultaten zijn van belang voor het verdere ophelderen van de biologische functie van SCIN als een specifieke remmer en stabilisator van convertase.

Structurele inzichten in de regulatie van complement

Het efficiënte mechanisme waarmee complement infecties bestrijdt en cellulaire restanten opruimt vereist een zeer precieze regulatie om ongewenste aanvallen op gezonde gastheer cellen te voorkomen. Een gevolg hiervan is dat zoogdieren een breed scala aan celoppervlak gebonden en vrije complement regulatoren tot expressie brengen. Deze regulatoren breken C3b op in fragmenten die geen convertase meer kunnen vormen en daarnaast beïnvloeden ze het natuurlijke

uiteenvallen van de C3 convertase om C3b productie te remmen. Deze regulatoren spelen een essentiéle rol in het beschermen van de gastheer en dus leiden genetische defecten in complement regulatoren tot een verhoogde kans op bepaalde ziektes. Een strategie dat virussen gebruiken om complement te ontwijken is de productie van eiwitten die structureel en functioneel lijken op de gastheer complement regulatoren; voorbeelden hiervan zijn VCP gecodeerd door het Vaccinia virus en SPICE gecodeerd door het pokken virus.

Alle complement regulatoren bestaan grotendeels uit meerdere kopieën van CCP domeinen. De eerste regulator waarop we ons richtten was complement factor H (FH) dat uit 20 CCP domeinen bestaat. De eerste 4 domeinen van FH bevatten cofactor activiteit en kunnen daarnaast ook het uiteenvallen van convertase versnellen. We bepaalden de structuur van het FH(1-4) fragment in complex met C3b. De structuur laat een uitgebreid contact oppervlak zien dat gevromd wordt door alle 4 domeinen van FH en verschillende domeinen van C3b. Zowel FH als C3b laten slechts kleine veranderingen zien ten opzichte van de vrije eiwitten. Dit suggereert dat de bindingsplekken in beide eiwitten voorgevormd zijn. De α'NT lus en het MG7 domein van C3b hebben nauw contact met de CCP1 en CCP2 domeinen van FH, die een significante bijdrage leveren tot complex formatie. Deze observatie is in overeenstemming met eerdere mutagenese studies aan de α'NT lus van C3b, die lieten zien dat een aantal zure aminozuren in α'NT een belangrijke rol spelen bij FH binding en daardoor activiteit.

De structuur geeft, op een moleculair niveau, inzicht in de regulerende werking van FH, de belangrijkste regulator van de alternatieve activatie route. FH(1-4) bindt C3b in de buurt van de twee peptidebindingen die door FI geknipt kunnen worden. De eerste peptidebinding is volledig toegankelijk (Arg1281-Ser1282), terwijl de tweede peptidebinding (Arg1298-Ser1299) verborgen ligt in het complex. Dit suggereert dat er na de eerste proteolytische knip er een conformatie verandering moet plaats vinden. In combinatie met data uit studies naar de functie suggereren onze resultaten dat de binding van een regulator aan C3b een bindingsplatform creëert voor FI. Dit verklaart dan ook de noodzakelijke aanwezigheid van een cofactor eiwit bij de verdere omzetting van C3b. Een recente publicatie over de structuur van FI bevestigt dit model. In dat artikel staat dat de binding van FI aan een C3b-regulator complex essentieel is voor de enzymatische werking van FI[3].

Als we de C3bFH(1-4) structuur vergelijken met de C3bBb-SCIN convertase structuur valt op dat er sterische hindering zou zijn tussen de eerste twee CCP domeinen van FH en Bb. Bovendien laat

een gemodeleerd complex zien dat naburige residuen van FH en Bb allen een negatieve lading hebben, wat suggereert dat electrostatische repulsie een rol speelt bij het uiteenvallen van de convertase. Recentelijk is getoond dat een atypische HUS mutant R35H in FH een sterk verlaagde activiteit had in het laten uiteenvallen van de convertase, terwijl de bindingsaffiniteit voor C3b onveranderd was[4]. Deze data laat zien dat residuen in dit gebied van FH van invoeld zijn op de destabilisatie van de C3-convertase.

De discussie over het mechanisme met betrekking op de aciviteit om het convertase uiteen te laten vallen hebben we verder uitgebreid door mutagenese data van een andere complement regulator, DAF, te analyseren. Het resultaat hiervan geeft aan dat residuen die belangrijk zijn voor de functie van DAF allemaal liggen in het gebied van FH dat 'botst' met Bb. Dit suggereert dat FH en DAF op een vergelijkbare wijze de C3-convertase uiteen laten vallen, maar dat het preciese mechanisme kan verschillen. De huidige studies naar de functie en structurele studies hebben inzichten geleverd in de interactie tussen regulatoren en het niet-katalytische deel van C3b. Een structuur van het Bb-DAF complex kan verdere informatie verschaffen over het interactiepatroon tussen deze regulator en het protease Bb. De vergelijking van zo'n structuur met bestaande structuren kan algemene mechanistische trends blootleggen.

Het complex geeft een verklaring op structuurniveau van het effect dat ziektegerelateerde mutaties in FH en C3b hebben op het uiteenvallen van de convertase. Deze mutanten en de mutanten uit mutagenesestudies werden aangegeven op de structuur van C3bFH(1-4) en hieruit bleek dat veel van de mutaties op de interface liggen, wat een verklaring verschaft voor de verandering in complement regulering van deze mutanten. Alhoewel de kristalstructuur van C3bFH(1-4) veel inzicht biedt in het mechanisme van complement regulering, kan het niet alle vragen beantwoorden die naarvoren komen als we de huidige data, van structurele studies en die naar de functie, van verscheidene complement regulatoren en hun virale homologen met elkaar vergelijken. Een deel van die data komt niet overeen met de inzichten die C3bFH(1-4) heeft verschaft, wat suggereert dat homologen op een andere manier interactie hebben met C3b. Om hierin meer inzicht te krijgen hebben we het structuuronderzoek uitgebreid met twee andere complement regulatoren, MCP en de potente virale complement modulator SPICE. De resultaten hiervan worden behandeld in **Hoofdstuk 4**.

De kristalstructuur van C3bMCP is opgehelderd tot een resolutie van 2.4 Å en vooralsnog is dit de dataset met de hoogste kwaliteit waarin C3b aanwezig is. Voor de kristallisatie hebben we intact

MCP, bestaande uit 4 CCP domeinen, gebruikt. In de structuur zijn alleen CCP 3 en 4 te zien, wat betekent dat CCP 1 en 2 dusdanig ongeordend zijn dat ze niet zichtbaar zijn. De flexibiliteit van CCP 1 en 2 komt waarschijnlijk door de het gebrek aan interactie tussen deze domeinen en C3b. Dit wordt ondersteund door bindingsdata waaruit blijkt dat CCP 1 en 2 nauwelijks bijdragen aan de C3b binding van MCP[5]. De relatieve domein orientatie van CCP 3 en 4 van MCP verschillen duidelijk met die van CCP 3 en 4 van FH. Een vergelijking van de twee complexen laat zien dat de twee regulatoren aan hetzelfde gebied van C3b binden. Dit gebied wordt gevormd door de MG1-2, CUB en TED domeinen. CCP 3 van MCP bindt C3b op een vergelijkbare manier als CCP3 van FH, terwijl CCP4 van MCP dezelde bindingsplek op C3b heeft als CCP4 van FH maar met een ander deel van het domein bindt. De structuur van C3bMCP laat duidelijk zien dat de residuen in CCP4, die geïdentificeerd zijn met mutagenesestudies, erg belangrijk zijn voor de binding aan C3b, terwijl deze eerder op basis van de C3bFH(1-4) structuur niet naarvoren kwamen als residuen die in de bindingsinterface zaten.

SPICE is een potente virale complement regulator die bestaat uit 4 CCP domeinen. De structuur van SPICE in complex met C3b is opgelost tot een resolutie van 2.7 Å. De eerste drie domeinen van SPICE binden aan C3b op een zeer vergelijkbare manier als FH, terwijl CCP 4 bindt zoals CCP 4 van MCP. SPICE en VCP, een vaccinia homoloog, verschillen in 11 aminozuren, maar SPICE remt complement 100 keer sterker dan VCP. Eerdere mutagenesestudies hebben 4 aminozuren in CCP 2 aangewezen die het meeste bijdragen aan de verhoging van de reguleringsactiviteit[6]. In onze structuur liggen deze residuen volledig bloot in de voorgestelde FI bindingsplaats, wat suggereert dat SPICE een beter bindingsplatform is voor FI en op die manier een verhooge cofactor activiteit heeft.

Op basis van alle beschikbare struturele informatie kunnen we concluderen dat C3b een algemeen bindingsplatform biedt aan regulatoren, dat al bestaat in ongebonden C3b en over verschillende domeinen verspreid is. In alle complexen is geen enkele grote conformatie verandering waarneembaar als een regulator bindt. Alhoewel de orientatie van CCP 3 en 4 van MCP erg verschilt van die van FH, wordt deze verandering niet veroorzaakt door binding aan C3b. In de structuur van MCP is dezelfde hoek tussen CCP 3 en CCP 4 te zien als in het complex met C3b, wat er op wijst dat deze bindingsorientatie al aanwezig is in de ongebonden staat van MCP. De C3bMCP en C3bSPICE structuren ondersteunen de theorie dat er een factor I bindingsplatform gevormd wordt door C3b en een regulator samen. Ondanks het ontbreken van het CCP 2 domein in de structuur van C3bMCP is dit domein wel noodzakelijk voor de cofactoractiviteit. We hebben

een positief geladen lysine residue geidentificeerd in CCP 2 dat een significante bijdrage levert aan de cofactoraciviteit. Dit wijst erop dat CCP2 een directe rol heeft in de binding van FI. De activiteit om de C3convertase uiteen te laten vallen berust met name op de interactie van regulatoren met de α'NT regio van C3b. Dit kan ook verklaren waarom MCP deze activiteit niet bezit, aangezien de binding aan C3b niet via de α'NT regio is. De huidige data geven nieuwe inzichten in het moleculaire mechanisme van de versnelling van het convertase verval, maar werpen tegelijkertijd ook veel vragen op die verder onderzoek behoeven.

REFERENCES

1. Laursen, N.S., *et al.* Substrate recognition by complement convertases revealed in the C5-cobra venom factor complex. *EMBO J* **30**, 606-616 (2011).
2. Pryzdial, E.L. & Isenman, D.E. Alternative complement pathway activation fragment Ba binds to C3b. Evidence that formation of the factor B-C3b complex involves two discrete points of contact. *J. Biol. Chem.* **262**, 1519-1525 (1987).
3. Roversi, P., *et al.* Structural basis for complement factor I control and its disease-associated sequence polymorphisms. *Proc Natl Acad Sci USA* **108**, 12839-12844 (2011).
4. Pechtl, I.C., Kavanagh, D., McIntosh, N., Harris, C.L. & Barlow, P.N. Disease-associated N-terminal complement factor H mutations perturb cofactor and decay-accelerating activities. *J Biol Chem* **286**, 11082-11090 (2011).
5. Adams, E.M., Brown, M.C., Nunge, M., Krych, M. & Atkinson, J.P. Contribution of the repeating domains of membrane cofactor protein (CD46) of the complement system to ligand binding and cofactor activity. *J Immunol* **147**, 3005-3011 (1991).
6. Yadav, V.N., Pyaram, K., Mullick, J. & Sahu, A. Identification of hot spots in the variola virus complement inhibitor (SPICE) for human complement regulation. *J Virol* **82**, 3283-3294 (2008).

Acknowledgement

There are many people that I would like to thank for making this thesis possible.

First of all, I would like to express my deep and sincere gratitude to my supervisor, Prof. dr. Piet Gros. All the time, you showed me your great enthusiasm and passion for science. I thoroughly enjoyed my experience at your lab with lots of fun in research. Only having your great efforts and full supports, I could finish my PhD studies with such success. “bedanken”: not only for your scientific training, but also I learned lots of things from you, which brings huge benefits for my life and career now and the future. I am so delighted and truly appreciate to have you as my supervisor for the last five years!

I am deeply grateful to Dr. John. D. Lambris, Professor of research medicine, department of pathology & laboratory medicine, University of Pennsylvania School of Medicine, for your constructive supervision and collaboration. I enjoyed very much to work together with you and people from your lab. I always have great time and enjoy our discussion on many things. I really enjoyed the conferences in Greek islands every time: the great scientific topics, the stimulating discussions, amazing views, delicious food and tasty ouzo! Thanks a lot for inviting me to your lab in the summer 2010. It was an unforgettable experience! I would also like to thank members of your lab: Daniel Ricklin, You-Qiang Wu, Georgia Sfyroera, Apostolia Tzekou, for your valuable discussions and showing me around Philadelphia.

I would like to sincerely thank my fellow labmates and colleagues, who are or were in the group of crystal and structural chemistry. Many of you are not only my colleagues, but also the dearest friends that I have in the Netherlands. Eric and Arie, it was great pleasure to work together with you in the past five years. Arjen, I enjoyed doing lots of things with you in the lab and outside! It was always fun (or we made it funny….)! I had the most fun trip to ESRF with you! I was deeply touched when you offered me all your help right before my leaving. Dennis thanks for all your help in the lab and daily life. I enjoyed the chatting, cooking and having beer with you! It was my most amazing Chinese cooking with you and your friends. Thanks for always offering me accommodation when I’m back in Utrecht. Els, you are always kind and I enjoyed our conversation during Veldhoven meeting. Arjen, Dennis and Els, wish your guys good luck in thesis writing and have a great future in your life and career! Harma, we started at the same time, shared one office and always shared hotel room. We always chat a lot and I miss it a lot! When I had questions for my project, I always came to you and asked. Thanks a lot for helping me and explaining things clearly in details. Tom, it is my pleasure to share the graphic office with you. I

truly appreciate your help for checking my thesis carefully. Bert, thanks for teaching me crystallization, data collection, structure determination, sharing your experiences, discussing with me. Michiel and Federico, thanks a lot for your valuable discussions and comments on projects as well as manuscripts. Federico, thank you for the home-made tiramisu, which is definitely the best tiramisu that I've ever had! Harma, Tom, Bert, Michiel and Federico, I wish all of you have great future and lots of success! Peng, we had lots of fun together! Good luck! 晓光，非常感谢你在我 PhD 最后阶段的帮助，真的非常感谢你！希望你坚持不懈悉心钻研，你会有很好的前途的！Xinyi and Lucy, I enjoyed our girl's evening together! Wish you happy life! Rachel, I had great time with your working in the lab. How are you? I hope you have a happy life in US! Lucio, thanks for showing me things in the lab when I started in the lab. Wieger, Roland and Lucio, thanks a lot for assisting the protein expression and discussion. Wish all of you great success!

Particularly, I would like to express my sincere gratitude to Arjen, Dennis and Harma for translating the summary session to Dutch. Without your kind and great help, I could not complete the thesis. Additionally, I want to thank Wei Zhou, for putting great effort to help me check and print the thesis, and bring all booklets to Europe! Thanks to all of you!

Lastly and importantly, I wish to thank my parents. They bore me, raised me, supported me, taught me, and loved me. This thesis would not have been possible without their encouragement and understanding. To them I dedicate this thesis.

Curriculumn Vitae

Jin Wu was born in Beijing, China, on 2nd Jan, 1981. In 2004, she completed her undergraduate studies in chemistry department at University of Science and Technology of China (USTC). Then she moved to Utrecht, the Netherlands, for her master study. In 2006, she received her MSc degree in Biomolecular Science program at Utrecht University. Since September 2006, she worked on her PhD research under the supervision of Prof. dr. Piet Gros at the group of Crystal and Structural Chemistry, Bijvoet Center for Biomolecular Research, Utrecht University.

List of Publications

Wu, J., Ricklin, D., Tzekou, A., Lambris, J. D., and Gros, P. Structures of C3b-MCP and C3b-SPICE reveal molecular modularity underlying complement regulator structure and function, *Manuscript in preparation*.

Forneris, F., Ricklin, D., **Wu, J.**, Tzekou, A., Wallace, R. S., Lambris, J. D., and Gros, P. Structures of C3b in complex with factors B and D give insight into complement convertase formation, ***Science 2010***, *330*, 1816-1820.

Jongerius, I., Puister, M., **Wu, J.**, Ruyken, M., van Strijp, J. A., and Rooijakkers, S. H. Staphylococcal complement inhibitor modulates phagocyte responses by dimerization of convertases, ***Journal of Immunology 2010***, *184*, 420-425.

Wu, J., Wu, Y. Q., Ricklin, D., Janssen, B. J., Lambris, J. D., and Gros, P. (2009) Structure of complement fragment C3b-factor H and implications for host protection by complement regulators, ***Nature Immunology 2009***, *10*, 728-733.

Wu, J.* and Rooijakkers, S. H.*, Ruyken, M., van Domselaar, R., Planken, K. L., Tzekou, A., Ricklin, D., Lambris, J. D., Janssen, B. J., van Strijp, J. A., and Gros, P. Structural and functional implications of the alternative complement pathway C3 convertase stabilized by a staphylococcal inhibitor, ***Nature Immunology 2009***, *10*, 721-727.

Wienk, H., Lammers, I., Hotze, A., **Wu, J.**, Wechselberger, R. W., Owens, R., Stammers, D. K., Stuart, D., Kaptein, R., and Folkers, G. E. The tandem zinc-finger region of human ZHX adopts a novel C2H2 zinc finger structure with a C-terminal extension, ***Biochemistry 2009***, *48*, 4431-4439.

*these authors contributed equally to this work.

Color Figures and Supplementary Figures

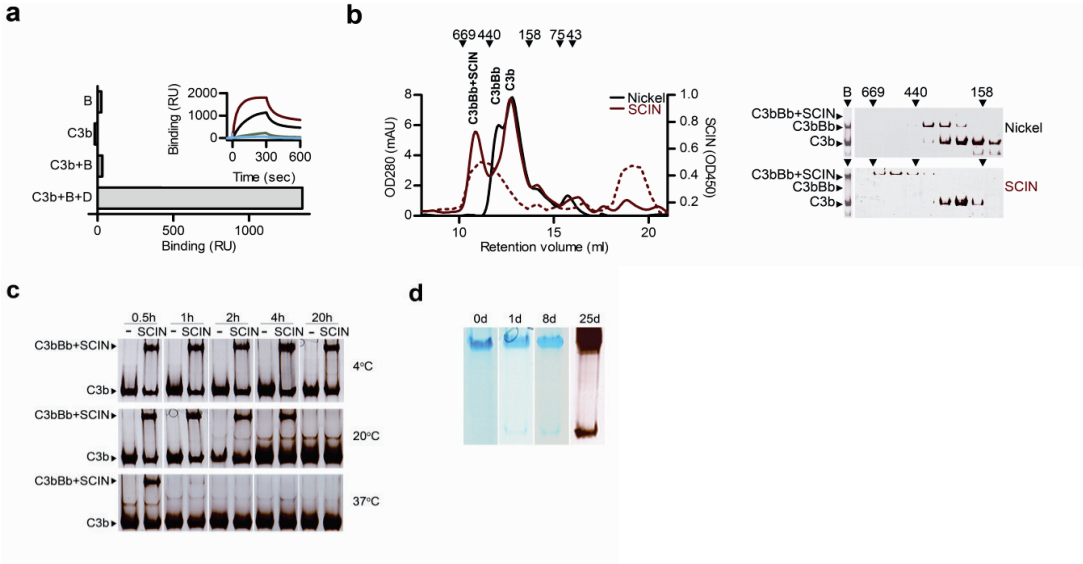

Chapter 2 Figure 1 SCIN induces the formation of dimeric convertases.
(**a**) Surface plasmon resonance analysis of the binding of soluble convertase components to surface-immobilized SCIN, showing responses at the end of injection (with all components at 100 nM). Inset, sensorgrams of injection with C3bBb, with C3b and FB at 10 nM (blue), 30 nM (green), 100 nM (black) or 300 nM (red), and FD at 100 nM. RU, resonance units. (**b**) Gel-filtration analysis (left) and native gel electrophoresis (right) of SCIN-inhibited convertases. Left, absorbance at 280 nm (A_{280}) of active convertases stabilized by Ni^{2+} (Nickel) and SCIN-inhibited convertases (SCIN). The 178-kDa peak corresponds to free C3b. Dashed red line, elution positions of SCIN determined by enzyme-linked immunosorbent assay (right axis; absorbance at 450 nm). mAU, milli-absorbance units. Right, electrophoresis of active convertase (Nickel) and SCIN-inhibited convertase (SCIN) before gel filtration (B) and of fractions eluted from the gel filtration column. (**c**) Analysis of the stability of C3b (500 nM), FB (500 nM), FD (250 nM) and SCIN (1 μM) incubated for various times (above) at 4 ºC, 20 ºC or 37 ºC and separated by native gel electrophoresis at 4 ºC. No complexes are present in the absence of SCIN (–). (**d**) Native gel electrophoresis of purified SCIN-convertase complexes after 0–8 d (left; Coomassie staining) and 25 d (far right; silver staining). Data are representative of three (**a–c**) or two (**d**) independent experiments.

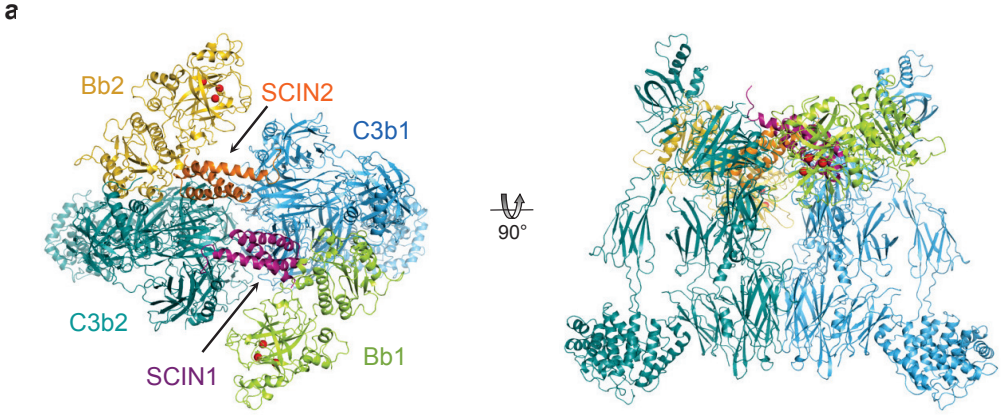

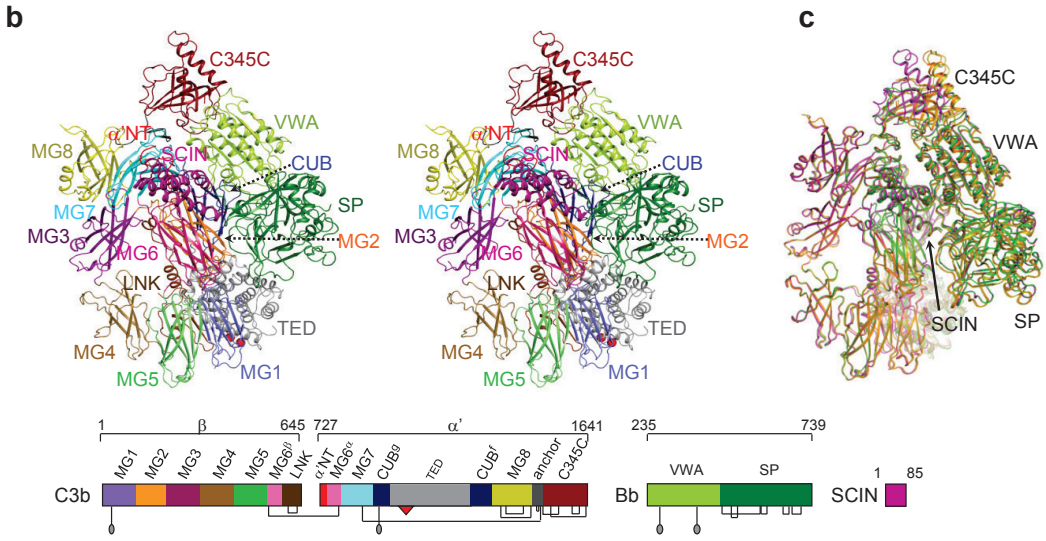

Chapter 2 Figure 2 Crystal structure of the C3 convertase C3bBb inhibited by SCIN.
(**a**) The C3bBb-SCIN dimeric complex, presented as a ribbon diagram with C3b in blue and turquoise, Bb in green and gold and SCIN in purple and orange. (**b**) 'Stereo' view of the monomeric C3bBb-SCIN extracted from the dimer, with colors indicating protein (SCIN) or protein domain (VWA and SP of Bb, and all 12 domains of C3b, with red spheres indicating thioester); below, domain composition (including disulfide bonds, glycosylation sites and thioester). α'NT, α' N-terminal tail. (**c**) Overlay of the four C3bBbSCIN complexes in the asymmetric unit (yellow, orange, green and magenta; additional details, **Chapter 2 Supplementary Fig. 8**).

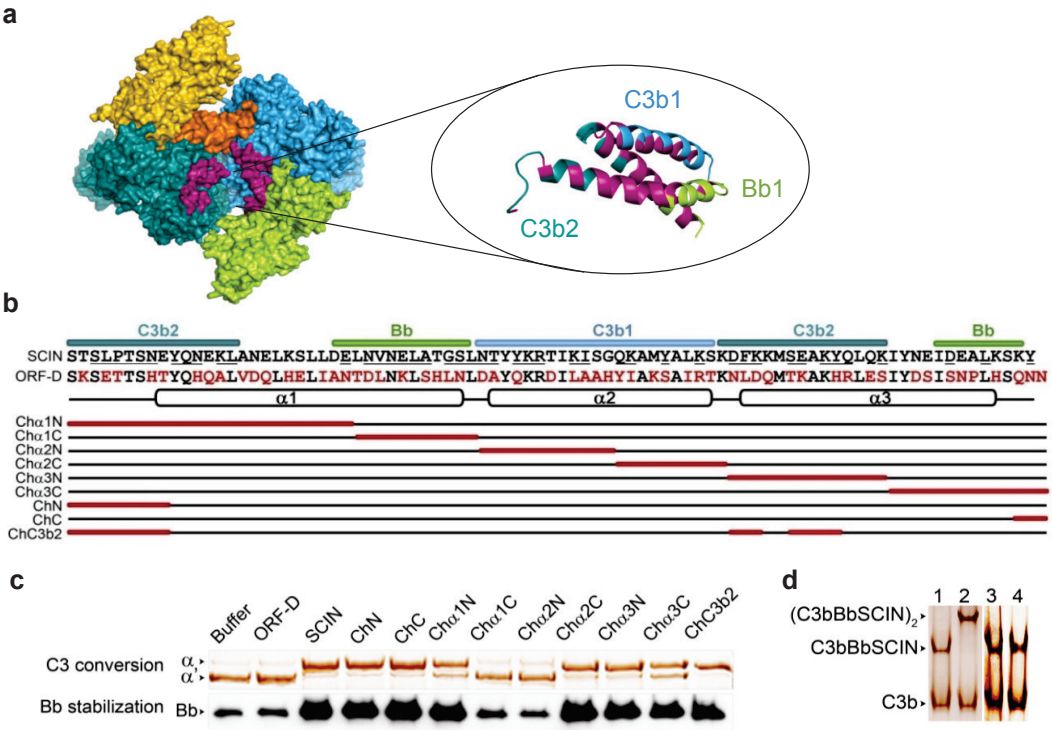

Chapter 2 Figure 3 Inhibition of C3bBb by SCIN.
(**a**) Contact sites of SCIN in the dimeric convertase with the SCIN binding pocket presented in surface representation (left) and a ribbon diagram of SCIN with colors indicating molecular contacts (right). (**b**) Amino acid sequence alignment of SCIN and the nonfunctional homolog ORF-D. Convertase contact sites in SCIN are underlined. Below, SCIN chimeras (red boxes indicate exchanged segments). (**c**) Convertase inhibition by SCIN chimeras, with C3 conversion by fluid-phase C3bBb (above) and Bb stabilization on bacterial surfaces (below). (d) Native gel electrophoresis of convertases in the presence of Ni^{2+} (lane 1), SCIN (lane 2), ChN (lane 3) or ChC3b2 (lane 4). Data (**c,d**) are representative of three independent experiments.

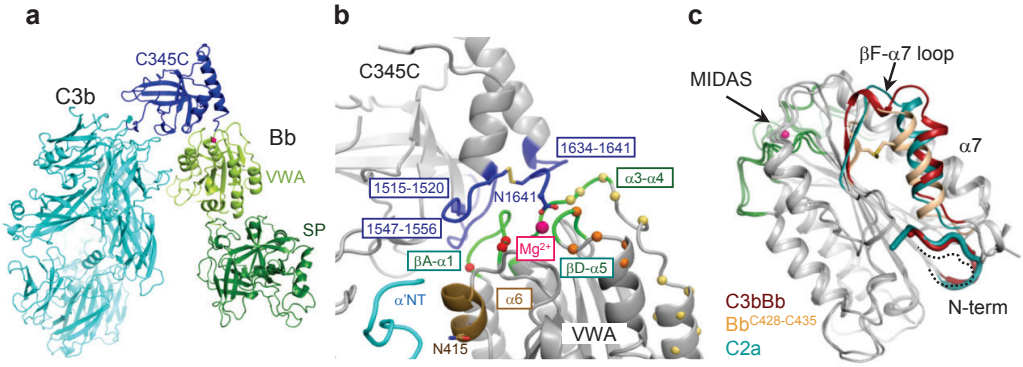

Chapter 2 Figure 4 The C3bBb structure derived from the C3bBb-SCIN complex.
(**a**) C3bBb complex, presented as a ribbon diagram with C3b in light and dark blue, Bb in light and dark green and Mg^{2+} as a pink sphere. (**b**) The C345C-VWA interface between C3b and Bb with the contact regions in blue (for the C345C domain of C3b) or green (for the VWA domain of Bb) and the disulfide bond of Cys1515-Cys1639 in C345C domain in a stick diagram. The residues substituted in FB chimeras are spheres (red, βA-α1 loop; beige, α3-α4 loop and α4 helix; orange, βD-α5 loop), based on reference 22. (**c**) Overlay of VWA domains of Bb in complex with C3b, Bb(C428-C435) (Protein Data Bank accession code 1RRK)[24] and C2a (Protein Data Bank accession code 2I6Q)[26], showing the position of helix α7 and the nascent N terminus. The MIDAS loop βA-α1, α3-α4 and βD-α5 are green; the N terminus of Bb (Cys428-Cys435) is missing (dashed line).

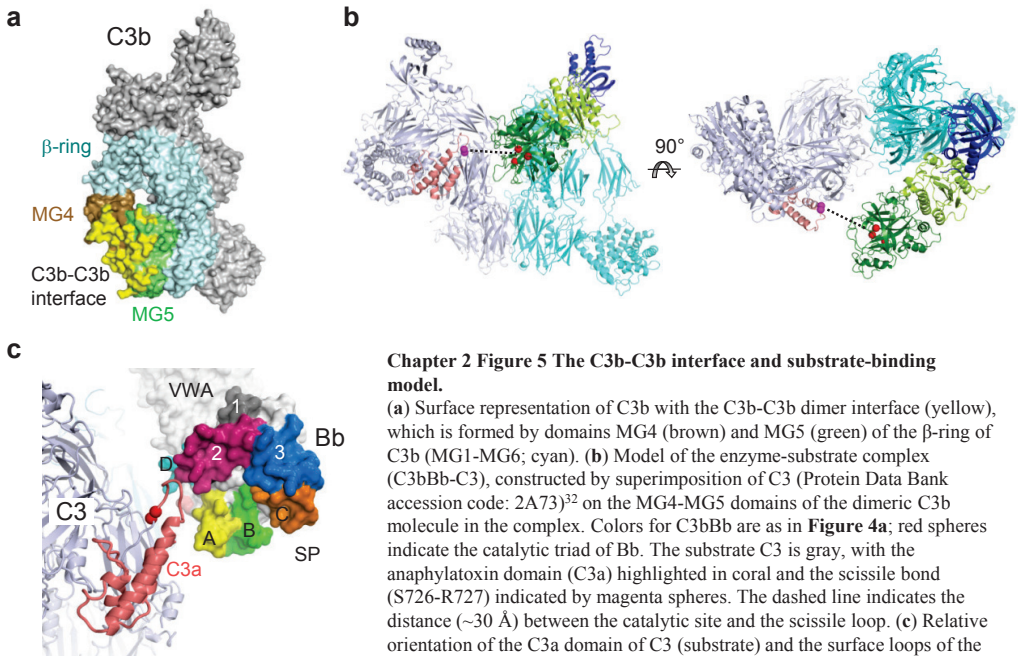

Chapter 2 Figure 5 The C3b-C3b interface and substrate-binding model.
(**a**) Surface representation of C3b with the C3b-C3b dimer interface (yellow), which is formed by domains MG4 (brown) and MG5 (green) of the β-ring of C3b (MG1-MG6; cyan). (**b**) Model of the enzyme-substrate complex (C3bBb-C3), constructed by superimposition of C3 (Protein Data Bank accession code: 2A73)[32] on the MG4-MG5 domains of the dimeric C3b molecule in the complex. Colors for C3bBb are as in **Figure 4a**; red spheres indicate the catalytic triad of Bb. The substrate C3 is gray, with the anaphylatoxin domain (C3a) highlighted in coral and the scissile bond (S726-R727) indicated by magenta spheres. The dashed line indicates the distance (~30 Å) between the catalytic site and the scissile loop. (**c**) Relative orientation of the C3a domain of C3 (substrate) and the surface loops of the SP domain of Bb forming the substrate-binding groove.

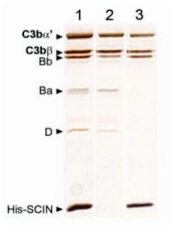

Chapter 2 Supplementary Fig. 1. SCIN binds C3bBb in solution.
His-tagged SCIN (1 μM) was incubated with C3b (500 nM), FB (500 nM) and FD (250 nM) in HBS-Mg for 1 hour at 4 ºC. SCIN complexes were captured by magnetic cobalt beads and bound proteins were visualized by SDS-PAGE under reducing conditions and silver staining. Lane 1: mixture before pull-down, lane 2: unbound proteins, lane 3: SCIN-bound proteins. SCIN bound complexes consist of C3b, Bb and SCIN. No specific bands were captured in the absence of FD or FB (data not shown). Data are representative of three independent experiments.

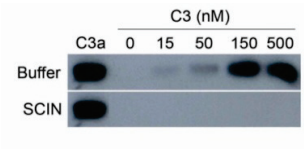

Chapter 2 Supplementary Fig. 2. SCIN inactivates preformed C3bBb.
Convertases were generated by mixing C3b (200 nM), FB (100 nM) and FD (50 nM) in HBS-Mg for 2 minutes at RT. Convertase formation was blocked with 5 mM EDTA and complexes were incubated with C3 (0-500 nM) in the presence or absence of SCIN (1 μM) for 20 minutes at RT. C3 cleavage was analyzed by immunoblotting using rabbit anti-C3a antibodies (Calbiochem). Data are representative of three independent experiments.

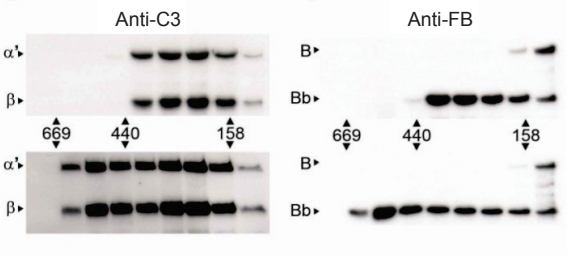

Chapter 2 Supplementary Fig. 3. Immunoblot analysis of fractions eluted from the gel filtration column.
Immunoblot analysis of convertase fractions eluted from the gel filtration column (as shown in **Fig. 1b**). Anti-C3 (*Left*) and Anti-FB (*Right*) immunoblot of active convertases stabilized by Ni^{2+} (top panels) and SCIN-inhibited convertases (bottom panels). The SCIN-inhibited convertase peak (~500 kDa) contains C3b and Bb. Data are representative of three independent experiments.

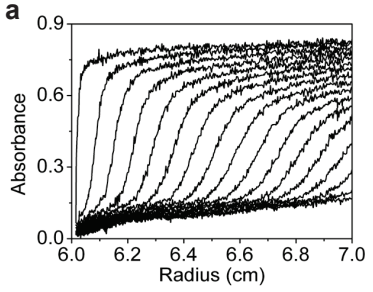

d

Component	Sphere	Prolate ellipsoid	Oblate ellipsoid
SCIN	1.6	1.2	1.2
Bb	5.2	3.9	4.0
C3b	11.3	8.6	8.8

Chapter 2 Supplementary Fig. 4. Analytical ultracentrifugation of the 500 kDa complex.
(**a**). Raw sedimentation data; B. Sedimentation data from which the time-invariant noise was subtracted. The graphs in panel (**a**) and (**b**) show the absorbance at 229 nm versus the radial distance from the center of rotation. During the time-course of the experiment, the solutes migrate radially outward (each scan corresponds to a certain time). (**c**) Differential (envelope) sedimentation coefficient distribution, enhanced van Holde-Weischet analysis[42], implemented in UltraScan[43] and panel (**d**), predicted sedimentation coefficients of convertase components in units of Svedberg (1 S = $1x10^{-13}$ s).

The enhanced van Holde-Weischet analysis on the TI-noise subtracted SV data revealed that the sample contained a complex that can be matched to a ~500 kDa complex consisting of $(C3bBb\text{-}SCIN)_2$. The peak at 15.2 S in the van Holde-Weischet differential (envelope) sedimentation coefficient distribution covered >70% of the total optical signal (**c**). The experimental sedimentation coefficient agreed with the prediction from theory and the observed crystal structure. The broadness of the 15.2 S peak is due to the relative low angular velocity at which the sedimentation velocity run was performed. A second significant peak at approximately 18 S may correspond to an end-to-end associated dimer of dimers. Furthermore, only a very small and insignificant amount of free C3b and a somewhat larger concentration of free SCIN were observed (**c**). Data are representative of one experiment.

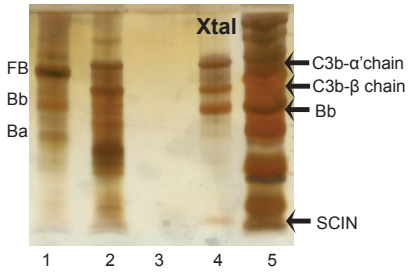

Chapter 2 Supplementary Fig. 5. Components of the crystal.
A single crystal was checked by SDS-PAGE (PhastGel Gradient 8-25). The crystal was washed with mother liquor three times. The gel was silver stained. Lane 1, FB; lane 2, C3b; lane 3, crystal droplet solution (control); lane 4, single crystal was washed with mother liquor; lane 5, marker. Data are representative of one experiment.

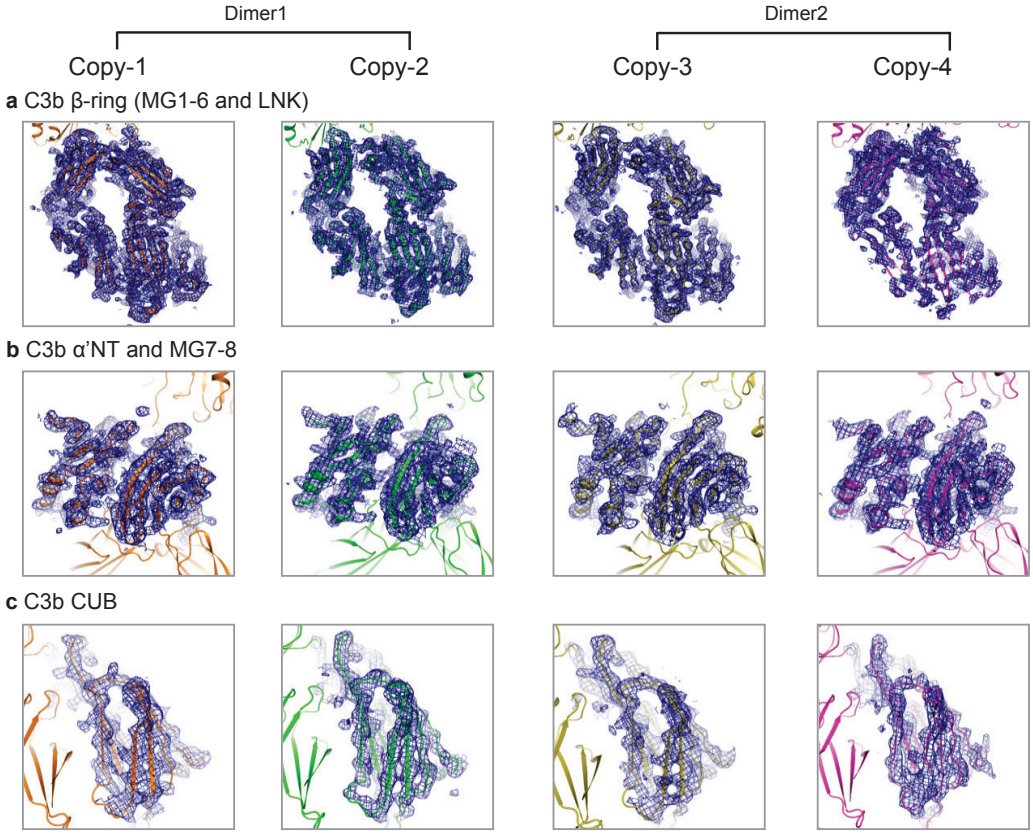

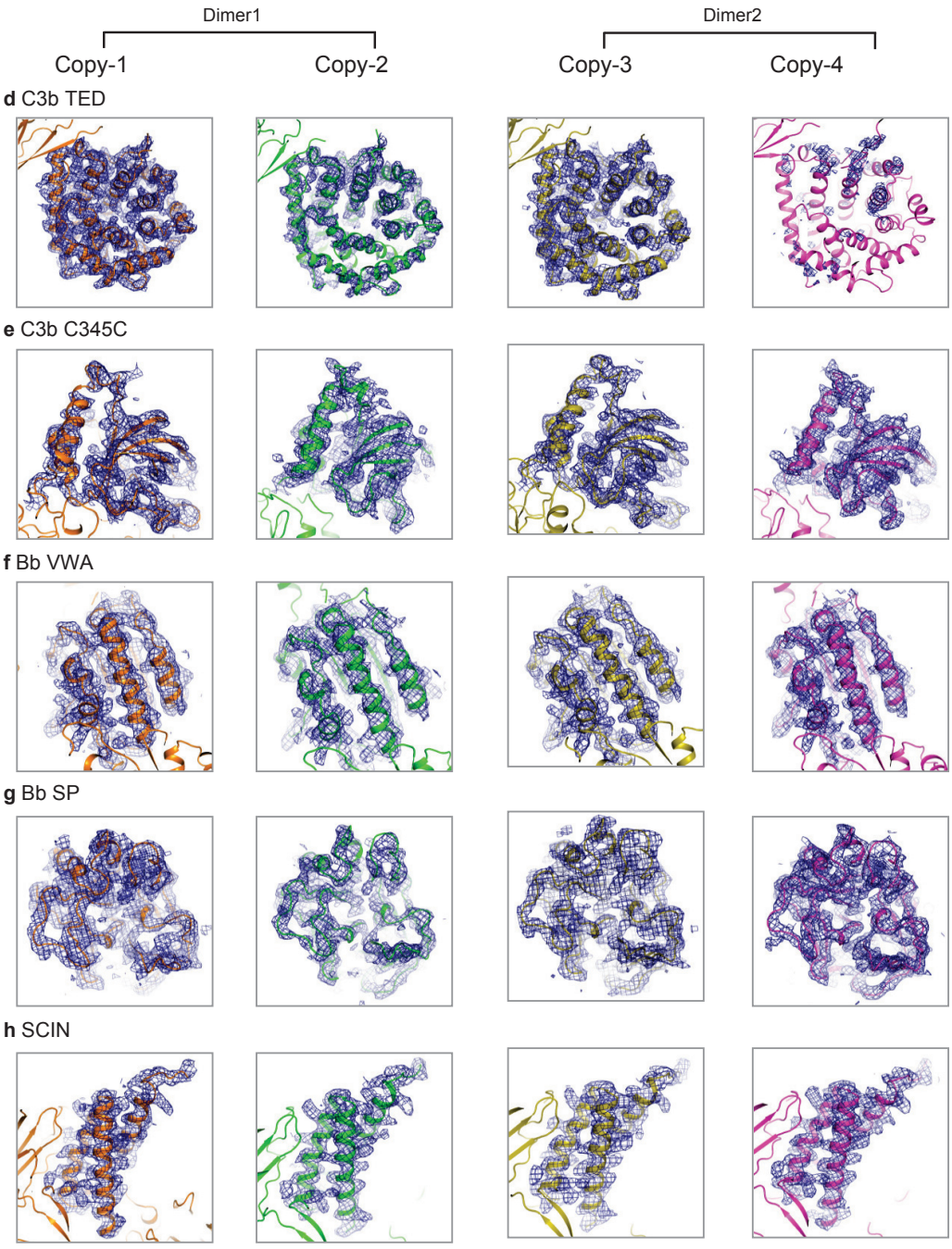

Chapter 2 Supplementary Fig. 6. Quality of the electron density map of the C3bBb-SCIN complexes.
Electron density (*2Fo-Fc* map, sharpened by B = -50 Å^2 and contoured at 1σ) of: (**a**) C3b β-ring (MG1-6 and LNK), (**b**) C3b α'NT and MG7-8, (**c**) C3b CUB, (**d**) C3b TED, (**e**) C3b C345C, (**f**) Bb VWA, (**g**) Bb SP and (**h**) SCIN.

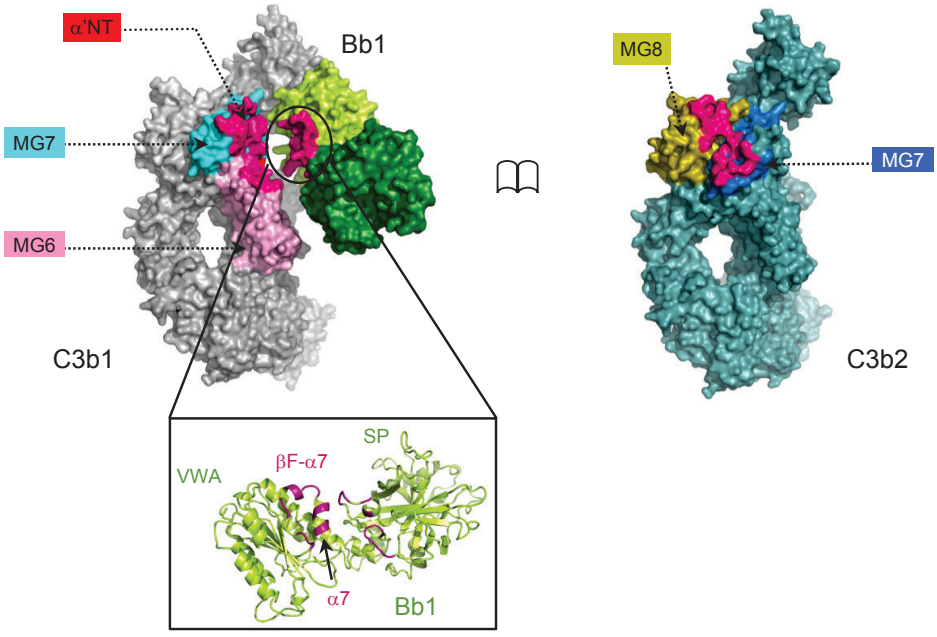

Chapter 2 Supplementary Fig. 7. SCIN binding pocket.
An "open" view of the C3bBb:C3b complex in surface representation. The domains forming the interface with SCIN are indicated. The footprint of SCIN binding sites are highlighted in magenta. The interaction sites involve hydrogen bonds, salt bridges and hydrophobic interactions. The insert shows the SCIN contact site on Bb (magenta; loop βF-α7 and helix α7 are indicated).

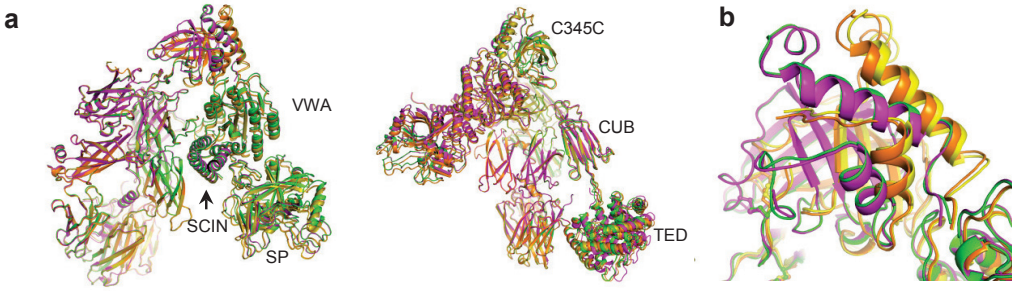

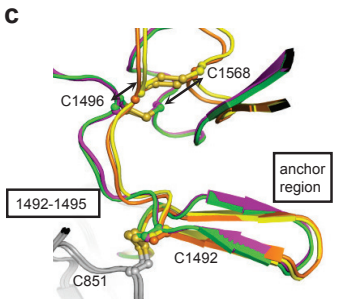

Complex	C345C		CUB		TED	
	Translation (Å)	Rotation (°)	Translation (Å)	Rotation (°)	Translation (Å)	Rotation (°)
C3bBb-SCIN 1	--	--	--	--	--	--
C3bBb-SCIN 2	5.9	26.2	0.5	3.3	2.7	9.4
C3bBb-SCIN 3	1.0	3.5	0.4	1.1	1.8	5.0
C3bBb-SCIN 4	6.1	26.9	1.3	5.1	--*	--*

Dimer1 Dimer2

*The TED domain is flexible in the corresponding copy.

	Complex	VWA		SP		SCIN	
		Translation (Å)	Rotation (°)	Translation (Å)	Rotation (°)	Translation (Å)	Rotation (°)
Dimer1	C3bBb-SCIN 1	--	--	--	--	--	--
	C3bBb-SCIN 2	1.9	2.7	2.3	4.0	0.4	1.3
Dimer2	C3bBb-SCIN 3	0.4	1.2	0.3	0.8	0.4	0.7
	C3bBb-SCIN 4	1.8	2.7	2.2	3.4	0.6	1.3

Chapter 2 Supplementary Fig. 8. Comparison of four C3bBb-SCIN complexes in the asymmetric unit.
(**a**) Four complexes are superposed on the β-ring of C3b1; the values of domain translation and rotation are given as calculated by SUPERPOSE in the CCP4 package. The major difference between C3b molecules is the location of the C345C domains as shown in (**b**) The C345C domains are divergent from loop 1492-1495, which is between two disulfide bonds C851-C1491 and C1496-C1568, as shown in (**c**). The orientation of the anchor region (1480-1491) is conserved among the four copies. The colour and numbering of the complexes are consistent with **Chapter 2 Supplementary Fig. 6**.

a

b

		C345C		CUB		TED	
		Translation (Å)	Rotation (°)	Translation (Å)	Rotation (°)	Translation (Å)	Rotation (°)
	C3b (2I07)	--	--	--	--	--	--
	C3b-CRIg (2ICF)	--*	--*	4.7	8.1	8.6	17.5
Dimer1	C3bBb-SCIN 1	8.2	40.4	5.3	15.4	8.6	17.8
	C3bBb-SCIN 2	5.3	24.2	4.8	15.5	6.2	9.8
Dimer2	C3bBb-SCIN 3	8.8	43.5	4.9	15.7	6.8	13.6
	C3bBb-SCIN 4	5.7	24.6	4.3	11.9	--*	--*

* These domains are flexible in the corresponding structures.

Chapter 2 Supplementary Fig. 9. Structural comparison of C3b.
(**a**) C3b in C3b-CRIg (pdb code: 2ICF)[16] and four copies of C3b-Bb/SCIN complexes were superposed on the crystal structures of C3b (pdb code: 2I07)[15] based on the core of C3b (MG2-3, MG 6-8, LNK, α'NT, 654 residues) (grey). (**b**) Domain translation and rotation calculated by SUPERPOSE of the CCP4 package.

a

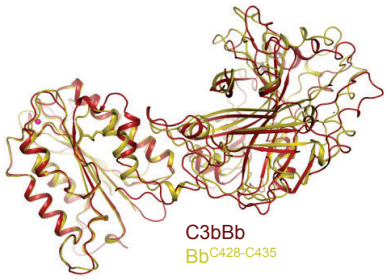

b

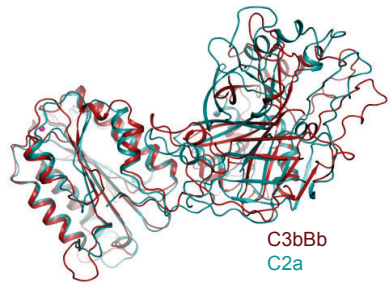

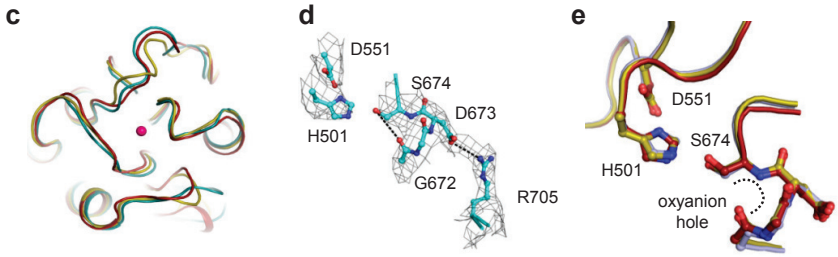

Chapter 2 Supplementary Fig. 10. Structural comparison of Bb in complex with isolated Bb, C2a and FB. (**a**) Comparison of Bb in complex with C3b with the isolated Bb structure (pdb code 1RRK)[24]. (**b**) Comparison of Bb in complex with C3b with the C2a structure (pdb code 2I6Q)[26]. (**c**) Comparison of MIDAS motif in structures of C3bBb-SCIN complex (dark red), isolated Bb (yellow) and C2a (turquoise); the Mg^{2+} is shown as a pink sphere. (**d**) The catalytic center in the SP domain of Bb in convertase complex; electron density (*2Fo-Fc* map) is contoured at 1σ. (**e**) Overlay of the catalytic center and oxyanion hole of Bb in C3bBb (dark red), isolated Bb (yellow) and pro-enzyme FB (light blue) (pdb code 2OK5)[25].

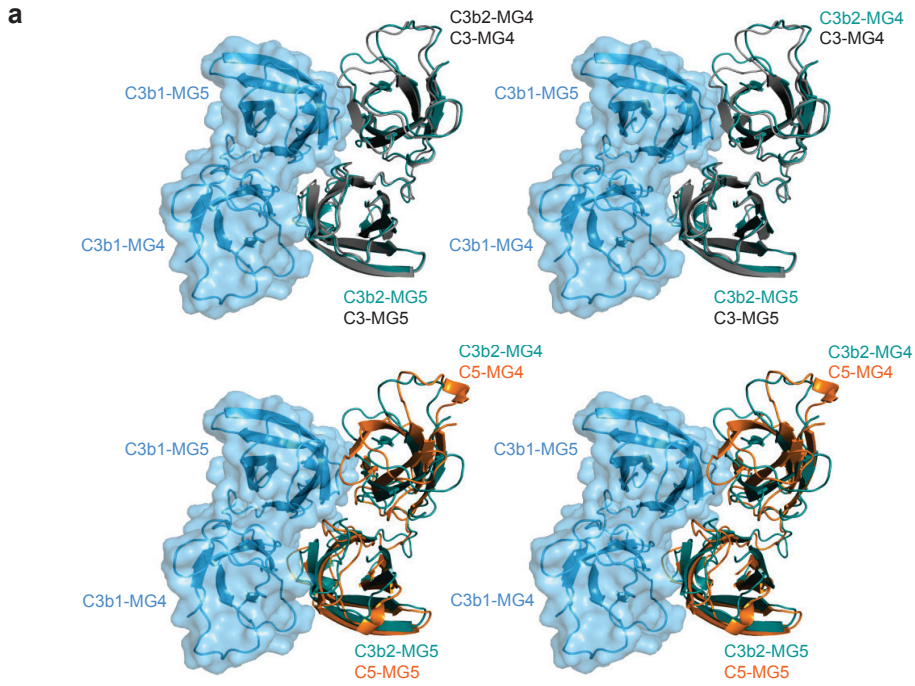

b

```
C3_MG45 329   SPYQIHFTKTPKYFKPGMPFDLMVFVTNPDGSPAYRVPVAVQGE----------DTVQSLT-QGDGVAKLSI  390
C4_MG45       SPFSLDLSKTKRHLVPGAPFLLQALVREMSGSPASGIPVKVSA----------TV-SPGSVPE-VQDIQD
C5_MG45       SPYKLNLVATPLFLKPGIPYPIKVQVKDSLDQLVGGVPVILNAQTIDVNQETSDLDPSKSVTRVDDGVASFVL
                                                  MG4

C3_MG45       NTHPS-QKPLSITVRTKKQELSEAEQATRTMQALPYSTVGN--SNNYLHLSVLRTELRPGETLNVNFLLRMDRA 461
C4_MG45       NTDGSGQVSIPIIIPQTISELQLSVSAGSPHPAIARLTVAAPPSGGPGFLSIERPDSRPPRVGDTLNLNLRAVG
C5_MG45       N-LPSGVTVLEFNVKTDAPDLPEENQAREGYRAIAYSSLSQ--SYLYIDWTDNHKALLVGEHL--NIIVTPKSP
                                  MG4                    MG5

C3_MG45       HEAKIRYYTYLIMNKGRLLKAGRQVREPGQDLVVLPLSITTDFIPSFRLVAYYTLIGASGQREVVADSVWVDVK 535
C4_MG45       SGATFSHYYYMILSRGQIVFM---NREPKRTLTSVSVFVDHHLAPSFYFVAFYYHG-----DHPVANSLRVDVQ
C5_MG45       YIDKITHYNYLILSKGKIIHFGTREKFSDASYQSINIPVTQNMVPSSRLLVYYIVTG-EQTAELVSDSVWLNIE
                                                  MG5
```

Chapter 2 Supplementary Fig. 11. Structural comparisons and sequence alignment of the C3b-C3b interface.
(**a**) Top: stereo view of the MG4-5 interface with C3 (pdb code: 2A73)[32] superposed on the MG4-5 domains of the right-hand side C3b in the C3b:C3b dimer. The domain-domain orientations of MG4 and MG5 are conserved in the C3 and C3b structures. Bottom: stereo view of the MG4-5 interface with C5 (pdb code: 3CU7)[33] superposed on the MG4-5 domains of C3b in the C3b:C3b dimer. (**b**) Sequence alignment of the MG4-5 domains from C3, C4 and C5. The alignment was performed in ClustalW2 (http://www.ebi.ac.uk/Tools/clustalw2/). Residues at the C3b:C3b interface are highlighted in green (conserved) and gray (not conserved). The pink dots indicate residues that interact with compstatin[30].

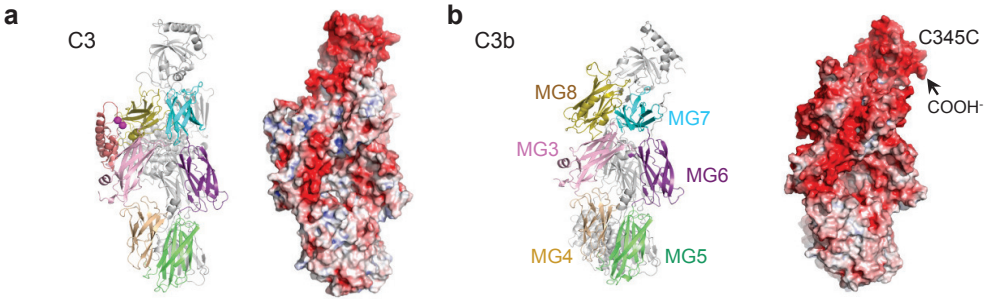

Chapter 2 Supplementary Fig. 12. Domain orientation and charge distribution of C3, C3b and Bb. (**a**) Domain organization of C3 in ribon representation (left side) and the solvent accessible surface of C3 colored by electrostatic potential from red (-10 k_bT/e_c) to blue (+10 k_bT/e_c) (right side)[32]. The orientation used is similar as in **Fig. 5a**. (**b**) Domain organization and electrostatic potential for C3b taken from the C3bBb-SCIN complex (same orientation and charge potential as in (**a**). (**c**) Electrostatic potential of Bb from red (-5 k_bT/e_c) to blue (+5 k_bT/e_c); orientation was chosen in order to show the charge distribution in MIDAS.

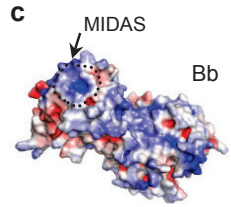

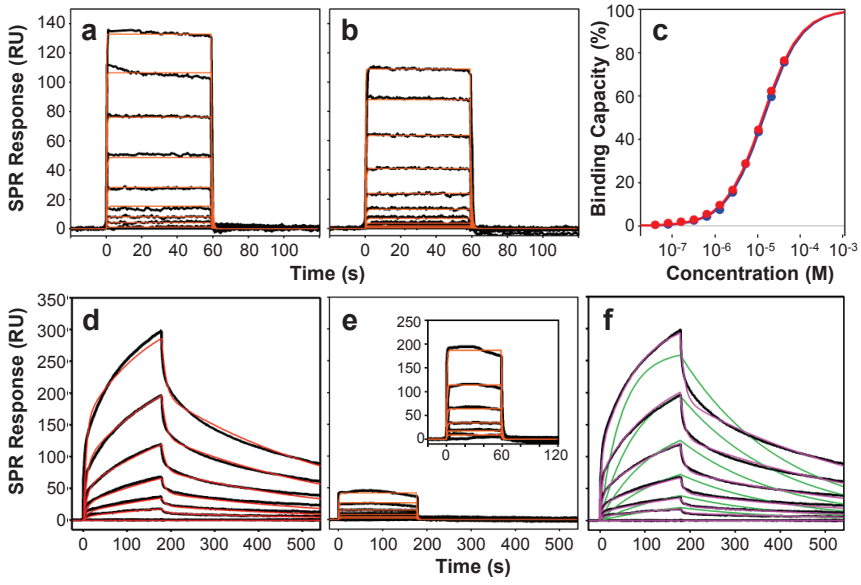

g

Analyte (Buffer) Kinetic Model	k_{on1} ($M^{-1}s^{-1}$)	k_{off1} (s^{-1})	K_{D1} (µM)	k_{on2} ($M^{-1}s^{-1}$)	k_{off2} (s^{-1})	K_{D2} (µM)	**Error** (ResSsq)
Ba (1 mM $MgCl_2$)							
Simple Bimolecular	1.4×10^5	1.9	13.2	n/a	n/a	n/a	2.3
Ba (3 mM EDTA)							
Simple Bimolecular	1.3×10^5	1.6	12.5	n/a	n/a	n/a	2.6
FB (1 mM $MgCl_2$)							
Simple Bimolecular [u]	(8.0×10^3)	(4.4×10^{-1})	(0.6)	n/a	n/a	n/a	14.5
Surface Heterogeneity	8.3×10^4	1.4×10^{-1}	1.7	4.8×10^3	2.3×10^{-3}	0.5	2.4
Conformational Change	2.9×10^4	1.1×10^{-1}	3.8	1.1×10^{-2} [v]	2.6×10^{-3}	n/a	2.9
Harris et al. [w]	*1.4×10^4*	*1.2×10^{-1}*	*(8.5)* [x]	*5.5×10^{-3}* [v]	*1.8×10^{-3}*	*n/a*	*(4.2)* [y]
FB (3 mM EDTA)							
Simple Bimolecular [z]	3.2×10^4	1.1	35.3	n/a	n/a	n/a	4.9

[u] The data set did not fit to this model; the values are only informative but do not reflect the real binding event.
[v] The unit for k_{on2} is s^{-1} in case of the *conformational change* model (conversion rate is independent on molarity).
[w] Rate constants provided by Harris *et al.*, based on a conformational change model[37].
[x] No K_D was specifically mentioned in ref. 37. Therefore, it was calculated as $K_D = k_{off}/k_{on}$.
[y] The kinetic fit and corresponding error calculation was performed using a different software (BIAevaluation).
[z] To improve on coverage, FB in absence of magnesium was measured at a higher concentration range (625 nM-20 µM). However, due to the still limited coverage, the extracted rate constants are of lower reliability (i.e. apparent).

Chapter 2 Supplementary Fig. 13. Kinetic analysis of C3b interactions with FB and Ba.
a-c, Binding of fragment Ba (40 nM – 40 µM) to immobilized C3b. Ba bound with highly similar binding kinetics in buffer containing either 1 mM $MgCl_2$ **(a)** or 3 mM EDTA **(b)**. Both data sets fitted very well to a *simple bimolecular* binding model (black: SPR signals, red: simulated curve) suggesting a single binding site and Langmuir 1:1 binding kinetics. The steady states of both Ba sets could be fitted to a single-binding-site model (with K_D values of 12 and 13 µM for Mg^{2+} and EDTA buffer, respectively) and showed a good overlay in the surface capacity plot **(c)**, therefore confirming the magnesium-independence of Ba binding. **d-f**, Binding of FB (63 nM - 2 µM) to C3b in the presence **(d)** or absence **(e)** of Mg^{2+}. In magnesium-containing buffer, the data set could be fit to a *conformational change* model with fast interaction and slow conversion component **(g)**. When magnesium was replaced by EDTA, both the binding kinetics changed to a simple bimolecular model with similar off-rates than for Ba and a significantly lower apparent affinity (a higher concentration range, i.e. 625 nM – 20 µM was used for the kinetic analysis; **e**, insert). It has to be noted that the FB data in magnesium buffer fitted similarly well to a *surface heterogeneity* model that considers two independent binding sites (**f**, magenta curves), whereas no suitable fit could be achieved for a *simple bimolecular* model (F, green curves). **(g)** Overview of kinetic profiles for FB and Ba in the presence or absence of magnesium. The rate constants for a *conformational change* model in case of FB were in good agreement with previously published data[37]. Data are representative of two to three independent experiments.

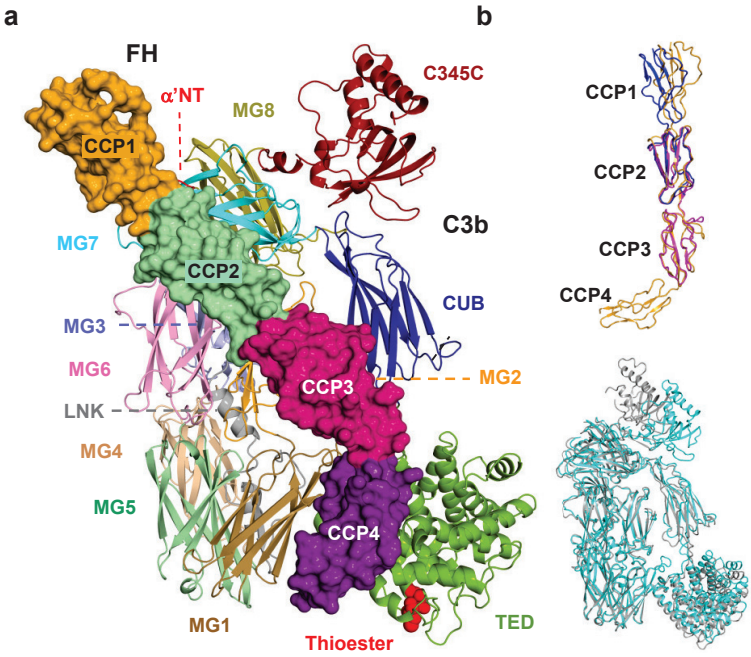

Chapter 3 Figure 2 Structure of C3b in complex with FH(1–4). (**a**) Overall structure of the C3b-FH(1–4) complex. C3b is presented as a 'ribbon' and FH is presented as surface representations; red spheres indicate thioesters. (**b**) Top, FH(1–4) in complex (orange) with NMR structures of CCP1–CCP2 (blue) and CCP2–CCP3 (magenta)[12]; bottom, C3b in complex with FH(1–4) (cyan) and free C3b (gray)[14]. Diagrams were generated with the PyMOL molecular visualization system.

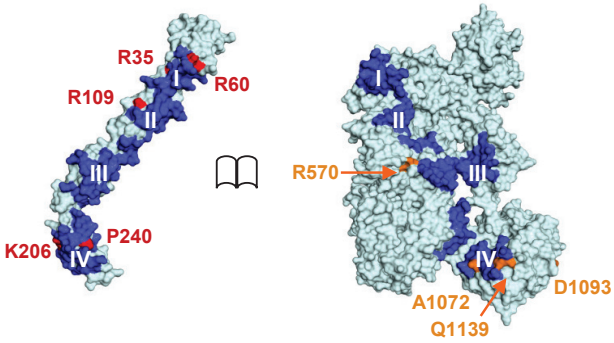

Chapter 3 Figure 3 Mapping of FH and C3 mutants on the complex structure.
Molecules are presented in surface representation with FH(1–4) on the left and C3b on the right. The four contact regions (I–IV) between FH(1–4) and C3b are in blue, with substitutions linked to AMD, MPGN-II and aHUS in red (for FH mutants) or orange (for C3b mutants).

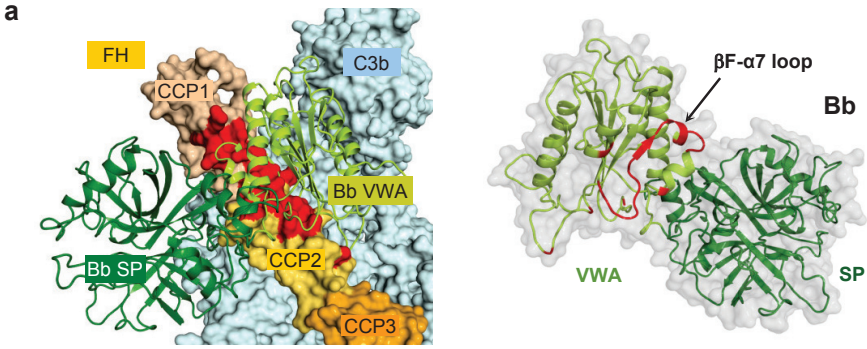

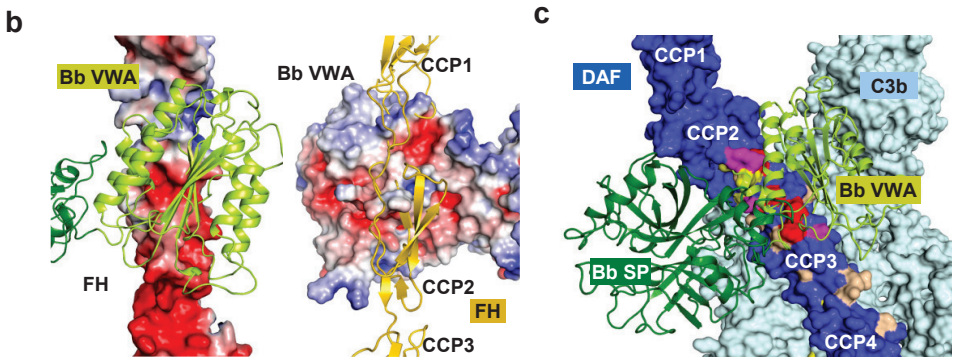

Chapter 3 Figure 4 Structural basis of decay-acceleration activity.
(**a**) Overlay of the C3b-FH and C3bBb complexes[21] (top) with C3b (light cyan) and CCP1–CCP3 of FH (beige, yellow-orange and orange, respectively) in surface representation and Bb in ribbon representation (light green, VWA domain; dark green, serine protease (SP) domain); the red surface area indicates the region where FH and Bb overlap (atomic distances of less than 2 Å). Below, overlap region (red) in Bb (Bb is rotated by 180° relative to the diagram above). (**b**) Electrostatic surface potential of FH and ribbon representation of Bb (left) and vice versa (right) in the regions facing each other. Potential contours are presented on a scale from $-5\ k_BTe_c^{-1}$ (red) to $+5\ k_BTe_c^{-1}$ (blue), where k_B is the Boltzmann constant, T is absolute temperature and e_c is elementary charge. (**c**) Superposition of CCP2–CCP4 of DAF[23] onto CCP1–CCP3 of FH, presented as in **a**. Colors of DAF substitutions indicate the degree of functional interference, from minor (beige), medium (yellow) and severe (magenta) to complete abortion (red) of decay-acceleration by DAF[24].

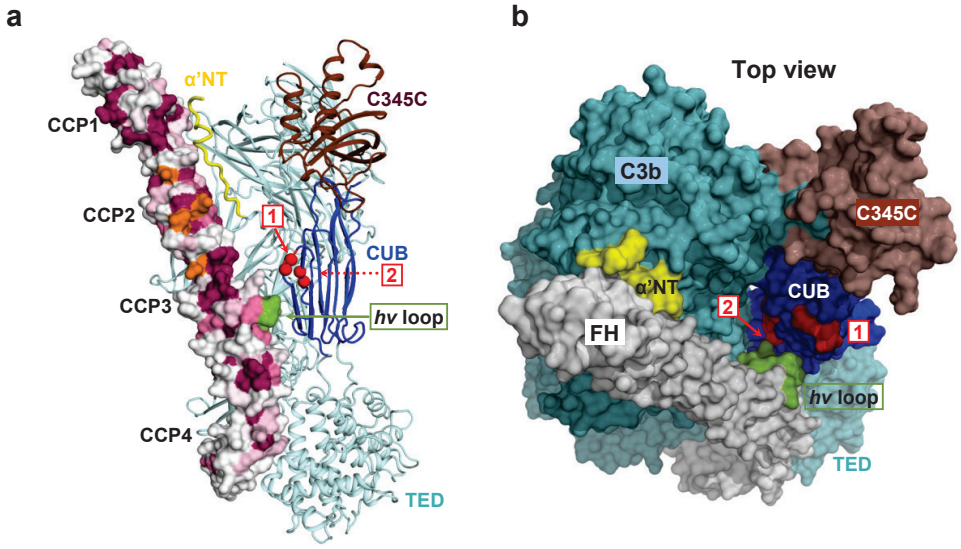

Chapter 3 Figure 5 Structural implications of cofactor activity.
(**a**) Sites of FI binding and cleavage. FH is presented in surface representation; colors indicate residue conservation with mutational data from ref. 30. Residues with the conservation scores of less than 5 are white; substitutions in VCP that enhance FI binding are orange; the hypervariable loop (*hv* loop) of CCP3 is green. C3b is cyan, with the CUB (blue), a'NT (yellow) and C345C (dark red) domains highlighted and the first and second scissile bonds in the CUB domain indicated by red spheres (conservation scale and corresponding colors, **Supplementary Fig. 4**). (**b**) Surface representation of the complex from the top view. Colors of the domains and FI cleavage sites are as in a; FH domains are gray.

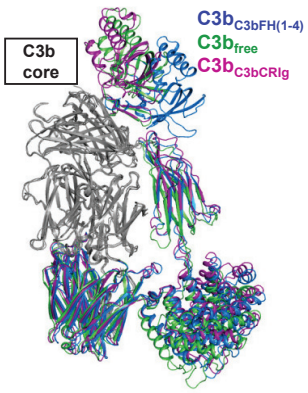

	C3b (pdb code: 2I07)		C3b (pdb code: 2ICF)	
	Translation (Å)	Rotation (°)	Translation (Å)	Rotation (°)
MG1	2.2	5.5	0.7	2.3
MG4	2.1	5.5	1.1	1.5
MG5	2.9	4.8	1.0	2.8
TED	6.9	11.8	3.7	7.5
CUB	5.2	12.9	1.4	6.0
C345C	19.2	25.8	--*	--*

	Rmsd (Cα) (Å)	
C3b core (41% of total model)	0.97	0.88

Chapter 3 Supplementary Figure 1. Structural comparison of C3b structures.
C3b in C3b-FH(1-4) complex (blue) was superposed on the crystal structures of free C3b (pdb code: 2I07)[14] (green) and C3b in complex of CRIg (pdb code: 2ICF)[15] (magenta) based on the C3b core consisting of MG2, MG3, MG6, LNK, α'NT, MG7 and MG8 (654 residues) (grey). The values of domain translation and rotation are calculated using SUPERPOSE in the CCP4 package[51].
* The C345C domain in C3b-CRIg structure had weak density and was not refined in the structure[15].

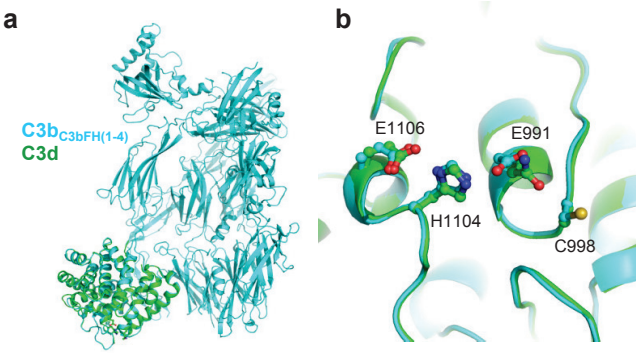

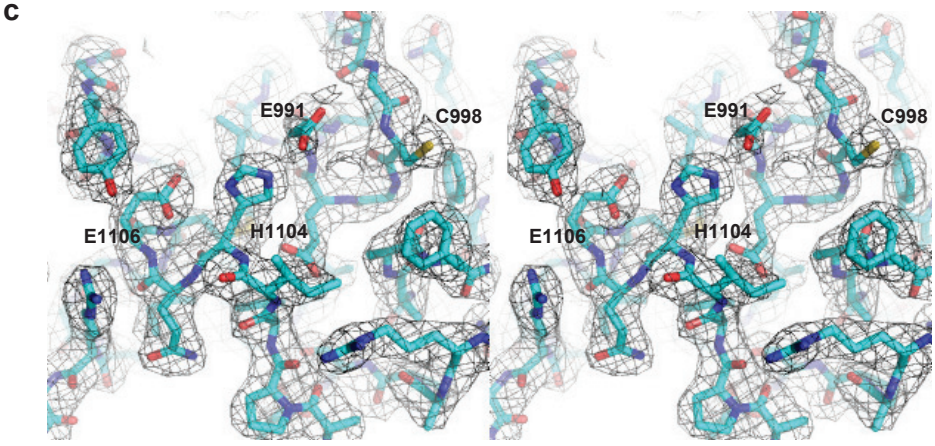

Chapter 3 Supplementary Figure 2. Thioester containing domain of C3b and comparison with C3d.
(**a**) Superposition of C3d (pdb code: 1C3D)[52] (green) with C3b in C3b-FH(1-4) complex (cyan). (**b**) Detail of thioester region. Glu-991, Cys-998, His-1104 and Glu-1106 are shown in ball-and-sticks. Cys-998 was mutated to Ala in C3d[52]. The two structures show similar conformations. C3b was treated with iodoacetamide after generation by limited trypsinization (see Methods). However, Cys-998 was exposed and no extra density was visible around it. (**c**) Stereo views of the electron density for the thioester region.

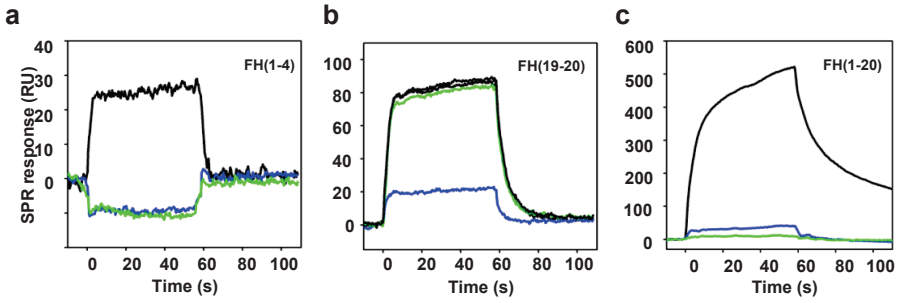

Chapter 3 Supplementary Figure 3. Effect of anti-C3b mAbs on FH(1-4) binding.
Antibodies against specific domains of C3b were used to investigate the contribution of these domains to the binding of FH(1-4). Using SPR, the binding signals of FH(1-4) (**a**), FH(19-20)(**b**), and FH(1-20)(**c**) were assessed before (black) and after injection of the antibodies onto immobilized C3b. In case of antibody C3-9, which is directed against the MG7/8 domains of C3b[53], only the binding of FH(1-4) and FH(1-20) but not FH(19-20) was impaired (green). In contrast, the TED-specific mAb311 also affected binding of FH(19-20), which is known to interact with the TED domain (blue). This confirms that both the TED and MG7 domain are involved in the binding of C3b to FH(1-4). Data are representative of two to three experiments.

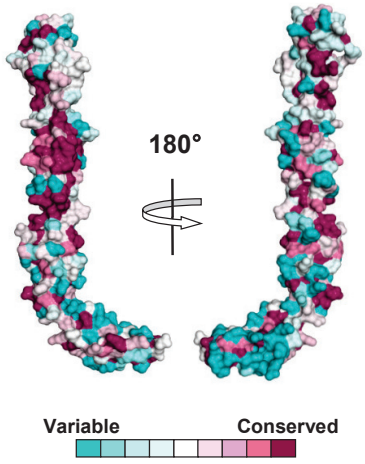

Organism	GenInfo Identifier	Similarity
Homo sapiens (human)	77744385	--
Pan troglodytes (chimpanzee)	114568537	98%
Macaca mulatta (rhesus monkey)	109018998	90%
Rattus norvegicus (Norway rat)	77861917	72%
Equus caballus (horse)	194227377	69%
Sus scrofa (pig)	47523636	67%
Canis familiaris (dog)	74005966	67%
Mus musculus (house mouse)	109627652	67%
Bos Taurus (cattle)	76677897	65%
Monodelphis domestica (opossum)	126306560	55%
Gallus gallus (red jungle fowl)	118094043	50%

Chapter 3 Supplementary Figure 4. CONSURF analysis of FH(1-4) from different species.
FH(1-4) is presented in the similar orientation as Fig. 2b (top), while the right-hand side is rotated by 180°. FH(1-4) is colored according to their conservation scores (1-9 from variable to conserved) based on CONSURF analysis[54]. The color scale is indicated above. The species chosen for the sequence alignment are listed in the Table.

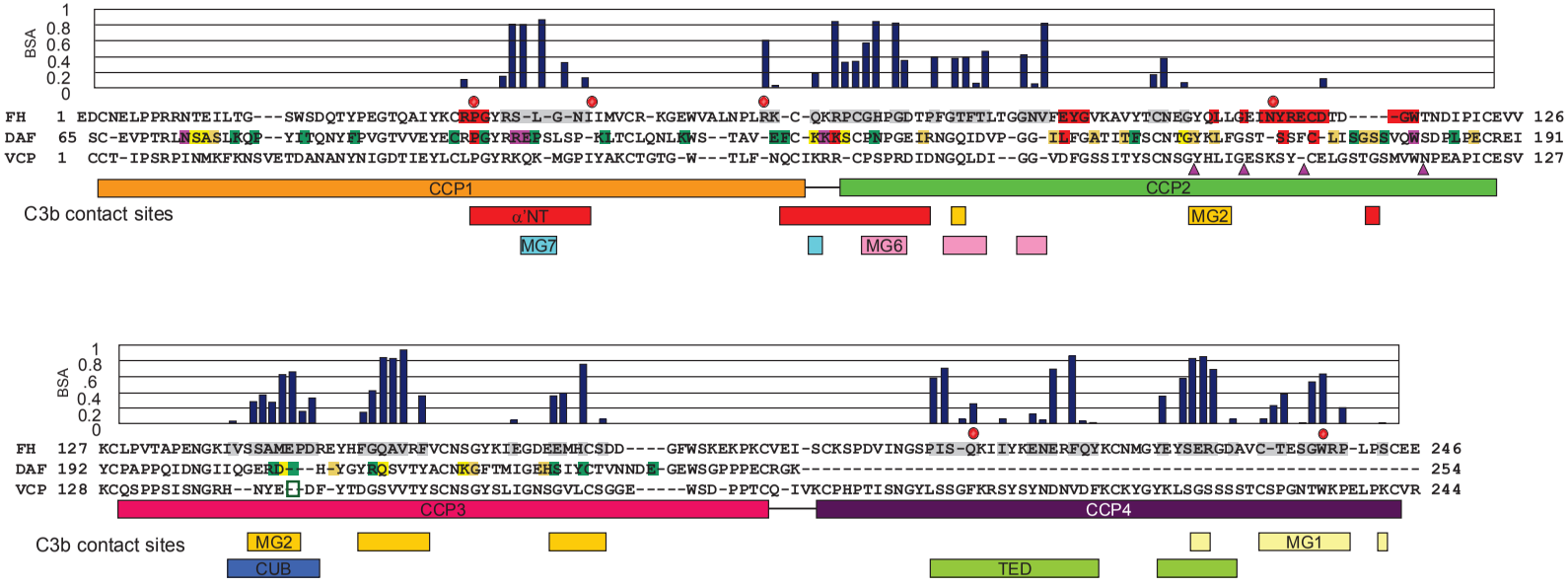

Chapter 3 Supplementary Figure 5. Structural-based sequence alignment of FH, DAF and VCP.
FH and DAF were aligned based on crystal structures, and VCP was aligned based on sequence using ClustalW2 (www.ebi.ac.uk/Tools/clustalw2/). The residues in FH making contact to C3b are shaded in grey; vertical bars indicate the fraction of the buried solvent-accessible surface area per residue (calculated by the protein interface analysis program PISA, www.ebi.ac.uk/msd-srv/prot_int/pistart.html). The corresponding C3b contact sites are indicated by blocks at the bottom of the alignment with the same color as indicated in **Chapter 3 Fig. 2a**. The disease-related mutants are labeled by the red dot on top of the residues, and the triangles are used to mark the important residues in VCP in cofactor activity assay based on ref. 30. Glu-144 of VCP located in the hyper-variant loop of CCP3 shows a significant effect on C3b binding (ref. 30) and is indicated by a green box. The region in FH overlapping with Bb (atomic distances shorter than 2Å) is highlighted in red. Mutations in DAF are highlighted according to the functional data in ref. 24 (red: critical for decay accelerating activity; magenta: severe effects on activity; yellow: medium effects, beige: minor effects; green: subtle or no effects).

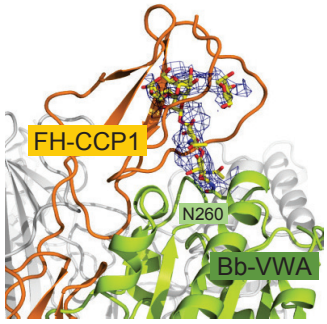

Chapter 3 Supplementary Figure 6. Steric hindrance between FH and the glycan attached to Asn-260 of Bb. C3b-FH(1-4) was superposed on the C3 convertase model[21] as shown in **Fig. 4a**. FH CCP1 clashes with the glycan attached to Asn-260 in the VWA domain of Bb. Electron density (*2Fo-Fc* map contoured at 1σ) of this glycan is shown.

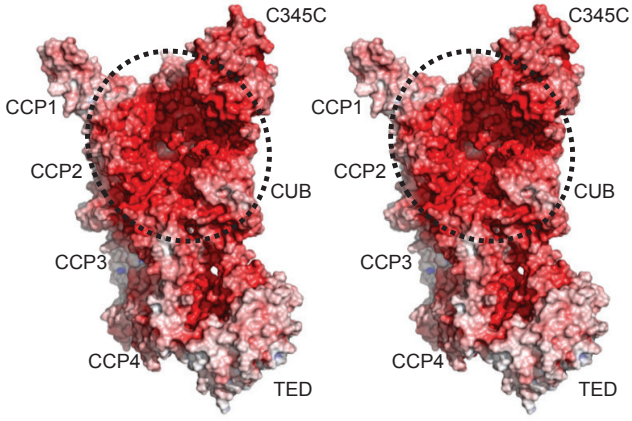

Chapter 3 Supplementary Figure 7. Stereo representation of the C3b-FH(1-4) complex coloured by electrostatic potential. The potential contours are shown on a scale from -15 (red) to + 15 $k_bTe_c^{-1}$ (blue). The dotted oval indicates the proposed FI binding region formed by FH domains CCP1-3 and C3b domains CUB and C345C.

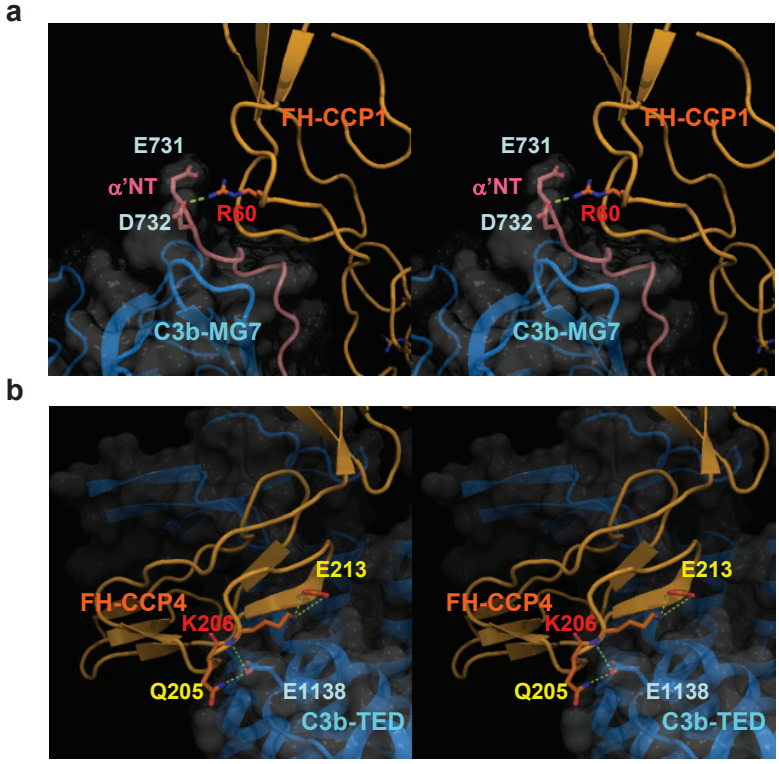

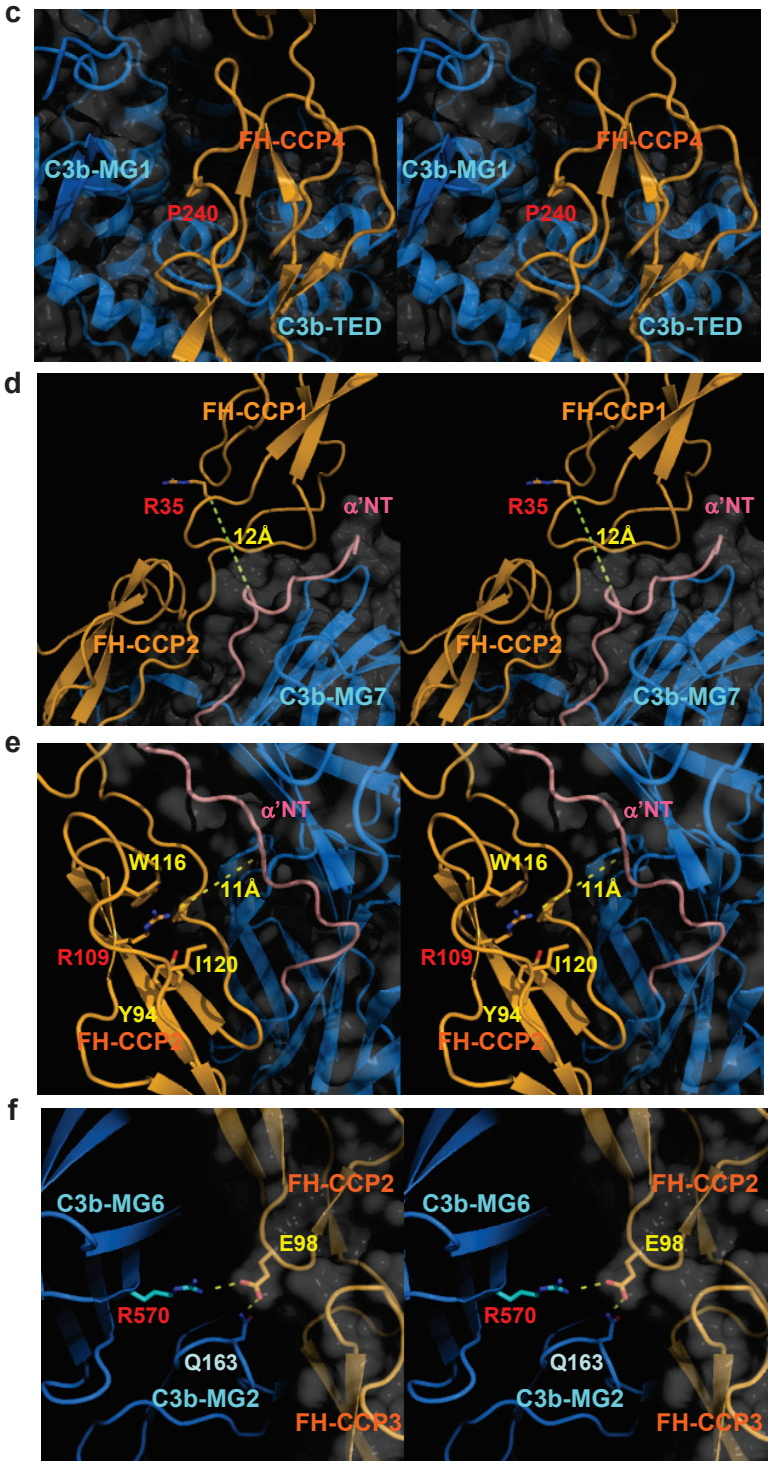
c
C3b-MG1
FH-CCP4
P240
C3b-TED
C3b-MG1
FH-CCP4
P240
C3b-TED
d
FH-CCP1
R35
α'NT
12Å
FH-CCP2
C3b-MG7
FH-CCP1
R35
α'NT
12Å
FH-CCP2
C3b-MG7
e
α'NT
W116
11Å
R109
I120
Y94
FH-CCP2
α'NT
W116
11Å
R109
I120
Y94
FH-CCP2
f
C3b-MG6
FH-CCP2
E98
R570
Q163
C3b-MG2
FH-CCP3
C3b-MG6
FH-CCP2
E98
R570
Q163
C3b-MG2
FH-CCP3

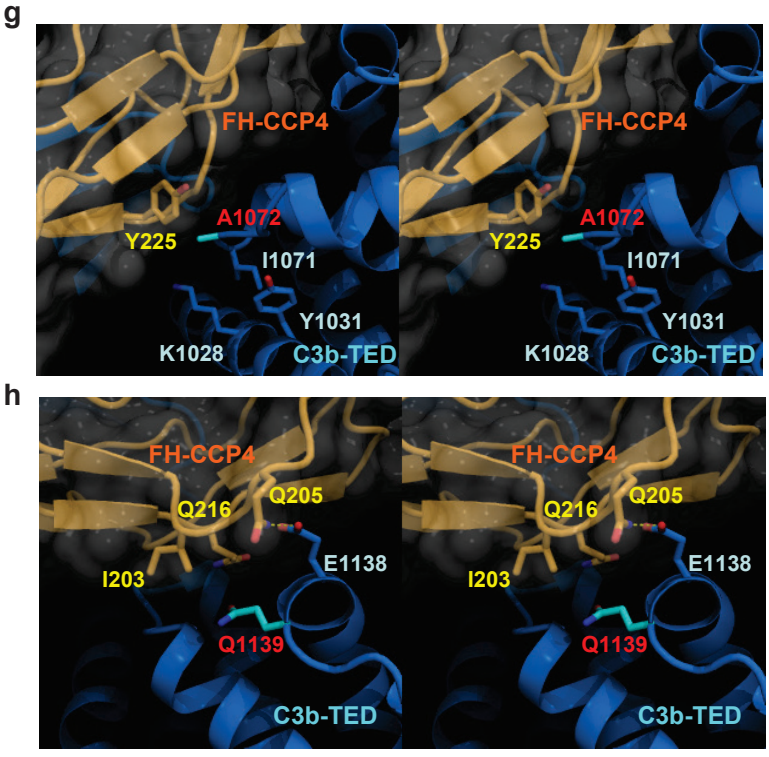

Chapter 3 Supplementary Figure 8. Detailed views of five disease-linked mutations.
Stereo views of FH residues Arg-60[35] (**a**), Lys-206[32] (**b**), Pro-240[33] (**c**), Arg-35[33] (**d**) and Arg-109[39] (**e**). Arg-60, Lys-206 and Pro-240 are at the C3b interface, while Arg-35 and Arg-109 are more than 10 Å away from the complex interface. (**f**), (**g**) and (**h**) are the stereo views of residues Arg-570, Ala-1072 and Gln-1139 in C3b[34].

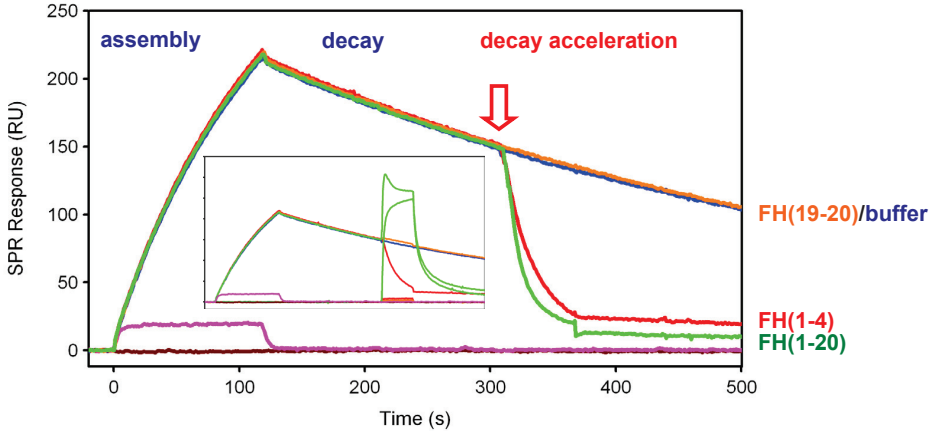

Chapter 3 Supplementary Figure 9. Decay of the C3 convertase by FH(1-4).
Formation, decay, and decay acceleration of the alternative pathway C3 convertase was monitored by SPR. The C3 convertase complex (C3bBb) was formed by injecting a mixture of FB and factor D (FD) on immobilized C3b. Only the combined factors but not FB (magenta) or FD (brown) alone led to the assembly of a stable complex. After observing regular convertase decay for 3 min, either FH(1-20) (green), FH(1-4) (red), FH(19-20) (orange), or buffer (blue) was injected for 1 min and the drop in post-injection signal was evaluated for decay acceleration. While FH(19-20) did not affect convertase decay, FH(1-4) accelerated the decay to a similar extent as FH(1-20). Extended analysis from **Chapter 3 Fig. 1d**. Binding data for convertase assay are representative of three individual experiments (controls with pure FB or FD were injected twice).

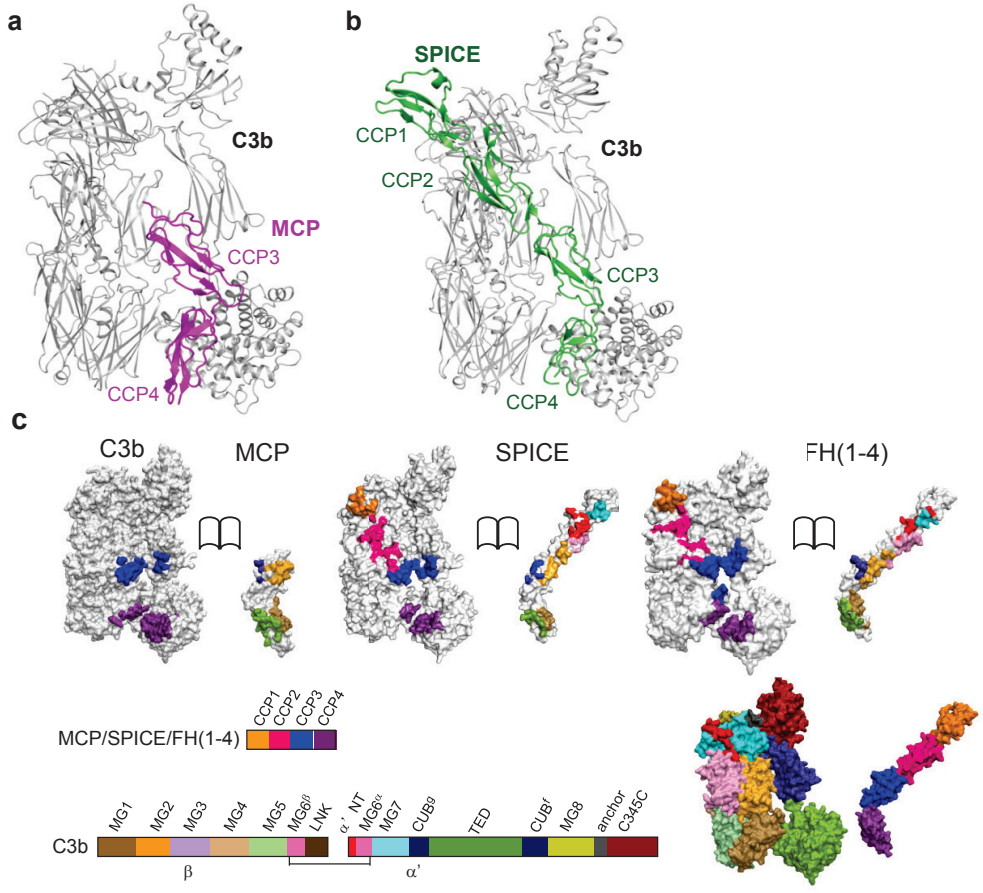

Chapter 4 Figure 1 Structures of C3b-MCP and C3b-SPICE.
Crystal structures of the C3b-MCP (**a**) and C3b-SPICE (**b**) complexes are shown in cartoon representation. Both MCP (pink) and SPICE (green) form a similar, extended interface with C3b (gray). (**c**) Opened view of the footprint of each complex interface. C3b and regulator domains are colored according to the color scheme depicted below. A schematic surface representation of the domain organization of regulators and C3b corresponding to this color scheme is shown at the bottom right.

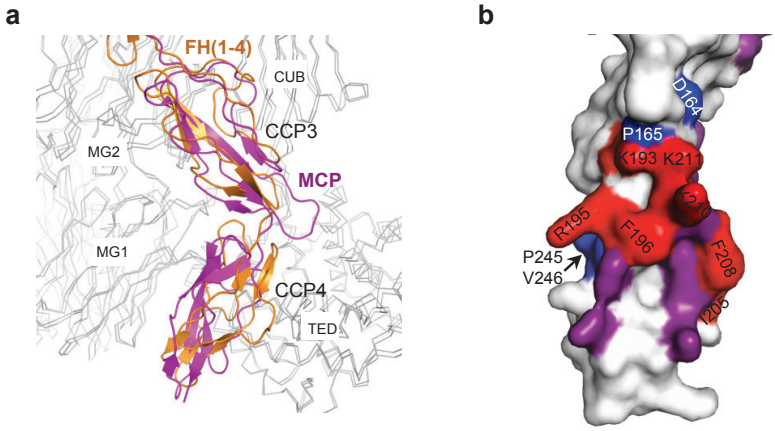

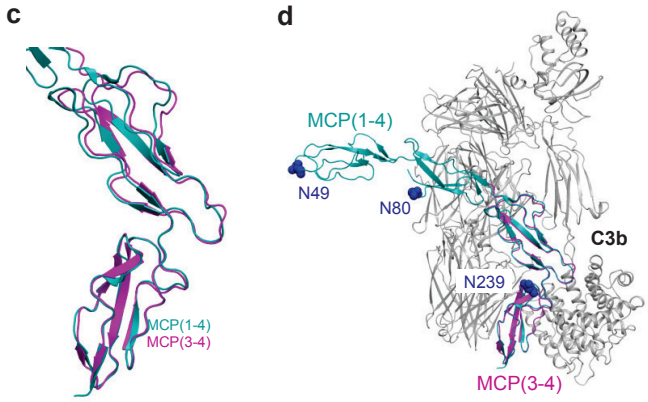

Chapter 4 Figure 2 Structural analysis of C3b-MCP complex.
(**a**) A structural comparison between C3b-FH(1-4) and C3b-MCP in the CCP3-4 region. (**b**) Mapping of the MCP residues that are important for C3b binding to the C3b-MCP complex structure. The interface is colored in purple. MCP mutants colored in red strongly affect C3b binding, while mutants colored in blue have medium effects[33]. These mutants are also at the complex interface. (**c**) Superposition of MCP(3-4) in C3b-MCP complex and MCP(1-4) in CD46-4D structure (PDB code: 3O8E). (**d**) A model of C3b-MCP(1-4) made by superposition of the C3b-MCP complex and MCP(1-4) in the CD46-4D complex based on domains of MCP CCP 3-4. Blue spheres indicate the position of N-linked glycans.

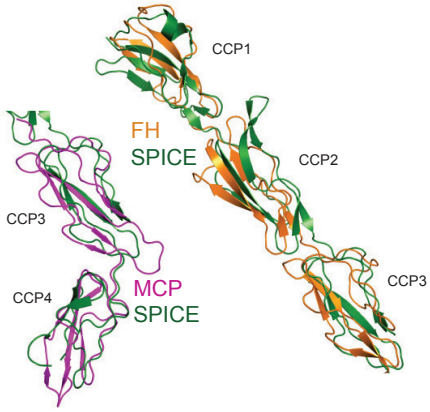

Chapter 4 Figure 3 Structural comparison of SPICE with MCP and FH(1-4), respectively.

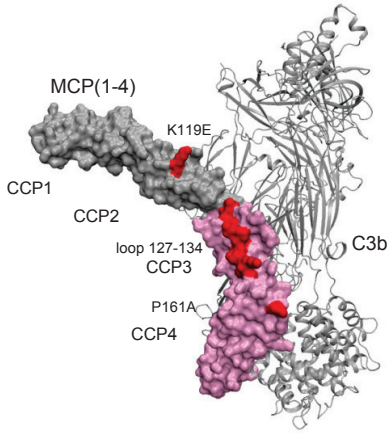

Chapter 4 Figure 4 Implication for cofactor activity.
A model of C3b-MCP(1-4) is shown in surface representation. Residue mutations that still bind to C3b but severely affect MCP cofactor activity are shown in red.

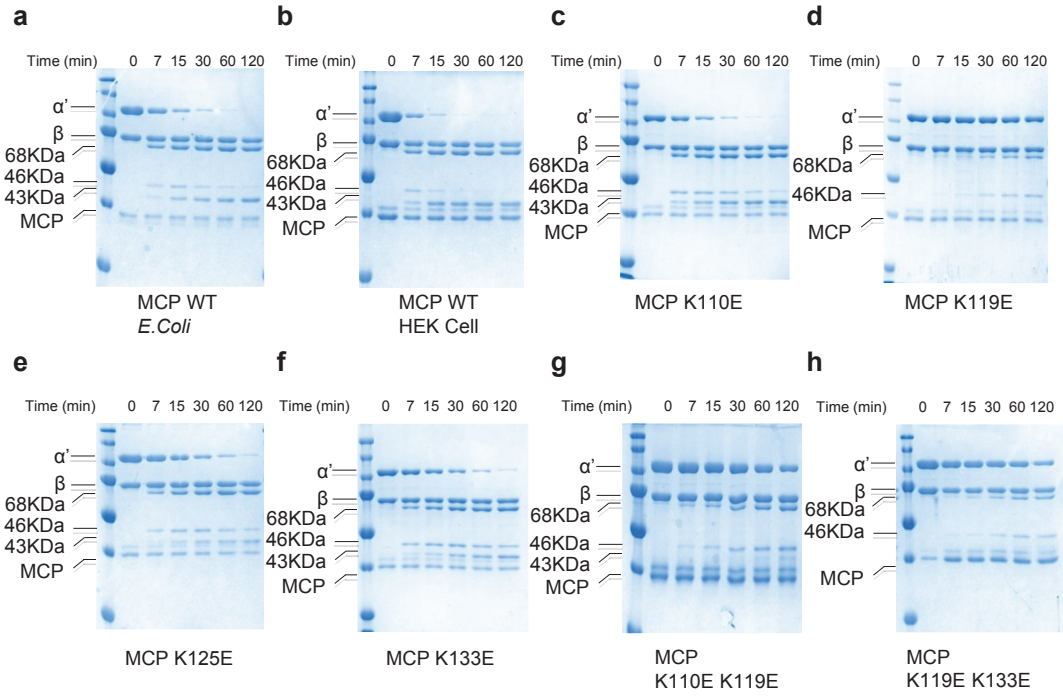

Chapter 4 Supplementary Figure 1. Time course analysis of FI-mediated cofactor activity of MCP and mutants.
(**a**) wild type MCP expressed in *E.coli*; (**b**) wild type MCP expressed in HEK cells; (**c-h**) MCP mutants expressed in HEK cells.

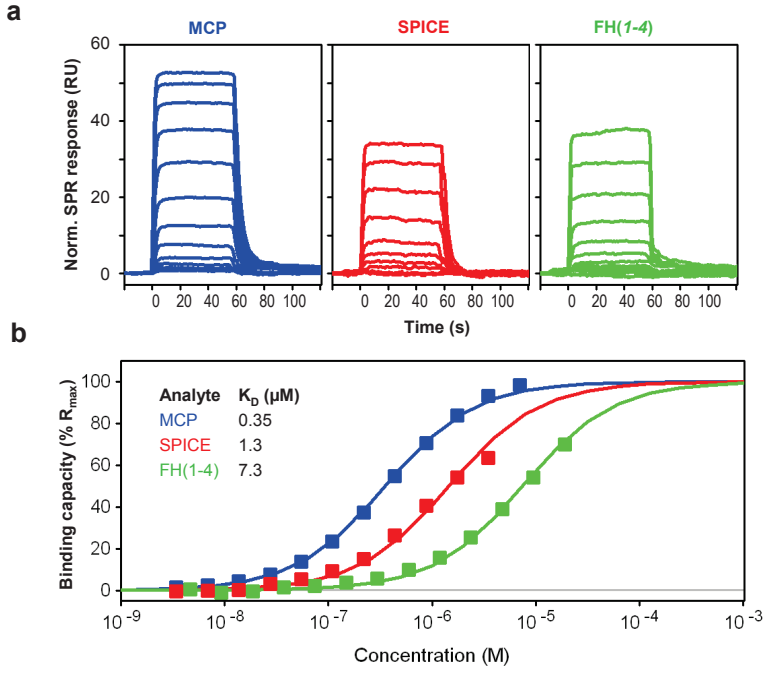

Chapter 4 Supplementary Figure 2. Binding of MCP, SPICE and FH(1-4) to immobilized C3b.
(**a**) Direct binding of three regulators to C3b results 1:1 (molar ratio) complex with binding affinity calculated (**b**).

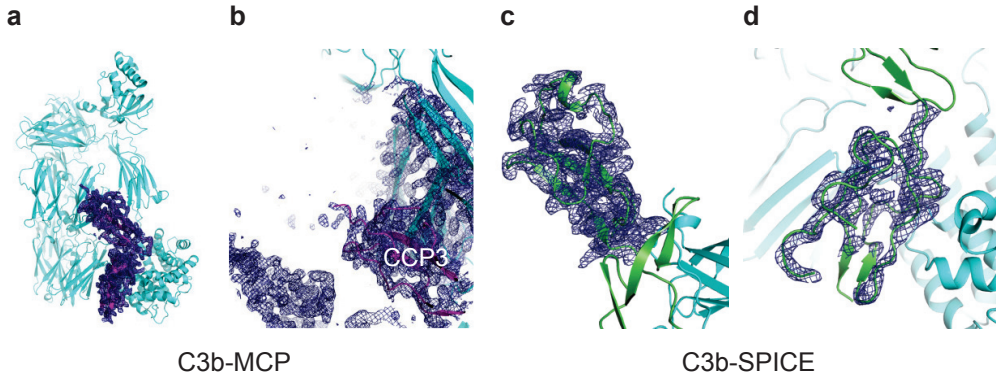

Chapter 4 Supplementary Figure 3. Electron density of structure C3b-MCP (a and b) and C3b-SPICE (c and d) in the region that well ordered and disordered.
(**a**) CCP3-4 of MCP; (**b**) tail of CCP2 and CCP3 of MCP; (**c**) CCP1 of SPICE; (**d**) CCP4 of SPICE.

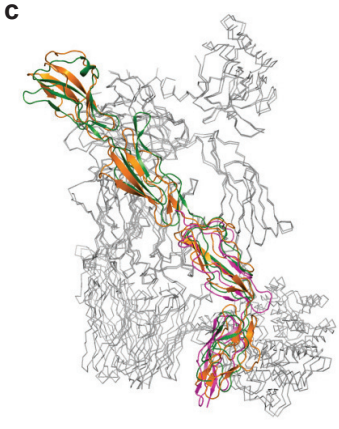

b

Domain	C3b-MCP		C3b-SPICE	
	Translation (Å)	Rotation (˚)	Translation (Å)	Rotation (˚)
MG1	1.7	7.6	0.4	3.4
MG4	3.1	6.4	1.1	2.3
MG5	3.0	7.6	0.5	2.8
TED	2.3	2.7	1.1	6.4
CUB	0.2	4.5	1.2	5.0
C345C	1.0	3.9	15.5	46.8
LNK	2.0	7.1	0.55	3.8

Domain	C3b-MCP		C3b-SPICE	
	Translation (Å)	Rotation (˚)	Translation (Å)	Rotation (˚)
MG2	0.5	3.2	0.7	3.8
MG3	0.3	4.3	0.47	4.5
MG7	0.5	2.4	0.45	2.0
MG8	0.3	3.5	0.47	2.5

d

Domain	Translation (Å)	Rotation (°)	Reference C3b-FH(-4)
CCP3	0.8	8.2	MG2 and CUB
CCP4	4.6	117	TED and MG1

e

Domain	Translation (Å)	Rotation (°)	Reference C3b-FH(1-4)
CCP1	4.3	18.6	α'NT and MG7
CCP2	0.7	3.3	MG2 and MG6
CCP3	1.0	4.3	MG2 and CUB
CCP4	4.7	113	TED and MG1

Domain	Translation (Å)	Rotation (°)	Reference C3b-MCP
CCP3	4.2	2.8	MG2 and CUB
CCP4	2.7	5.4	TED and MG1

Chapter 4 Supplementary Figure 4. Domain rotations and translations among structures of C3b in complex with different regulators.
(**a**) C3b (pdb code: 2I07, blue), C3b in C3b-MCP (pink), C3b-SPICE (green) and complexes was superposed on C3b-FH(1-4) (pdb code: 2WII, orange) based on domains of MG2-3, MG 6-8, α'NT) (grey). (**b**) The values of domain translation and rotation are calculated using SUPERPOSE in the CCP4 package. Structure of C3b-FH(1-4) is used as reference in calculating the values. (**c**) Superpose structures of C3b-MCP (pink), C3b-SPICE (green) on C3b-FH(1-4) (pdb code: 2WII, orange) based on domains involved in C3b-regulator interaction (i.e. MG1-2, MG6-7, α'NT, CUB and TED). (**d**) C3b-MCP was superposed on C3b-FH(1-4) based on the basis of domains as reference indicated in each column. The translation and rotation value are calculated. (**e-f**) C3b-SPICE was superposed on C3b-FH(1-4) (**e**) and C3b-MCP (**f**) respectively, based on the basis of domains as reference indicated in each column.

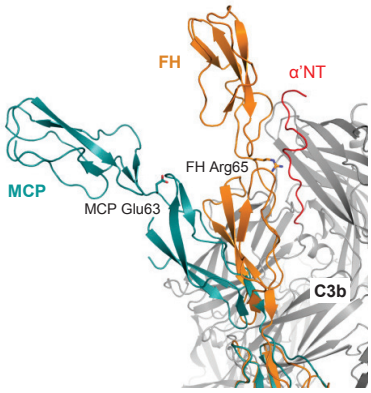

Chapter 4 Supplementary Figure 5. Interaction between α'NT of C3b and CCP1-2 linker of FH(1-4), and comparison with MCP CCP1-2 linker.

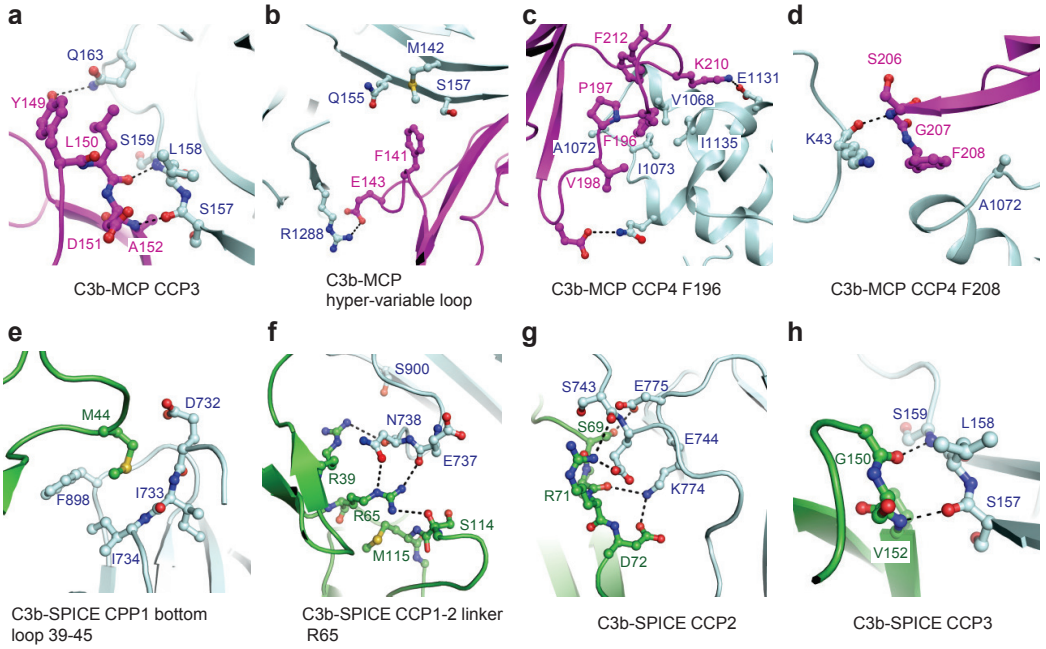

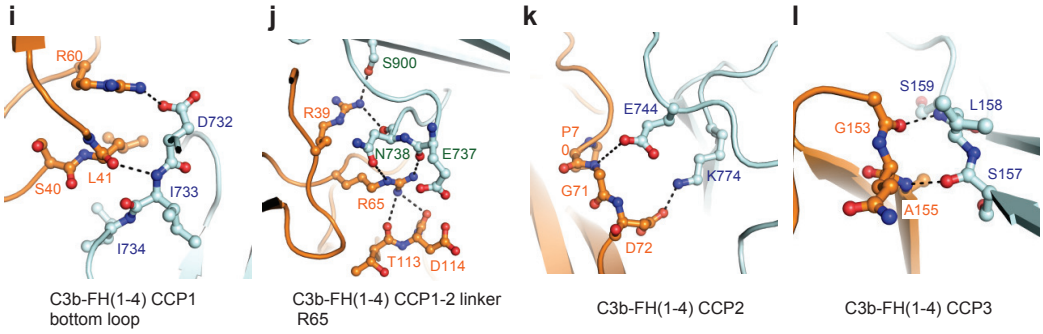

Chapter 4 Supplementary Figure 6. Interaction between C3b with MCP, SPICE and FH(1-4).
Detailed view of contact regions of C3b-MCP **(a-d)**, C3b-SPICE **(e-h)** and C3b-FH(1-4) **(i-l)**. C3b is colored in light blue, MCP in pink, SPICE in green and FH(1-4) in orange. Hydrogen bonds and salt bridges are shown with dashed lines.

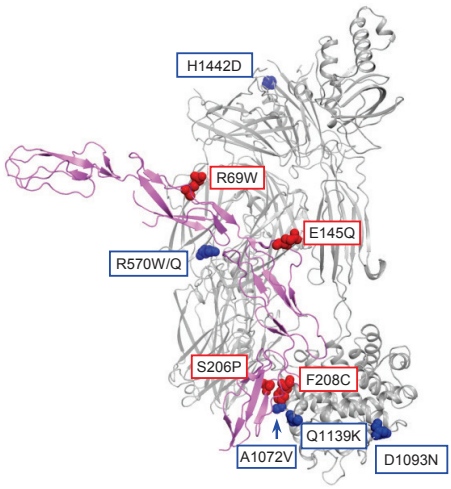

Chapter 4 Supplementary Figure 7. Mutants reported in MCP and C3b leading to aHUS.
The C3b-MCP(1-4) model is derived by superposition of structure MCP(1-4) (pdb code: 3O8E) on structure C3b-MCP on domains CCP(3-4) of MCP. The MCP(1-4) colored in magenta and C3b in grey. The identified aHUS associated mutants in MCP is shown in red spheres and mutants in C3b is shown in blue spheres.

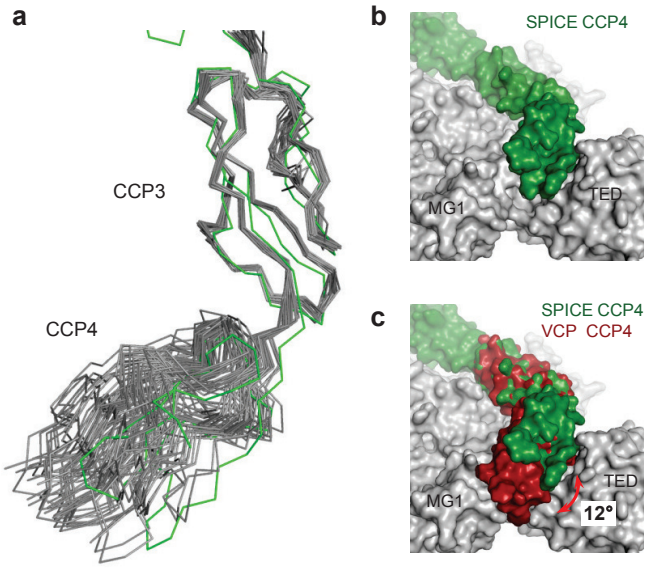

Chapter 4 Supplementary Figure 8. Comparison between SPICE in complex and VCP(3-4) determined by NMR.
(**a**) Structure comparison between SPICE(3-4) (green) in C3b-SPICE complex and NMR structure VCP(3-4) (grey, pdb code: 1VVD). (**b**) Binding platform in C3bS-PICE structure formed by TED and MG1 domains of C3b. (**c**) Comparison the orientation of VCP(3-4) (pdb code: 1VVC) with SPICE CCP4 in complex. The structure are superposed on CCP3 domain of SPICE/VCP.

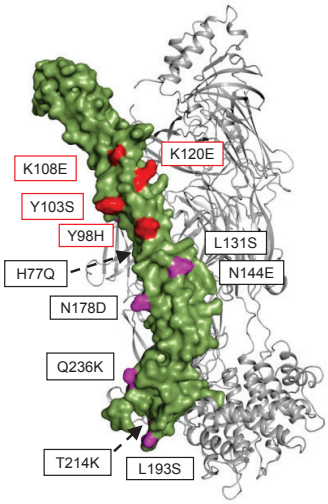

Chapter 4 Supplementary Figure 9. Mapping 11 different amino acids between SPICE and VCP on C3b-SPICE structure.
The 11 different amino acids between SPICE and VCP are colored in magenta and labeled. Y98H, Y103S, K108E and K120E are highlighted in red, as these four residues have the most contribution to the enhanced activity of SPICE.

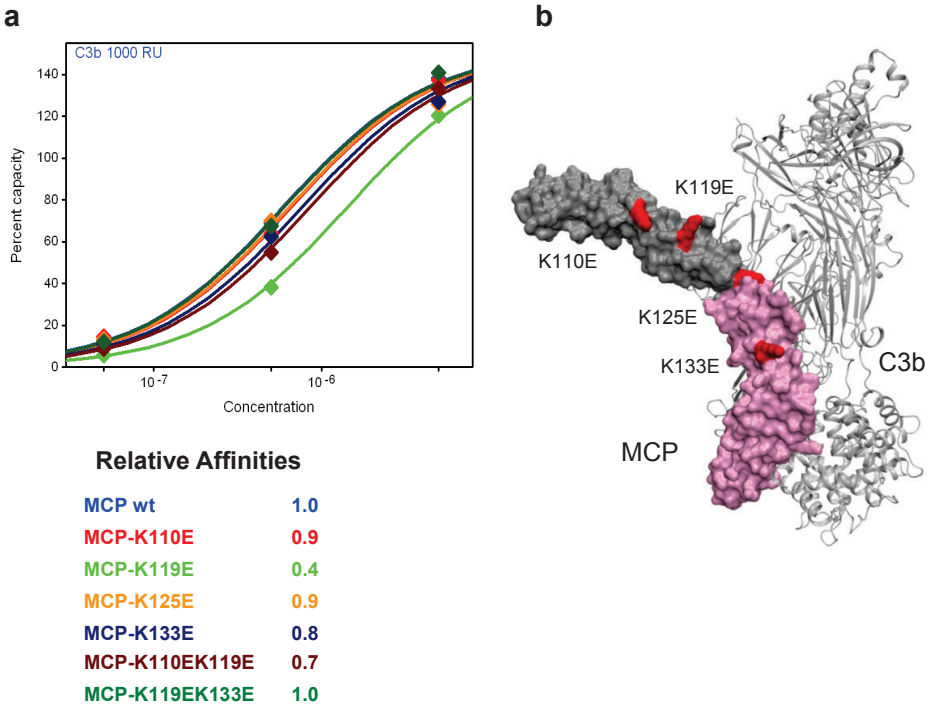

Chapter 4 Supplementary Figure 10. Binding of MCP and the charge reverse mutants of MCP.
(**a**) Direct binding of MCP and MCP mutants to surface-bound C3b. The relative affinities of mutants to wild type MCP were calculated. (**b**) Mapping charge reverse mutant to C3b-MCP(1-4) derived from C3bMCP and MCP(1-4) structures.